ESD-TR-76-67

Dee 1473

(12)

AD A024311

Project Report

TT-7

A. P. Modica

H. Kleiman

Statistics of Global IR Atmospheric Transmission

3 March 1976

Prepared for the Defense Advanced Research Projects Agency under Electronic Systems Division Contract F19628-76-C-0002 by

Lincoln Laboratory

MASSACHUSETTS INSTITUTE OF TECHNOLOGY

LEXINGTON, MASSACHUSETTS

Approved for public release; distribution unlimited.

The work reported in this document was performed at Lincoln Laboratory, a center for research operated by Massachusetts Institute of Technology. This work was sponsored by the Defense Advanced Research Projects Agency under Air Force Contract F19628-76-C-0002 (ARPA Order 2752).

This technical report has been reviewed and is approved for publication.

FOR THE COMMANDER

Eugene C. Raabe

Eugene C. Raabe, Lt. Col., USAF
Chief, ESD Lincoln Laboratory Project Office

MASSACHUSETTS INSTITUTE OF TECHNOLOGY

LINCOLN LABORATORY

STATISTICS OF GLOBAL IR ATMOSPHERIC TRANSMISSION

A. P. MODICA

H. KLEIMAN

Group 53

PROJECT REPORT TT-7

3 MARCH 1976

LEXINGTON MASSACHUSETTS

ABSTRACT

RAND weather data tapes have been used to obtain statistics of visibility, relative humidity and cloud ceiling heights for a number of global weather stations to generate probabilities for atmospheric attenuation in the infrared spectral region. LOWTRAN atmospheric models for clear-air and rural fog-haze transmission have been used to correlate the observed photopic visibility (.55 - .66μm) and humidity to the IR attenuation. A maritime fog-haze model of Barhydt has been incorporated in the analysis to predict atmospheric attenuation losses for the 8.0 - 11.5μm band. Statistics for rain attenuation in the 0.6 to 10.6μm region were computed using the extinction data reported by Rensch and Long. The basic results of the study are global seasonal probabilities for horizontal sea level transmission losses for several narrow IR bands (1.0 - 1.2), (3.8 - 4.2), (8.0 - 11.5μ) and four laser lines (1.06), (3.83), (4.73), and (10.6μm). Correction factors are provided to scale horizontal transmission losses to slant path transmittances.

CONTENTS

PREFACE

Weather statistics are extremely important in the design of electro-optical systems for tactical operations. In the HOWLS Program, several such systems are being considered. Existing analyses and weather statistics were inadequate for effectiveness evaluations and it was necessary to initiate an effort to extrapolate available data. The present study is an attempt to correlate extensive meteorological data from a network of global weather stations sufficiently different in climatological conditions to establish a representative data base on world-wide atmospheric attenuation in the 1.0-14.0μm IR radiation band. Weather histories of photopic visibility and relative humidity were obtained from the RAND Weather Data Bank and were reduced to IR atmospheric propagation models. The transmission models used in the analysis are continuously being updated by current HOWLS weather measurements and through ongoing measurements programs under Project OPAQUE. The results of this work should prove valuable to many users concerned with electro-optical, global all-weather performance.

1. Introduction

Under the HOWLS Program, the analysis of FLIR imaging systems and IR sensor devices for target acquisition and PGM (precision-guided munitions) terminal guidance applications has led to the need to assess the impact of weather statistics and atmospheric attenuation in the infrared on the effectiveness of such types of tactical weapon systems. The primary objective of IR-weather analysis is to collate meteorological data for a number of worldwide weather stations and to determine the extent and frequencies of IR attenuation losses extrapolated from photopic visibilities and relative humidity measurements. RAND Weather Tapes[1] have been processed by a computer to determine the seasonal and geographical variations of these weather parameters for a number of selected Northern Hemisphere weather stations: Berlin, Dresden, Essen, and Hamburg in Germany; Nicosia, Cyprus; Cairo, Egypt; Hue, South Vietnam; Hanoi, North Vietnam; and Falmouth, MA, USA. These statistics and the AFCRL LOWTRAN atmospheric models for clear air and fog-haze transmission[2] have been correlated to generate probability curves for horizontal sea level atmospheric attenuation losses for three narrow IR radiation bands (1.0-1.2), (3.8-4.2), (8.0-11.5μm) and four laser lines (1.06), (3.83), (4.73), (10.6μm). Joint probabilities of transmission losses with cloud ceiling height have also been computed and indicate the seasonal and worldwide variability. Synoptic weather statistics for precipitation, cloud ceiling heights and photopic visibilities have been included for examination to demonstrate similarities and differences in weather between the various geographical locations.

2. RAND Weather Data Bases

Weather data have been compiled by the RAND Corporation[1] for a network of global weather stations and are available on 9 track, 1600 bpi density magnetic tapes. The data bank of each weather station is a chronology of atmospheric variables including the parameters of dew point temperature (relative humidity), photopic visibility, weather conditions (rain, fog, haze, drizzle, etc.) and cloud data (cloud amounts, ceiling heights). The principle source of the RAND Weather Data Bank (RAWDAB) is derived from weather observation records collected by the USAF Environmental Technical Applications Center[3]. The RAWDAB tapes are written in EBCDIC Code having a physical record block of 50 logical records, 96 characters in length. Groups of weather stations in close proximity were chosen to compare similarities in local weather conditions. Sufficient groups were chosen with widely varying weather patterns to provide a representative global weather data base.

3. Atmospheric Transmission Models

In the present study, the atmospheric attenuation of radiation in the 1.0-14.0μm infrared region is of primary interest. Models for atmospheric transmission in the IR deal primarily with molecular absorption by atmospheric CO_2 and water vapor gases, and with the scattering of radiation by various types of aerosols (rural, continental, maritime), whose normalized extinction coefficients are shown for comparison in Figure 1. The AFCRL LOWTRAN computer program[2] has been used to compute atmospheric transmittances for three narrow IR radiation bands (1.0-1.2), (3.8-4.2), and the (8.0-11.5μm) thermal band for horizontal sea level paths. The LOWTRAN code was run for a sequence of relative humidities and visibility ranges with the resultant transmittances being fitted to exponential laws of the form[4]:

3.1 Clear Air Transmission Equation

$$T_A = \exp\left[-R(A/W + B)\right] \qquad (1)$$

and

3.2 Fog-Haze Transmission Equation

$$T_F = \exp\left[-R(A/V^C)\right] \qquad (2)$$

where R is the optical path length, km, W is the amount of H_2O absorber, ft per mm of precipitable H_2O (Ft/mm-prec H_2O), V is the photopic visibility range, km, and A, B, and C are the coefficients derived from a three-point average curve fit. The amount of water vapor absorber in ft/mm-prec H_2O is given in terms of the percent relative humidity, RH, and the air temperature, TK $(^{o}K,)$ by[5]

$$W = 3.3(10^5) \Big/ \left[RH\left(\frac{TK}{247}\right)^{16.8} - .616RH\right] \qquad (3)$$

or in terms of the H_2O partial pressure[6], P_{H_2O}

$$W = 0.114(10^2)\ TK/P_{H_2O} \qquad (4)$$

Similar clear air and fog-haze transmission expressions were derived for four IR laser lines using spectral absorption and extinction coefficients obtained from AFCRL[7]. Barhydt's maritime fog-haze model[5] was used as a lower bound to the LOWTRAN rural aerosol model for the (8.0-11.5μm) band. Clear air transmission for the 10.6μm laser line was calculated with the expression given by Long, et al, in a study of water vapor continuum absorption of CO_2 laser radiation near 10μm[6]. A comparison of Barhydt's and Long's transmission curves with the LOWTRAN Model is shown in Figure 2. Figure 3 shows the clear air and fog-haze transmission curves for the IR radiation bands calculated with the LOWTRAN code. A summary of the atmospheric clear air and fog-haze transmission models used in the meteorology statistical analysis is given in Table 1. The difference in the transmission equations for the bands and lines reflects the fact that the band coefficients are related to vibrational-rotational line spectral absorption and extinction factors integrated over the bandwidth. Based on the work of Eldridge[8], the fog-haze atmospheric boundary occurs abruptly and represents a transition at about a 1.2 km visibility. Hulbert[9] has found that the haze-clear boundary condition is more diffusive, approximately a 15 km visibility range. Table 2 catalogs the different types of fogs according to their photopic visibilities and compares the attenuation loss performances for the (3.8-4.2) and (8.0-11.5μm) bands, and the 1.06 and 10.6μm laser lines.

TABLE 1

IR NARROW BAND AND LASER LINE ATMOSPHERIC TRANSMISSION EQUATIONS

Narrow Band Atmospheric Transmission in the Infrared

Radiation:	Clear Air Transmission	Fog Haze Transmission
[a](1-1.2)µm	$T_W = \exp\{-R[35.9/(W) + .065]\}$	$T_F = \exp\{-2.02R/(V)^{.997}\}$
(3.8-4.2)µm	$T_W = \exp\{-R[10.47/(W) + .098]\}$	$T_F = \exp\{-.796R/(V)^{.855}\}$
[b](8-11.5)µm	$T_W = \exp\{R[.987/(W)^{.384} + 5930/(W)^{1.86}]\}$	$T_F = \exp\{-0.8R/(V)^{1.26}\}$

a. Ref. 2, b. Ref. 5

Laser Line Atmospheric Transmission in the Infrared

Radiation:	[a]Clear Air Transmission	[a]Fog-Haze Transmission
(1.06)µm	$T_W = \exp\{-0.R/w\}$	$T_F = \exp\{-2.20R/(V)\}$
(3.83)µm	$T_W = \exp\{-R(.002078 + 1.937/w)\}$	$T_F = \exp\{-.526R/(V)\}$
(4.73)µm	$T_W = \exp\{-R(.0013 + 16.366/w)\}$	$T_F = \exp\{-.44R/(V)\}$
(10.6)µm	[b]$T_W = \exp\{-R\,[144.(295./TK)^{1.5}\,(10)^{-970/TK} + .0374\,(TK/W) + .1078\,(TK/W)^2]\}$	$T_F = \exp\{-.391R/(V)\}$

Units, W(FT/MM - prec H_2O, V(KM), R(KM), TK(°K)

a. Ref. 7, b. Ref. 6

TABLE 2

COMPARISON OF FOG-HAZE VISIBLE/INFRARED
ATMOSPHERIC TRANSMITTANCES

*TYPE	H_2O CONTENT (G/M^3)	VISIB (KM)	IR BANDS μM DB KM^{-1} (3.8-4.2)	(8-11.5)	LASER LINE μM DB KM^{-1} 10.6	1.06
THICK	0.4	.03	69.9	45.3	58.1	318.4
MEDIUM	.16	.085	28.9	17.7	21.4	112.4
LIGHT	.063	.170	16.4	10.1	11.5	56.2
MIST	.027	.30	10.3	6.6	7.2	31.8
HAZE	.005	1.0	4.1	3.2	3.2	9.6

* Inland Fog @ 70°, 90% relative humidity

LOWTRAN rural fog-haze model

The slant path correction factor $\tilde{\Delta}$ is used to convert sea level horizontal attenuation losses to slant path attenuation losses and is given by the expression.[6]

3.3 Slant Path Correction Factor

$$\tilde{\Delta} = L^{-1} \csc\phi \int_0^L e^{-\frac{h}{\tilde{H}_0}} \, dh \qquad (5)$$

where $e^{-\frac{h}{\tilde{H}_0}}$ is the geometric mean vertical scale factor for the water vapor number density and aerosol particle number density, L is the slant path range, km, h is the vertical height, and ϕ is the elevation angle. Equation 5 was evaluated using the vertical scale normalized distributions shown in Table 3. Values of the slant path correction factors are given in Figure 4 for slant angles between 0 and 90^0 elevation and slant ranges from 0.5 to 10 km. The geometric mean slant path correction factors are used for atmospheres having 2 km to 10 km visibilities. Limiting exact solutions for scaling sea level horizontal attenuation losses to slant path losses are obtained by using the exact aerosol or water vapor slant path correction factor for atmospheric visibilities < 2 km and > 10 km, respectively.

4. Rain Attenuation

In the visible and IR spectral region, attenuation by rain is expected to be independent of wavelength because the raindrop radius (typically, about 0.5 cm) is much larger than the wavelength where the Mie extinction efficiency factor asymptotically approaches the value 2. Measured values of the

TABLE 3

NORMALIZED VERTICAL SCALE FACTORS FOR ATMOSPHERIC WATER VAPOR AND AEROSOL DISTRIBUTIONS

$$Z(h) = N(h)/N_o$$

(KM)	0	1	2	3	4	5	6	7	8	9	10
[1] WATER VAP	1.0	.71	.51	.34	.19	.109	.06	.024	.01	.0046	.0039
[2] AEROSOL	1.0	.37	.13	.049	.018	.0065	.0046	.0042	0044	.0042	.0041
[3] GEOM. MEAN	1.0	.51	.26	.129	.058	.027	.017	.010	.006[illegible]	.0044	.004

1. Handbook of Geophysics and Space Environment (1965)
2. Elterman, L., Appl. Opt. 9, 1804 (1970)
3. Geom. Mean = $\left[Z(h)_{H_2O} \cdot Z(h)_{AERO}\right]^{1/2}$

visible and IR extinction coefficients through rain are found to compare favorably with theoretical prediction[10] as shown in Figure 5. These rain attenuation results and the LOWTRAN clear air transmission models were used to reduce meteorological relative humidity and visibility data to IR attenuation losses through rain.

5. Cloud Free Line-of-Sight Probabilities

The cloud free line-of-sight (CFLOS) probability is another important weather parameter used in optical-systems analysis and is defined as the frequency of time an observer will find a line-of-sight unobstructed by clouds along a viewing angle from ground level to a given point above ground. RAND meteorological data have been queried to obtain seasonal (CFLOS) statistics as a function of viewing angle, α and line-of-sight from ground level to points, h in space. The CFLOS probabilities are computed from the equation

$$P_{CFLOS} = \sum_{k=0}^{8} c\ (\alpha,k) \cdot D\ (h,k), \qquad (6)$$

where D (h,k) is the cumulative probability that the cloud cover in eights, k (Octas sky cover) will be equal to or less than a given height, and c (α,k) is the clear view function (Table 4) related to the probability that a cloud free line-of-sight will exist through cloud cover at or below the viewing point along the viewing angle[11]. CFLOS probabilities have been determined from available cloud data for Berlin, Essen, Hamburg, Nicosia, Cairo, Hue and Falmouth USA representing the HOWLS weather data base. These

TABLE 4

CLOUD COVER CLEAR VIEW PROBABILITY FUNCTION

CLOUD COVER(EIGHTS)	ELEVATION ANGLE(DEG) 0.0	5.0	10.0	15.0	20.0	25.0	30.0	35.0	40.0	45.0	50.0	55.0	60.0	90.0
	PROBABILITY													
0	.962	.965	.970	.973	.975	.978	.980	.983	.985	.988	.990	.993	.995	1.000
1	.640	.730	.820	.875	.895	.910	.920	.930	.940	.945	.950	.952	.954	0.960
2	.490	.600	.695	.750	.805	.825	.850	.860	.875	.880	.890	.895	.898	0.900
3	.370	.490	.590	.645	.700	.730	.775	.790	.300	.815	.825	.830	.840	0.850
4	.275	.380	.485	.540	.600	.645	.680	.695	.710	.725	.740	.750	.765	0.780
5	.195	.280	.360	.420	.490	.525	.575	.595	.610	.630	.650	.660	.675	0.680
6	.095	.180	.250	.300	.365	.400	.430	.460	.480	.500	.510	.520	.525	0.545
7	.040	.090	.130	.190	.225	.250	.275	.290	.300	.320	.325	.330	.340	0.350
8	.020	.025	.030	.035	.040	.045	.050	.055	.060	.065	.070	.075	.080	0.085

results are given in Table A-2 of the appendix for viewing angles of 1, 2, 3, 5, 15, 45, 90 degree-elevation and line-of-sight paths from ground to .333, .5, 1. and 2 km cloud heights.

6. Stations Selected for IR Weather Analysis

The RAND Weather Data Bank (RAWDAB) was used in the present study to provide visibility, relative humidity, cloud ceiling heights and synoptic weather parameters for four typical regions of the Northern Hemisphere; Europe, North Africa, Southeast Asia and Eastern USA. A general meteorological description of each geographic area is given below as summarized by Rosen and Schutz.[11]

Europe: (Berlin, Essen, Dresden, Hamburg)

These weather stations lie in the rolling hills of northern German plains and come under the influence of a prevailing westerly flow of moist polar air generated in the North Atlantic high. There is extensive cloudiness throughout the year and little regional variation in climate. In winter, the moist Atlantic polar air becomes cool and stabilizes, resulting in persistent low broken-to-overcast stratus or strato-cumulus cloud cover. In summer, the highest cloud amounts occur during the day, since the land is warmer than the surrounding ocean creating unstable convective currents in the moist polar air mass. Overcast conditions are half that of winter, although the frequency of broken cloud cover remains about the same. Cumulus and cumulonimbus clouds (rain clouds) tend to dominate. The frequency of this cumulonimbus activity takes place on the average 4 to

6 days per month. These line squalls are similar to those experienced across the eastern United States, but are less violent because the polar air masses tend to be less moist than the tropical air masses influencing eastern United States.

North Africa: (Nicosia and Cairo)

These weather stations lie on the coastal reaches of the eastern Mediterranean, and come under the influence of the Atlantic polar air mass moving clockwise around the North Atlantic high. Expansion and compression of this air mass while crossing the east-west mountain chain of western Europe causes a loss in moisture. Before reaching the Nicosia and Cairo areas, however, some moisture is again added to the lower levels by passage over the warm Mediterranean. This added moisture accounts for the high percentage of scattered to broken clouds annually. Characteristically, Cairo and the eastern Mediterranean coast are wet in winter and dry in summer. In winter, storms intensify over the eastern portion of the polar front in the vicinity of Cyprus on an average of 4 to 6 times per month and account for the high percentage of broken-to-overcast cloud layers. In summer, low strato-cumulus clouds move inland as the land cools in the late afternoon. They remain through the night and then dissipate or form small cumulus clouds by late morning as the land becomes warmer. During the early morning period to early evening, the cloud cover increases rapidly between 2 and 4000 ft then remains constant. The low stratus or cumulus-type clouds provide the only obscuration of the ground from all levels above. Weak upper-level disturbances occasionally pass the eastern Mediterranean area but have little or no effect on the cloud pattern below 16,000 ft.

Southeast Asia: (Hue, Hanoi)

Vietnam and the remaining peninsula of Southeast Asia come under the influence of two major monsoonal flows. From May to September, the southwest monsoon brings dried tropical ocean air to the Hue area. In October a shift begins, so that from November to March the northeast monsoon prevails, sending moist polar continental air into Hue and the surrounding coast. These area masses are somewhat similar to those that influence the area south and east of the Great Lakes. Winter conditions at Hue and along the coastal slopes of the Annam Range (from about 12^{o}N latitude to the Red River delta) give broken-to-overcast low clouds approximately 70 percent of the time. This results from dry stable polar continental northeast flow over the Gulf of Tonkin and the South China Sea and accounts for the sharp increase below 6000 ft of persistent low stratus and strato-cumulus weather. From May to September, the period of the southwest monsoon, cloudiness during the daytime (0600 to 1800 LST) decreases caused by a drying of the unstable tropical ocean air through an adiabatic cooling and heating process as the air mass moves across the Annam Range from the southwest. Cloud cover is predominantly scattered-to-broken cumulus-type clouds with base heights around 2500 ft.

Eastern United States: (Falmouth)

The east coast region of the United States comes under the influence of the continental polar air mass in winter and a tropical ocean air mass in summer. In winter, the eastern United States has clear weather about 8 percent of the time and has only 10 percent scattered cloudiness. The Gulf Stream which carries moist tropical ocean air along a frontal path extending to the western coast of Europe (England) is modified by the cooler polar North Atlantic high, creating infrequent extended periods of fog for this area. In winter, the same Gulf Stream is turned westward by this polar Canadian high creating similar fog conditions along the eastern border of the United States. Winter fogs in western Europe are similar to those of eastern United States, both regions being fed by the same moist tropical air masses. Summer weather is less complicated by extensive storms, although line squalls in late spring and early fall sometimes prevail. The predominant cloud is cumulus within the dominating moist, unstable Atlantic air mass.

Of the stations considered in this study, from an annual viewpoint, Eastern United States and Europe represent the cloudiest stations. Hue or Southeast Asia is next in amount of cloud-cover and the Cairo area, being represented by a relatively dry polar air mass, has a minimum of cloud cover. The information provided by these global weather areas represents in this report a broad sample of the kind of climatic variation suitable to form the basis for a statistical analysis applicable to atmospheric IR attenuation losses on a worldwide scale.

7. Statistics

Some meteorological data for certain weather stations were not available on the RAWDAB tapes for statistical analysis. It was found for example that the Berlin and Falmouth tapes did not contain records on synoptic weather conditions. Also, the Dresden and Hanoi tapes did not have data on cloud ceiling heights. For clarification, a definition of the statistical quantities used in the analysis will be briefly discussed here.

Frequency of occurrence: the fraction of time a statistical parameter is recorded within a given data group.

Synoptic probability: the frequency of occurrence of a given weather condition, i.e., rain, fog, haze, fraction of cloud cover.

Seasonal probability: frequency of occurrence during winter, DEC. JAN. FEB.; Spring, MAR. APL. MAY; summer, JUN. JUL. AUG.; and fall, SEPT. OCT. NOV.

Atmospheric attenuation probability: the integrated frequency of occurrence where the meteorological parameter is equal to or greater than its value (independent of cloud ceiling height).

Joint probability of cloud ceiling height and atmospheric attenuation: probability that the attenuation is equal to or greater than its value and the cloud ceiling height is equal to or below the indicated cloud height.

Cloud ceiling height probability: defines the integrated frequency of occurrence of the cloud height being equal to or below the indicated value.

Photopic visual probability: defines the integrated frequency of occurrence of the (.5 - .6μm) visual range being equal to or less than the indicated value.

Attenuation losses of selected narrow band and laser line transmittances in the 1.0-14.0μm IR region were calculated from relative humidity and photopic visibilities, using clear air and rural fog-haze expressions given by the AFCRL LOWTRAN atmospheric models. The LOWTRAN models for rural, continental and urban aerosols show relatively small differences in their normalized extinction coefficients for the 1.0-14.0μm spectral region, thereby making the present analysis less sensitive to the types of inland fogs and almost completely general for correlation with photopic visibilities. For the 8.0-11.5μm band, atmospheric attenuation losses were computed with the maritime fog-haze transmission model of Barhydt.

8. Weather Statistics and IR Atmospheric Attenuation Averages for Germany

Synoptic weather, photopic visibility and cloud ceiling height: The synoptic weather averages for Germany (Figure 6) show that the frequency of occurrence of clear days during the year varies from about 55 percent of the time in winter and increases to about 70 percent of the time for summer. The second dominant weather condition is rain, occurring about 25-30 percent of the time throughout the year. The occurrence of fog appears to be greater in winter and fall, but slightly less in spring and summer and averages between 5 and 10 percent of the total weather events. The standard deviations from the mean values suggest that for Germany or European weather there is little regional variation in climate throughout the year, in agreement with the meteorological description of Rosen and Schutz.

Average meteorological visibilities for Germany (Figure 7) show that visibilities equal to or less than 10 km occur about 80 percent of the time in winter and about 40 percent of the time in summer. Poor weather, where visibilities are equal to 1 km and less, appears to take place with a frequency between 5 and 10 percent throughout the four seasons and tends to correlate well with the synoptic weather data for fog and haze frequencies. Plots of short-term (6-hour time intervals) visibility data for three European cities; Leipzig, Dresden, and Prague (Oct. 10-30, 1960) are shown in Figure 8. These data have been cross-correlated[12], also, to show the degree of temporal similarities in visibility for typical European weather.

Cloud ceiling height averages (Figure 9) show that base heights equal to or below 1 km occur between 60 and 80 percent of the time for winter, spring, and fall. In summer, base heights that are equal to 1 km and below occur about 55 percent of the time, again reflecting the year round cloudy characteristics of European weather. Figure 10 shows that the short-term variability of cloud ceiling height for Leipzig, Dresden and Prague. The almost complete correlation in cloud heights for these three weather zones indicates that cloud cover extends uniformly over large distances in Europe.

IR atmospheric attenuation loss averages: Average IR attenuation losses for Germany were computed for the three narrow band wavelengths, (1.0-1.2), (3.8-4.2), and (8.0-11.5)μm shown in Figure 11. The error bars in the figure indicate typically about a 10 percent standard deviation from the mean values calculated from the Berlin, Dresden, Essen and Hamburg weather data. The results show that for the (8.0-11.5)μm band, the attenuation loss in winter for clear and fog-haze weather conditions is equal to or more than 1.5-1.75 dB/km about 10-5 percent of the time, respectively. In summer, the (3.8-4.2)μm band shows about the same statistics on the average. The reason for the high performance of the (8.0-11.5)μm band in winter and the high performance of the (3.8-4.2)μm band in summer is accounted for by the low relative humidity in winter, since the (8.0-11.5)μm band is more sensitive to water vapor absorption and less sensitive to fog-haze scattering. The (3.8-4.2)μm band is better in summer, since this spectral band is less sensitive to water vapor absorption or high relative humidity and only moderately affected by fog-haze conditions. The (1.0-1.2)μm band which is most sensitive to aerosol scattering gives attenuation losses about a factor of two greater for the same frequency of occurrence.

Rain attenuation loss averages: The average frequency for rain attenuation losses in Germany is shown in Figure 12. The attenuation losses were calculated for the (1.0-1.2), (3.8-4.2), (8.0-11.5)μm IR bands and the visible wavelength interval (.5 - .6)μm. These calculations included clear-air water vapor absorption and losses due to rain drop scattering and liquid absorption. These data show little variation in attenuation losses for the IR-bands and the visible region, indicating that the attenuation loss here is dominated by rain scattering and absorption and less by clear-air water vapor absorption. The results show that for

Germany, about 50 percent of the time, the atmospheric losses on the average can be expected to be equal to or greater than 3 dB/km in rain.

Figure 13 is shown to compare the probability of atmospheric attenuation losses for clear weather, fog-haze and rain atmospheric conditions. This figure also shows rain rates correlated to attenuation losses for the visible (.5 - .6)μm band. The results indicate clearly the advantages of the IR bands for fog-haze transmission over the visible band. It is also noticed that in the visible, attenuation losses are greater in fog than in rain all of the time. In the infrared, attenuation losses less than 2 dB/km occur in fog between 20 and 35 percent of the time. These conditions never exist in the rain.

Attenuation due to rain is always greater than 2 dB/km, with 50 percent of the rain having attenuation between 2 and 3 dB/km. However, for infrared attenuation above 3 dB/km, an inversion takes place between rain and fog transmission, where attenuation losses equal to or less than 3 dB/km occur more frequently in rain than during foggy conditions.

9. Use of IR-Weather Data: Examples

Weather statistics and probabilities for IR and visible attenuation losses are compiled in the Appendix according to the weather stations studied in this report. A number of examples are treated here to illustrate the use of these figures.

- <u>Synoptic Weather Statistics</u> (Figures A*.1)

These figures provide the fraction of time during the four seasons that clear weather, haze, fog, drizzle and rain occur, respectively.

- Probability of Cloud Ceiling Height (Figures A*.2)

These figures give the cumulative probability, $P_{CH}(h)$, that a cloud base will be equal to or less than a given altitude, h. The cumulative probability that a cloud base will be equal to or greater than this altitude is

$$P_{CH} = 1 - P_{CH}(h).$$

The probability, $P_{CH}(S)$, that a cloud base will occur at or below a slant range, L and elevation angle ϕ is

$$P_{CH}(S) = P_{CH}(H),$$

where $H = L \sin \phi$, the terminal altitude of the slant path.

- Probability of Photopic Visibility (Figures A*.3)

These figures give the cumulative probability, $P_{vis}(\nu)_o$, that the horizontal sea level visibility will be equal to or less than a given meteorological range, ν. The probability that the visibility will be equal to or greater than this range is

$$P_{vis} = 1 - P_{vis}(\nu)_o.$$

The probability, $P_{vis}(V)_s$, that the visibility along a slant path, $(V)_s$ of range, L and slant angle, ϕ is equal to or less than a given value is the probability along an equivalent horizontal sea level visibility path, $(V)_o$, i.e.,

$$P(V)_s = P(V)_o$$

where

$$(V)_o = (V)_s \times \tilde{\Delta}_{aero}$$

and $\tilde{\Delta}$ is the slant path correction factor for a slant range, L and angle, ϕ (Figure 4).

- Probability of Atmospheric Attenuation (Figures A*.4 and A*.5 bands and laser lines)

These figures give the cumulative probability, $P_a(\beta_\lambda)_o$ that the horizontal sea level attenuation loss is equal to or greater than a given value, β_λ for a particular band or laser line (λ). The probability that the attenuation loss is equal to or less than this value is

$$P_a = 1 - P_a\,(\beta_\lambda)_o.$$

The probability, $P_a(\beta_\lambda)_s$ along a slant path of range, L and slant angle ϕ is

$$P_a(\beta_\lambda)_s = P_a(\beta_\lambda)_o$$

where $(\beta_\lambda)_o$ is the equivalent sea level attenuation loss

$$(\beta_\lambda)_o = (\beta_\lambda)_s \times \tilde{\Delta}^{-1}$$

and $\tilde{\Delta}$ is the corresponding slant path correction factor. The joint probability $P_a^{\lambda_1\lambda_2}$, that the attenuation loss is equal to or greater than a given value is

$$P_a^{\lambda_1\lambda_2} = P_a(\beta_{\lambda_1})_o \cdot P_a(\beta_{\lambda_2})_o$$

for a horizontal sea level path and two wavelength intervals λ_1 and λ_2. The corresponding probability for the attenuation loss to be equal to or less than a certain value is

$$P_a^{\lambda_1\lambda_2} = \left[1 - P_a(\beta_{\lambda_1})_o\right]\left[1 - P_a(\beta_{\lambda_2})_o\right]$$

For slant path joint probabilities the equations are

$$P_a^{\lambda_1\lambda_2}(s) = P_a(\beta_{\lambda_1})_s \cdot P_a(\beta_{\lambda_2})_s \equiv P_a(\beta_{\lambda_1})_o \cdot P_a(\beta_{\lambda_2})_o$$

where

$$(\beta_{\lambda_n})_o = (\beta_{\lambda_n})_s \times \tilde{\Delta}^{-1}$$

and n is either λ_1 or λ_2.

- Joint Probability of Cloud Height/Atmospheric Attenuation (Figures A*.6 and A*.7 IR Bands and Laser Lines)

These figures give the joint probability $P_{CH,a}$, that the horizontal sea level attenuation loss $(\beta_\lambda)_{o,CH}$ for a band or laser line will be equal to or greater than a given value for cloud ceiling heights equal to or less than a given altitude. The slant path probability that the attenuation loss along the path is equal to or greater than a given value for a cloud ceiling height equal to or less than a given altitude is

$$P_{CH,a}\,(\beta_\lambda)_{s,CH} = P_{CH,a}\,(\beta_\lambda)_{o,CH}$$

where

$$(\beta_\lambda)_{o,CH} = (\beta_\lambda)_{s,CH} \cdot \tilde{\Lambda}_{s,CH}^{-1}$$

and $\tilde{\Delta}_{s,CH}$ is the slant path correction factor evaluated for a slant range L, and slant angle $\phi = \arcsin\left(\frac{h}{L}\right)$. The conditional probability that the slant path attenuation loss for two wavelengths be equal to or greater than a given dB loss becomes

$$P_{CH,a_s}^{\lambda_1\lambda_2} = P_{CH,a}(\beta_{\lambda_1})_s \cdot P_{CH,a}(\beta_{\lambda_2})_s .$$

The probability that the slant path attenuation loss for two wavelengths be equal to or less than a given dB loss is

$$'P_{CH,a_s}^{\lambda_1\lambda_2} = \left[1 - P_{CH,a}(\beta_{\lambda_1})_s\right] \left[1 - P_{CH,a}(\beta_{\lambda_2})_s\right]$$

The conditional probability that the cloud ceiling height be equal to or greater than a given altitude, and the slant path attenuation for two wavelengths be equal to or less than a given dB loss is

$$''P_{CH,a_s}^{\lambda_1\lambda_2} = \left[1 - P_{CH}(h)\right] \cdot {}'P_{CH,a_s}^{\lambda_1\lambda_2}$$

- <u>HOWLS Application of These Data: Examples</u>

1. Calculate for a 2-color IR passive homing sensor the probability that the cloud ceiling height will be equal to or greater than .33 km altitude along a 3 km slant path where the attenuation loss for both the (3.8 - 4.2)μm band and the (8.0 - 11.5)μm band is less than or equal to 10 dB for winter (Hamburg, Germany, data). From Figure A4.2, the probability for the cloud height to be equal to or greater than .33 km is

$$'P_{CH} = 1 - P_{CH}(1) = 0.92$$

The slant angle, ϕ is

$$\phi = \arcsin\left(\frac{.33}{3}\right) = 6^{o}$$

The slant path correction factor $\tilde{\Delta}_{geom}$ for a slant range of 3 km and 6^{o} slant angle is (Figure 4)

$$\tilde{\Delta}_{geom} = 0.8$$

The equivalent horizontal sea level attenuation loss for the (3.8 - 4.2)μm and (8.0 - 11.5)μm bands are

$$(\beta_{3.5})_o = (\beta_{8.0})_o = (3.3) / .8 \cong 4 \text{ dB/km.}$$

The corresponding probabilities that the attenuation loss will be equal to or greater than 4 dB/km for cloud ceiling heights equal to or below .33 km (Figure A4.6) are

(3.8-4.2)μm band

$$P_{CH,a}\,(.33_{3.8})_{o,1} = .07$$

(8.0-11.5)μm band

$$P_{CH,a}\,(.33_{8.0})_{o,1} = .05$$

The conditional probability that the cloud ceiling height be equal to or greater than .33 km, and the 3 km slant path attenuation for the two wavelengths be equal to or less than 10 dB loss is

$$''P_{CH,a_s}^{\lambda_1\lambda_2} = [.92][1 - .07][1 - .05] \cong .81$$

i.e., about 80 percent of the time this conditional probability will occur.

2. Calculate for the IR Countermortar System the joint probability as a function of slant angles (1^o, 2^o, 3^o) that the cloud ceiling will be equal to or greater than the terminal altitude for the slant range of 5 km and a transmittance equal to or less than 12 dB in attenuation losses for the (8.0-11.5)μm band in winter (Hamburg, Germany, data). Using the same procedure as in the previous example, the results of this problem are given in Table 5. It is seen in this case, that the system will work about 40 percent of the time in winter for a slant stare-angle of 3^o, and that the systems utility is increased to about 60 percent of the time for a stare-angle of 1^o.

TABLE 5

RESULTS OF A JOINT PROBABILITY PROBLEM

CASE I
RADIATION: (8.0-11.5)μm Band
ATTENUATION LOSS: 12 db Winter (Hamburg, Germany)
SLANT RANGE: 5km

Slant Angle (°)	Cloud Height (km)	γ_{GEOM}	$(\beta_{8.0})_s \frac{db}{km}$	$(\beta_{8.0})_o \frac{db}{km}$	$P_{CH}(H)$	$P_{CH,a}(\beta_{8.0})_{o,CH}$
1.0	.087	.94	2.4	2.55	.1	.32
2.0	.174	.93	2.4	2.58	.25	.30
3.0	.262	.92	2.4	2.60	.40	.28

JOINT PROBABILITIES FOR CASE I

Slant ∢ (°)	$1-P_{CH} \cdot 1-P_{CH,a}(\beta_{8.0})_{o,CH}$
1.0	.61
2.0	.53
3.0	.43

APPENDIX

The appendix contains the detailed results for each of the stations used in this work. Seven sets of plots (where data were available) are given for each location, as follows:

- Probability of Synoptic Weather (for each season)
- Probability of Cloud Ceiling Height
- Probability of Photopic Visibilities
- Probability of Atmospheric Attenuation for IR Bands (for each of 8.0-11.5, 3.8-4.2, and 1.0-1.2μm bands)
- Probability of Atmospheric Attenuation for IR Lines (for each of 10.6, 4.73, 3.8, and 1.06μm laser lines)
- Joint Probability of Cloud Heights and Atmospheric Attenuation for IR Bands (for each of three bands and altitudes of 0.33, 0.5, 1.0, and 2.0 km)
- Joint Probability of Cloud Height and Atmospheric Attenuation for IR Lines (for each four lines and four altitudes)

Probability curves are given for each of the nine stations listed below.

Berlin, Germany	(52^o-28'N, 13^o-24'E)
Dresden, E. Germany	(51^o-08'N, 13^o-46'E)
Essen, Germany	(51^o-24'N, 6^o-58'E)
Hamburg, Germany	(53^o-38'N, 9^o-59'E)
Cairo, Egypt	(30^o-8'N, 31^o-34'E)
Nicosia, Cyprus	(35^o-9'N, 33^o-17'E)
Hue, S. Vietnam	(16^o-24'N, 107^o-51'E)

Hanoi, N. Vietnam (21^{o}-1'N, 105^{o}-51'E)

Falmouth, Mass. USA (41^{o}-39'N, 70^{o}-31'W)

Table A-1 indicates the figure number which presents each of these sets of data.

Table A-2 gives seasonal cloud free line-of-sight statistics as a function of viewing angle and line-of-sight path above ground for the same geographic area.

TABLE A-1

FIGURES IN APPENDIX PRESENTING STATISTICAL

WEATHER AND ATMOSPHERIC ATTENUATION

	Berlin	Dresden	Essen	Hamburg	Cairo	Nicosia	Hue	Hanoi	Falmouth
Prob. Synoptic Weather	----	A2.1	A3.1	A4.1	A5.1	A6.1	A7.1	A8.1	----
Prob. Cloud Ceiling	A1.2	----	A3.2	A4.2	A5.2	A6.2	A7.2	----	A9.2
Prob. Photopic Visibility	A1.3	A2.3	A3.3	A4.3	A5.3	A6.3	A7.3	A8.3	A9.3
Prob. Atmo. Atten. IR Bands	A1.4	A2.4	A3.4	A4.4	A5.4	A6.4	A7.4	A8.4	A9.4
Prob. Atmo. Atten. IR Laser Lines	A1.5	A2.5	A3.5	A4.5	A5.5	A6.5	A7.5	A8.5	A9.5
Joint Prob. Cloud/Atmo. Atten. IR Bands	A1.6	****	A3.6	A4.6	****	A6.6	****	****	A9.6
Joint Prob. Cloud/Atmo. Atten. IR Laser Lines	A1.7	****	A3.7	A4.7	****	A6.7	****	****	A9.7

**** Joint meterorological data not available

---- Meteorological data not available

TABLE A-2

GLOBAL CLOUD FREE LINE-OF-SIGHT STATISTICS

BERLIN, GERMANY
DAYTIME HOURS- 600 TO 1800 LST
FROM 1946 3 31 TO 1947 5 23

CLOUD BASE HEIGHT 0.333

ANG(DEG)	1.0	2.0	3.0	5.0	15.0	45.0	90.0
FREQ							
UNTR	762	763	763	765	774	784	806
SPRG	893	894	895	896	904	[illegible]	933
SUMR	885	885	886	887	896	913	927
FALL	702	702	753	[illegible]	716	737	758

CLOUD BASE HEIGHT 0.500

ANG(DEG)	1.0	2.0	3.0	5.0	15.0	45.0	90.0
FREQ							
UNTR	672	673	674	676	686	709	724
SPRG	858	860	861	862	871	888	903
SUMR	847	848	849	850	859	870	891
FALL	668	670	671	673	686	711	726

CLOUD BASE HEIGHT 1.000

ANG(DEG)	1.0	2.0	3.0	5.0	15.0	45.0	90.0
FREQ							
UNTR	513	514	516	518	536	558	575
SPRG	706	708	709	712	723	757	773
SUMR	716	717	719	722	738	767	783
FALL	543	545	547	553	572	600	627

CLOUD BASE HEIGHT 2.000

ANG(DEG)	1.0	2.0	3.0	5.0	15.0	45.0	90.0
FREQ							
UNTR	428	429	431	434	449	480	498
SPRG	564	567	570	575	601	647	668
SUMR	581	584	587	593	620	647	686
FALL	458	461	464	470	486	543	563

ESSEN, GERMANY
DAYTIME HOURS- 600 TO 1800 LST
FROM 1949 1 1 TO 1962 6 4

CLOUD BASE HEIGHT 0.333

ANG(DEG)	1.0	2.0	3.0	5.0	15.0	45.0	90.0
FREQ							
UNTR	647	648	650	652	663	686	701
SPRG	775	775	776	778	787	806	822
SUMR	869	870	871	872	881	899	913
FALL	739	740	741	742	753	776	790

CLOUD BASE HEIGHT 0.500

ANG(DEG)	1.0	2.0	3.0	5.0	15.0	45.0	90.0
FREQ							
UNTR	484	485	486	488	503	532	549
SPRG	704	705	706	708	720	743	758
SUMR	813	814	815	817	828	849	863
FALL	654	655	[illegible]	658	671	695	711

CLOUD BASE HEIGHT 1.000

ANG(DEG)	1.0	2.0	3.0	5.0	15.0	45.0	90.0
FREQ							
UNTR	267	270	272	277	301	345	365
SPRG	435	438	441	448	478	529	549
SUMR	545	548	552	558	591	643	663
FALL	408	411	414	419	446	491	511

CLOUD BASE HEIGHT 2.000

ANG(DEG)	1.0	2.0	3.0	5.0	15.0	45.0	90.0
FREQ							
UNTR	178	181	184	190	218	268	290
SPRG	296	301	306	318	367	423	447
SUMR	377	[illegible]	[illegible]	[illegible]	443	515	536
FALL	244	248	[illegible]	[illegible]	296	364	378

HAMBURG, GERMANY
DAYTIME HOURS- 600 TO 1800 LST
FROM 1949 1 1 TO 1950 2 21

CLOUD BASE HEIGHT 0.333

ANG(DEG)	1.0	2.0	3.0	5.0	15.0	45.0	90.0
FREQ							
UNTR	625	626	627	628	640	663	679
SPRG	753	754	755	757	767	789	803
SUMR	798	798	799	801	818	834	848
FALL	750	751	[illegible]	753	761	776	793

CLOUD BASE HEIGHT 0.500

ANG(DEG)	1.0	2.0	3.0	5.0	15.0	45.0	90.0
FREQ							
UNTR	536	537	538	541	555	583	599
SPRG	685	687	688	690	704	720	[illegible]
SUMR	767	768	769	772	784	[illegible]	[illegible]
FALL	672	673	674	676	687	710	[illegible]

CLOUD BASE HEIGHT 1.000

ANG(DEG)	1.0	2.0	3.0	5.0	15.0	45.0	90.0
FREQ							
UNTR	353	355	358	363	385	427	447
SPRG	508	511	514	518	546	[illegible]	[illegible]
SUMR	544	547	551	558	591	643	[illegible]
FALL	513	515	518	522	544	583	[illegible]

CLOUD BASE HEIGHT 2.000

ANG(DEG)	1.0	2.0	3.0	5.0	15.0	45.0	90.0
FREQ							
UNTR	274	277	279	[illegible]	310	357	370
SPRG	456	459	[illegible]	[illegible]	[illegible]	[illegible]	[illegible]
SUMR	487	491	[illegible]	[illegible]	[illegible]	[illegible]	[illegible]
FALL	416	418	421	[illegible]	[illegible]	[illegible]	[illegible]

FALMOUTH MA USA
DAYTIME HOURS- 600 TO 1800 LST
FROM 1961 1 1 TO 1968 8 21

CLOUD BASE HEIGHT 0.333

ANG(DEG)	1.0	2.0	3.0	5.0	15.0	45.0	90.0
FREQ							
UNTR	793	794	794	795	804	828	836
SPRG	781	782	783	784	[illegible]	753	[illegible]
SUMR	696	697	698	700	718	737	754
FALL	702	702	703	706	711	735	756

CLOUD BASE HEIGHT 0.500

ANG(DEG)	1.0	2.0	3.0	5.0	15.0	45.0	90.0
FREQ							
UNTR	760	761	762	763	772	792	[illegible]
SPRG	704	705	706	707	718	737	752
SUMR	682	684	685	687	700	726	742
FALL	654	655	656	658	668	691	706

CLOUD BASE HEIGHT 1.000

ANG(DEG)	1.0	2.0	3.0	5.0	15.0	45.0	90.0
FREQ							
UNTR	694	695	696	698	710	738	750
SPRG	627	628	629	632	643	668	[illegible]
SUMR	653	654	655	658	673	701	717
FALL	613	614	615	617	626	654	[illegible]

CLOUD BASE HEIGHT 2.000

ANG(DEG)	1.0	2.0	3.0	5.0	15.0	45.0	90.0
FREQ							
UNTR	640	641	[illegible]	[illegible]	[illegible]	[illegible]	701
SPRG	[illegible]	[illegible]	[illegible]	[illegible]	[illegible]	[illegible]	[illegible]
SUMR	[illegible]	[illegible]	[illegible]	[illegible]	[illegible]	[illegible]	[illegible]
FALL	670	670	673	676	[illegible]	[illegible]	[illegible]

NICOSIA
DAYTIME HOURS- 600 TO 1800 LST
FROM 1964 1 1 TO 1969 11 21

CLOUD BASE HEIGHT 0.333

ANG(DEG)	1.0	2.0	3.0	5.0	15.0	45.0	90.0
FREQ							
UNTR	[illegible]	[illegible]	[illegible]	[illegible]	[illegible]	[illegible]	[illegible]
SPRG	[illegible]	[illegible]	[illegible]	[illegible]	[illegible]	[illegible]	[illegible]
SUMR	[illegible]	[illegible]	[illegible]	[illegible]	[illegible]	[illegible]	[illegible]
FALL	[illegible]	[illegible]	[illegible]	[illegible]	[illegible]	[illegible]	[illegible]

CLOUD BASE HEIGHT 0.500

ANG(DEG)	1.0	2.0	3.0	5.0	15.0	45.0	90.0
FREQ							
UNTR	[illegible]	[illegible]	[illegible]	[illegible]	[illegible]	[illegible]	[illegible]
SPRG	[illegible]	[illegible]	[illegible]	[illegible]	[illegible]	[illegible]	[illegible]
SUMR	[illegible]	[illegible]	[illegible]	[illegible]	[illegible]	[illegible]	[illegible]
FALL	[illegible]	[illegible]	[illegible]	[illegible]	[illegible]	[illegible]	[illegible]

CLOUD BASE HEIGHT 1.000

ANG(DEG)	1.0	2.0	3.0	5.0	15.0	45.0	90.0
FREQ							
UNTR	[illegible]	[illegible]	[illegible]	[illegible]	[illegible]	[illegible]	[illegible]
SPRG	[illegible]	[illegible]	[illegible]	[illegible]	[illegible]	[illegible]	[illegible]
SUMR	[illegible]	[illegible]	[illegible]	[illegible]	[illegible]	[illegible]	[illegible]
FALL	[illegible]	[illegible]	[illegible]	[illegible]	[illegible]	[illegible]	[illegible]

CLOUD BASE HEIGHT 2.000

ANG(DEG)	1.0	2.0	3.0	5.0	15.0	45.0	90.0
FREQ							
UNTR	[illegible]	[illegible]	[illegible]	[illegible]	[illegible]	[illegible]	[illegible]
SPRG	[illegible]	[illegible]	[illegible]	[illegible]	[illegible]	[illegible]	[illegible]
SUMR	[illegible]	[illegible]	[illegible]	[illegible]	[illegible]	[illegible]	[illegible]
FALL	[illegible]	[illegible]	[illegible]	[illegible]	[illegible]	[illegible]	[illegible]

HUE, S. VIETNAM
DAYTIME HOURS- 600 TO 1800 LST
FROM 1960 1 1 TO 1968 8 21

CLOUD BASE HEIGHT 0.333

ANG(DEG)	1.0	2.0	3.0	5.0	15.0	45.0	90.0
FREQ							
UNTR	743	744	745	746	755	774	759
SPRG	[illegible]	[illegible]	[illegible]	[illegible]	[illegible]	[illegible]	[illegible]
SUMR	[illegible]	[illegible]	[illegible]	[illegible]	[illegible]	[illegible]	[illegible]
FALL	[illegible]	[illegible]	[illegible]	[illegible]	[illegible]	[illegible]	[illegible]

CLOUD BASE HEIGHT 0.500

ANG(DEG)	1.0	2.0	3.0	5.0	15.0	45.0	90.0
FREQ							
UNTR	[illegible]	[illegible]	[illegible]	[illegible]	[illegible]	[illegible]	[illegible]
SPRG	[illegible]	[illegible]	[illegible]	[illegible]	[illegible]	[illegible]	[illegible]
SUMR	[illegible]	[illegible]	[illegible]	[illegible]	[illegible]	[illegible]	[illegible]
FALL	[illegible]	[illegible]	[illegible]	[illegible]	[illegible]	[illegible]	[illegible]

CLOUD BASE HEIGHT 1.000

ANG(DEG)	1.0	2.0	3.0	5.0	15.0	45.0	90.0
FREQ							
UNTR	[illegible]	[illegible]	[illegible]	[illegible]	[illegible]	[illegible]	[illegible]
SPRG	[illegible]	[illegible]	[illegible]	[illegible]	[illegible]	[illegible]	[illegible]
SUMR	[illegible]	[illegible]	[illegible]	[illegible]	[illegible]	[illegible]	[illegible]
FALL	[illegible]	[illegible]	[illegible]	[illegible]	[illegible]	[illegible]	[illegible]

CLOUD BASE HEIGHT 2.000

ANG(DEG)	1.0	2.0	3.0	5.0	15.0	45.0	90.0
FREQ							
UNTR	[illegible]	[illegible]	[illegible]	[illegible]	[illegible]	[illegible]	[illegible]
SPRG	[illegible]	[illegible]	[illegible]	[illegible]	[illegible]	[illegible]	[illegible]
SUMR	[illegible]	[illegible]	[illegible]	[illegible]	[illegible]	[illegible]	[illegible]
FALL	[illegible]	[illegible]	[illegible]	[illegible]	[illegible]	[illegible]	[illegible]

REFERENCES

1. E. Rodriguez and R. Huschke, "The RAND Weather Data Bank (RAWDAB): An Evolving Base of Accessible Weather Data," RAND Report R-1269-PR (March 1974).

2. J. Selby and R. McClatchey, "Atmospheric Transmittance from 0.25 to 28.6μm: Computer Code LOWTRAN 2," Air Force Cambridge Research Laboratories Report AFCRL-72-0745 (29 December 1972).

3. "AWS Data Families 12-13: Electronic Data Processing Reference Manual (Synoptic Observation, Chapter 3, The Obsersation)," Vols. I and II (September 1960).

4. L. Biberman and G. duMais, "Modeling the Effects of Weather on 8.5-11 Micrometer FLIR Performance: An Analysis Using Real Data," IDA Technical Report (1975).

5. H. Barhydt, "Sea Level Atmospheric Transmission in the 8-11.5 μ Band," Interdepartmental Correspondence, Hughes Aircraft Company (May 1974).

6. J. McCoy, D. Rensch and R. Long, "Water Vapor Continuum Absorption of Carbon Dioxide Laser Radiation Near 10 μ," Appl. Opt. 7, 1471 (1969).

7. R. McClatchey and J. Selby, "Atmospheric Attenuation of Laser Radiation from 0.76 to 31.25 μm," Air Force Cambridge Research Laboratories Report AFCRL-TR-74-0003 (3 January 1974).

8. R. G. Eldridge, Bull. Am. Meteorol. Soc. 50, 422 (1969).

9. E. O. Hulbert, J. Opt. Soc. Am. 31, 467 (1941).

10. D. B. Rensch and R. K. Long, "Comparative Studies of Extinction and Backscattering by Aerosols, Fog, and Rain at 10.6 μ and 0.63 μ," Appl. Opt. 9 1563 (197[illegible]).

11. J. Rosen and C. Schutz, "The Effectiveness of a New Air Defense Weapon in Cloudy Weather: Methodology and Applications," RAND Report R-1256-ARPA (December 1973).

12. Y. Lubkin, An Introduction to Correlation, (Federal Scientified Corporation, New York, 1 May 1973).

18-5-6371

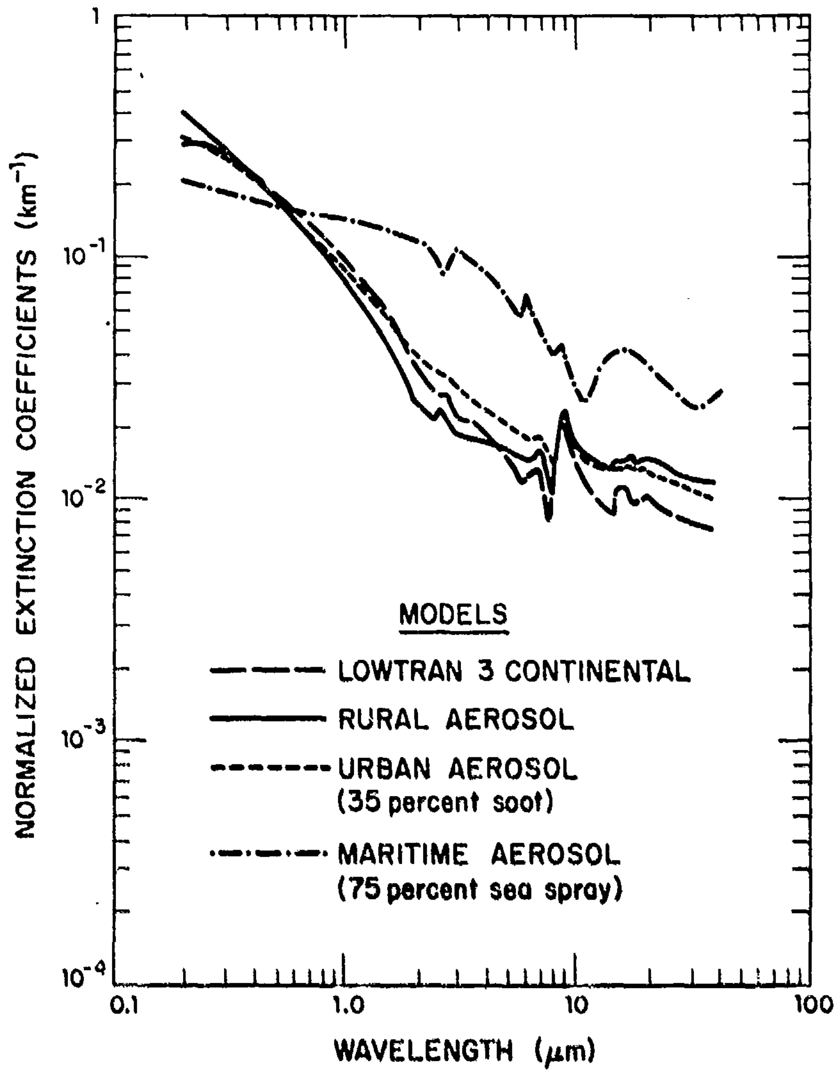

Fig. 1. Aerosol normalized extinction coefficients.

TT-7 (2)

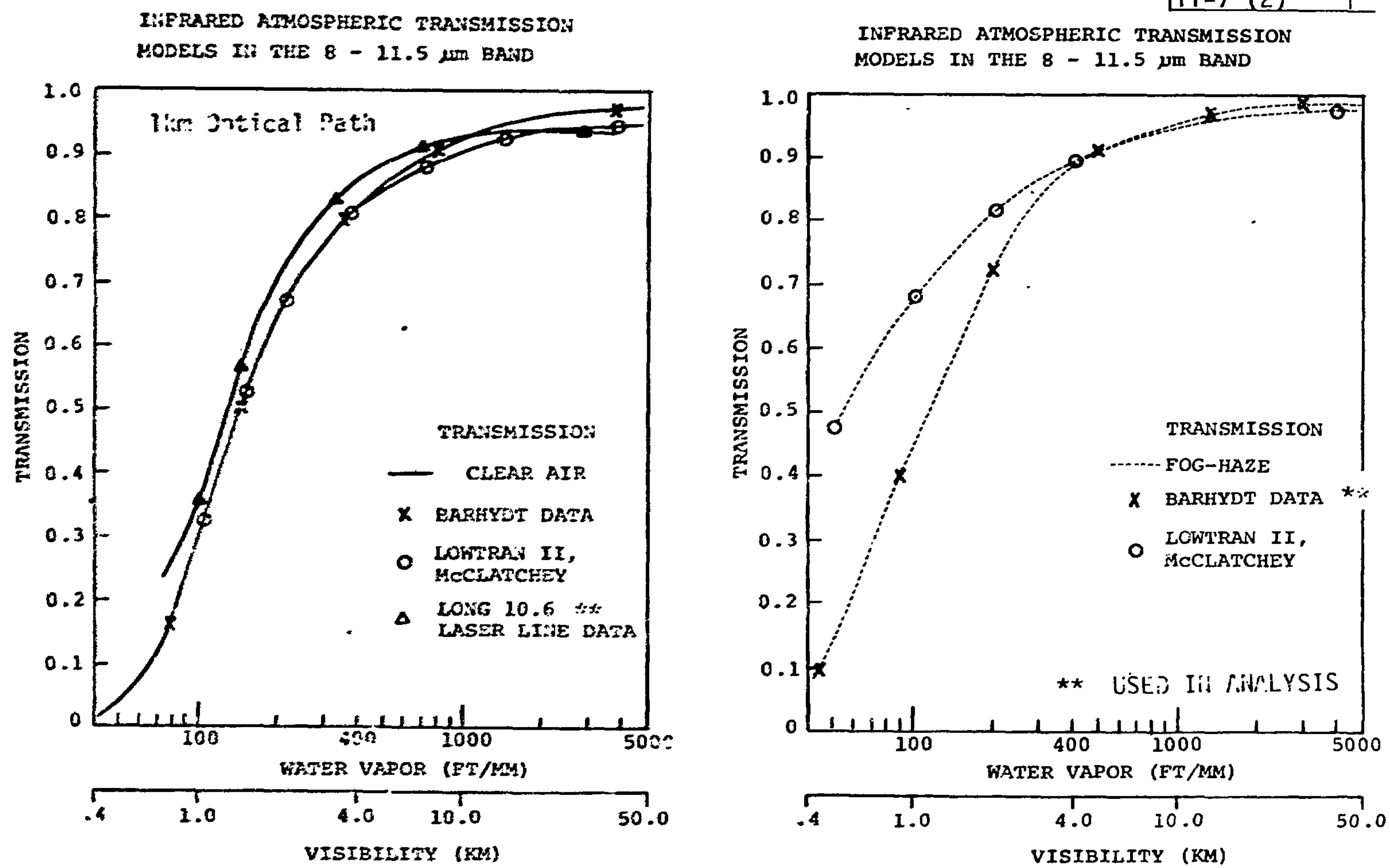

Fig. 2. Comparison of atmospheric attenuation models for clear-air and fog-haze transmission in the 8-11.5µm IR band.

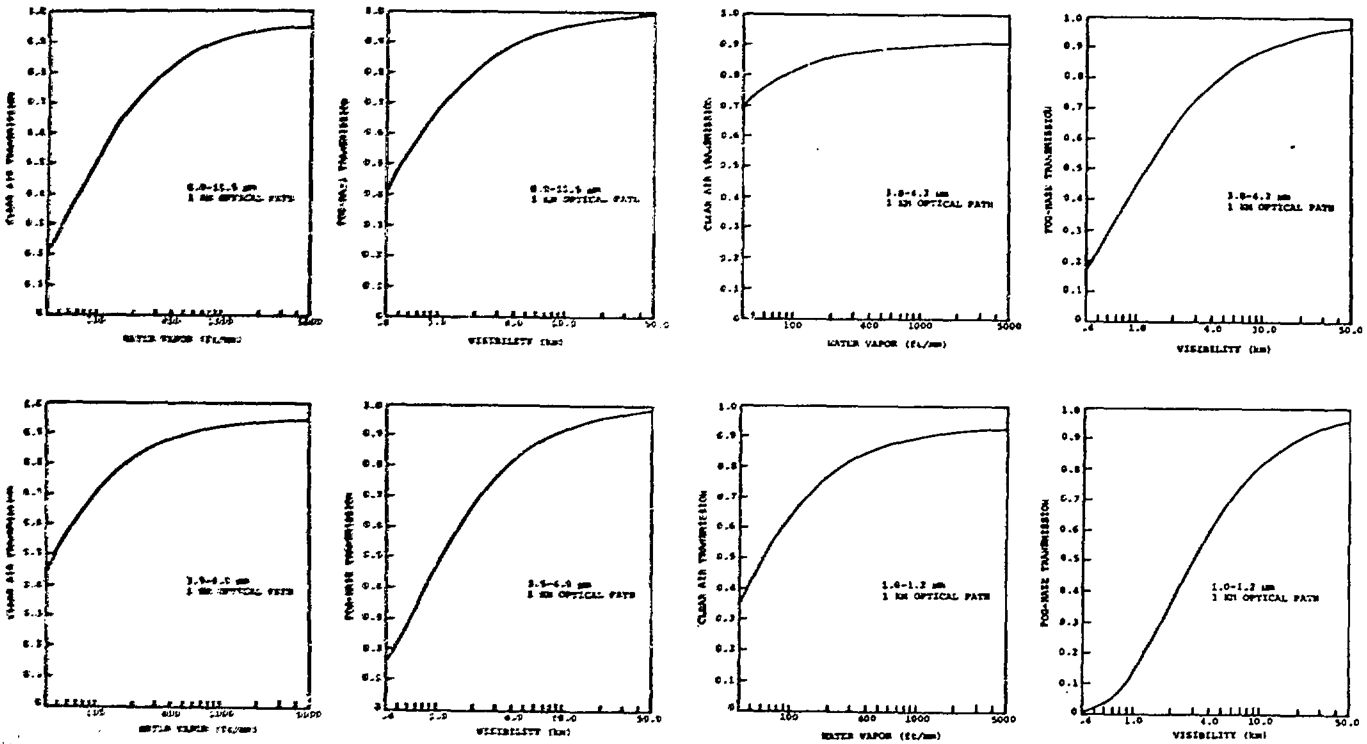

Fig. 3. LOWTRAN clear-air and rural fog-haze transmission curves for several atmospheric windows in the 1.0-14.0μm IR spectral band.

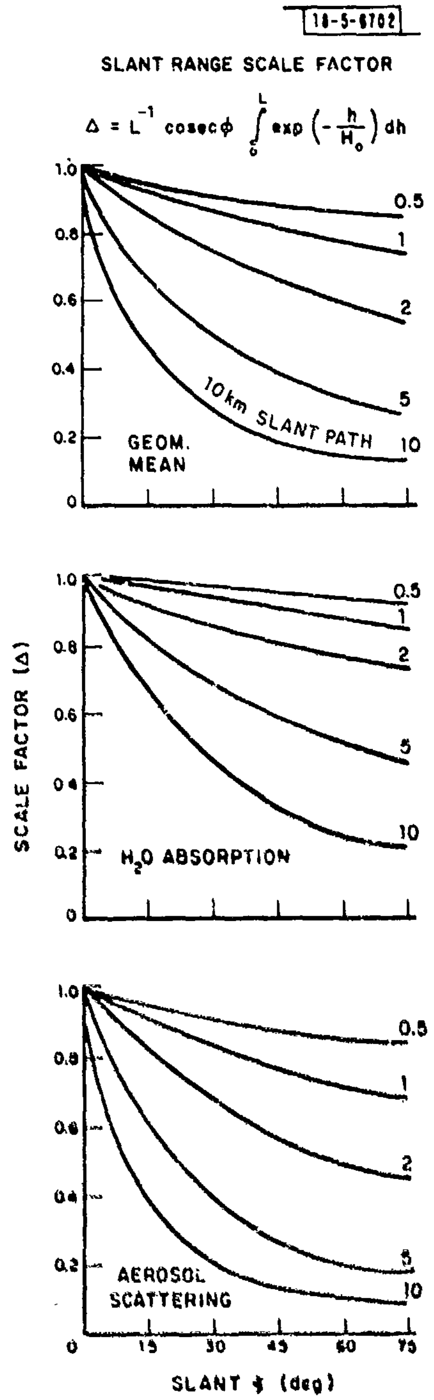

Fig. 4. Slant path correction factors for horizontal atmospheric attenuation losses.

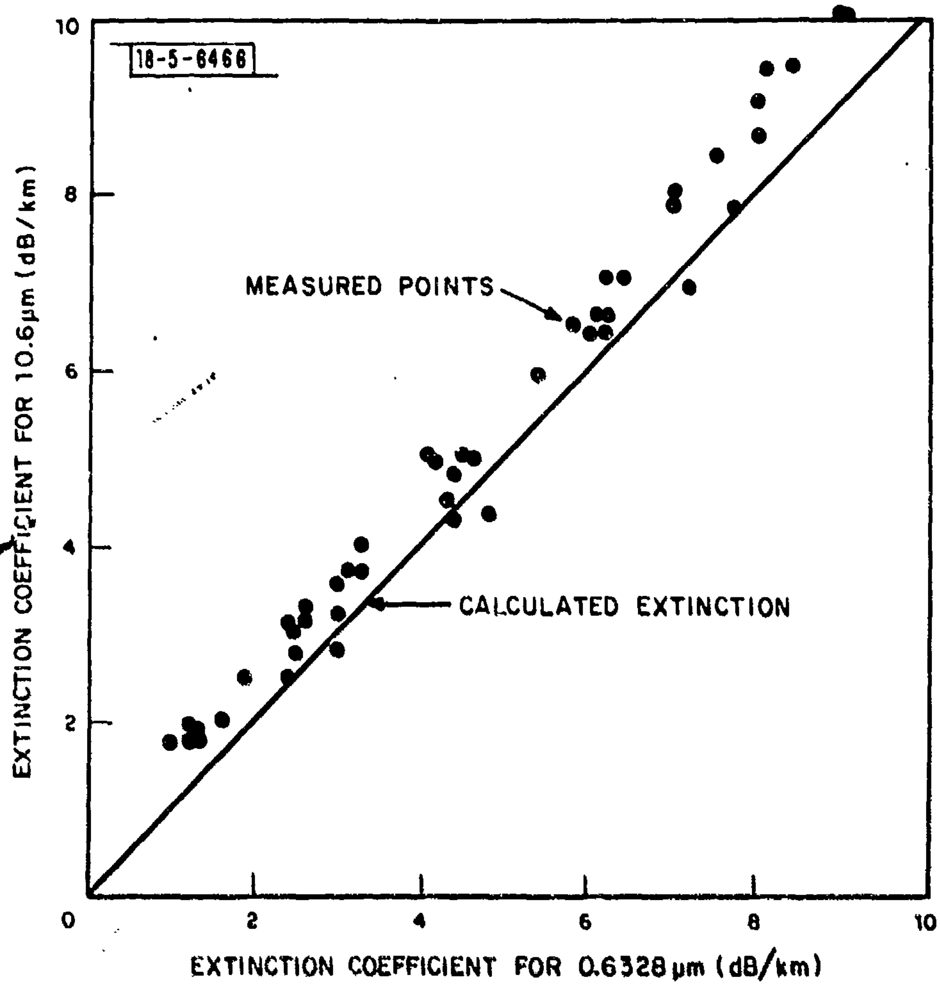

Fig. 5. Experimental and theoretical IR extinction coefficients through rain.

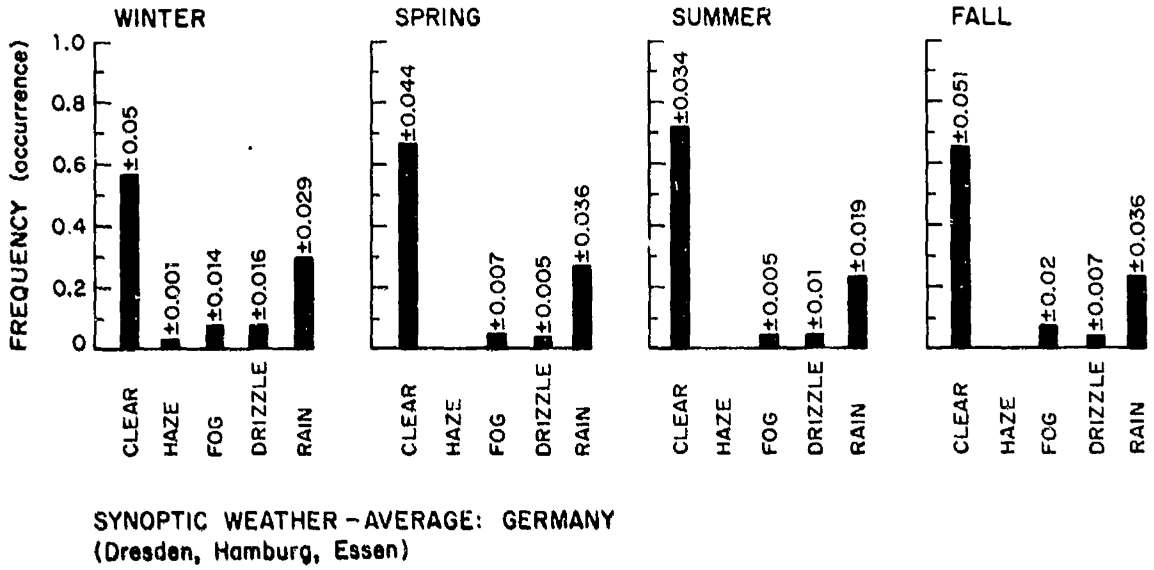

Fig. 6. Synoptic weather averages for Germany.

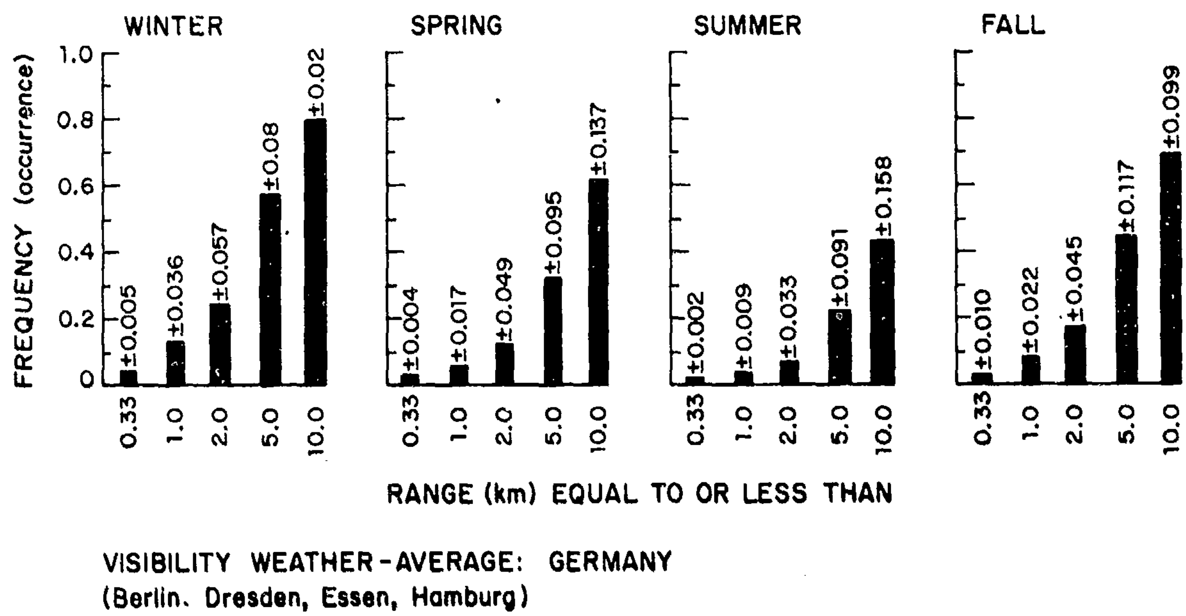

Fig. 7. Average meteorological visibilities for Germany.

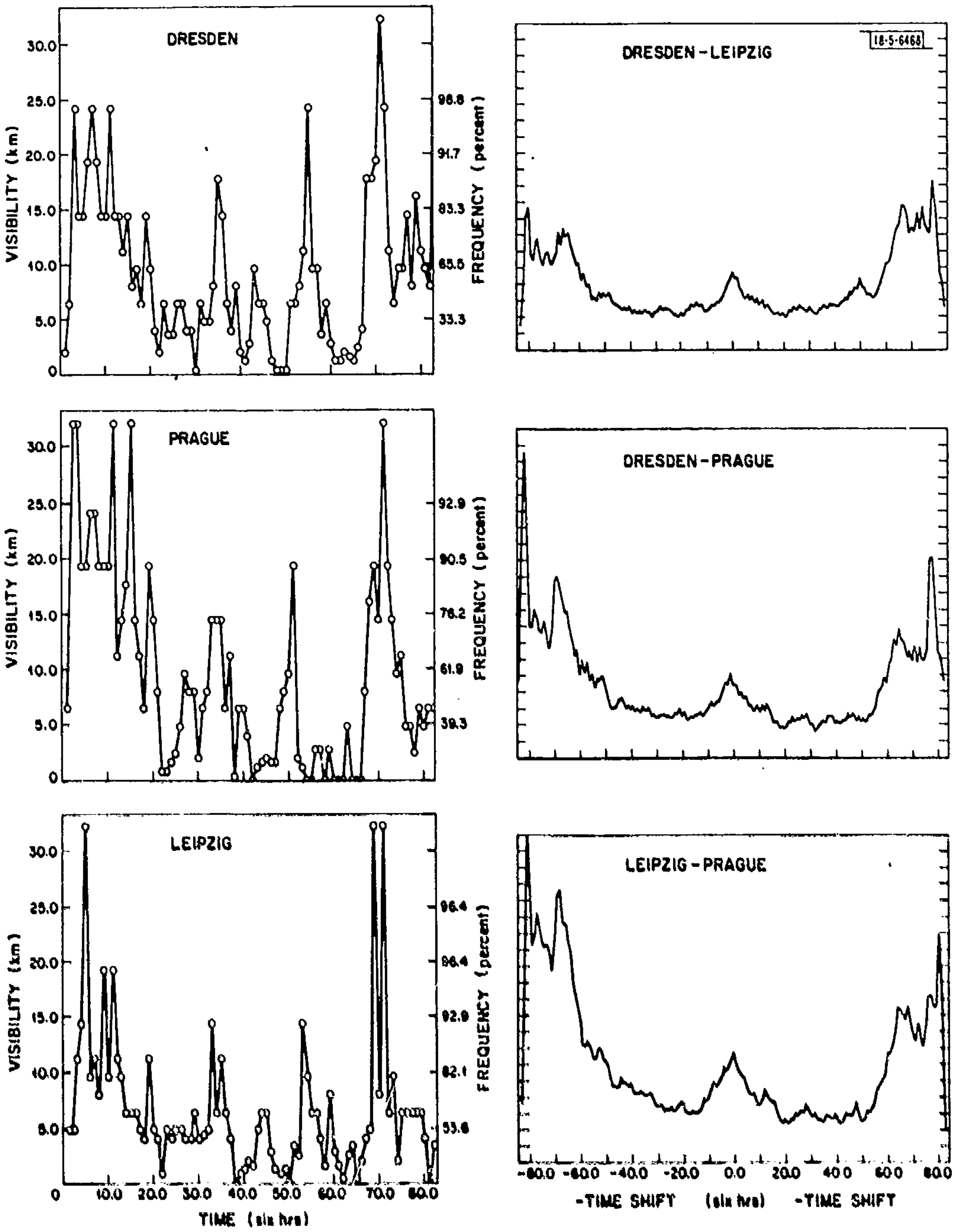

Fig. 8. Short-term visibility and cross-correlation for three European cities.

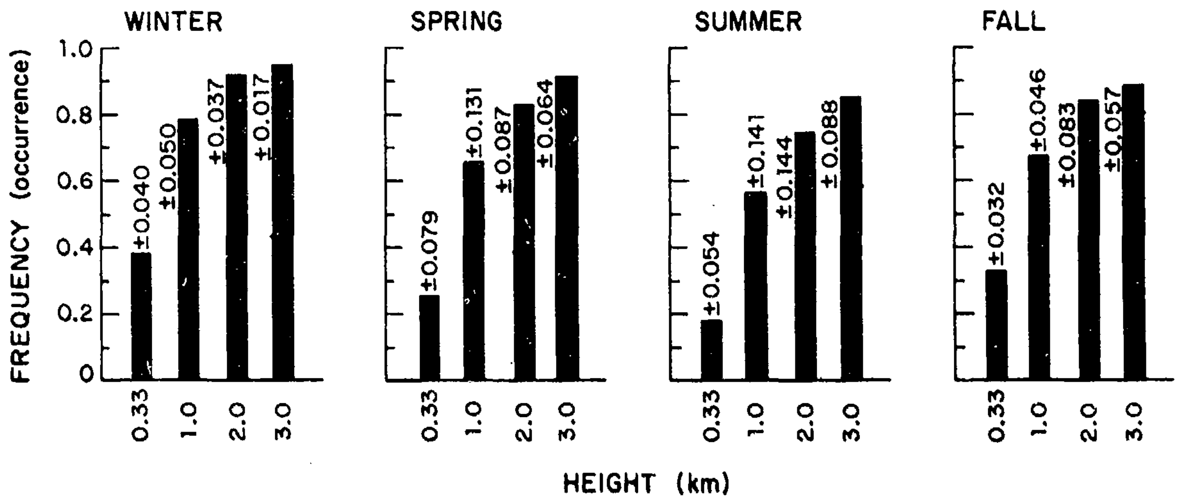

CLOUD CEILING AVERAGE: GERMANY
(Berlin, Essen, Hamburg)

Fig. 9. Cloud ceiling height averages for Germany.

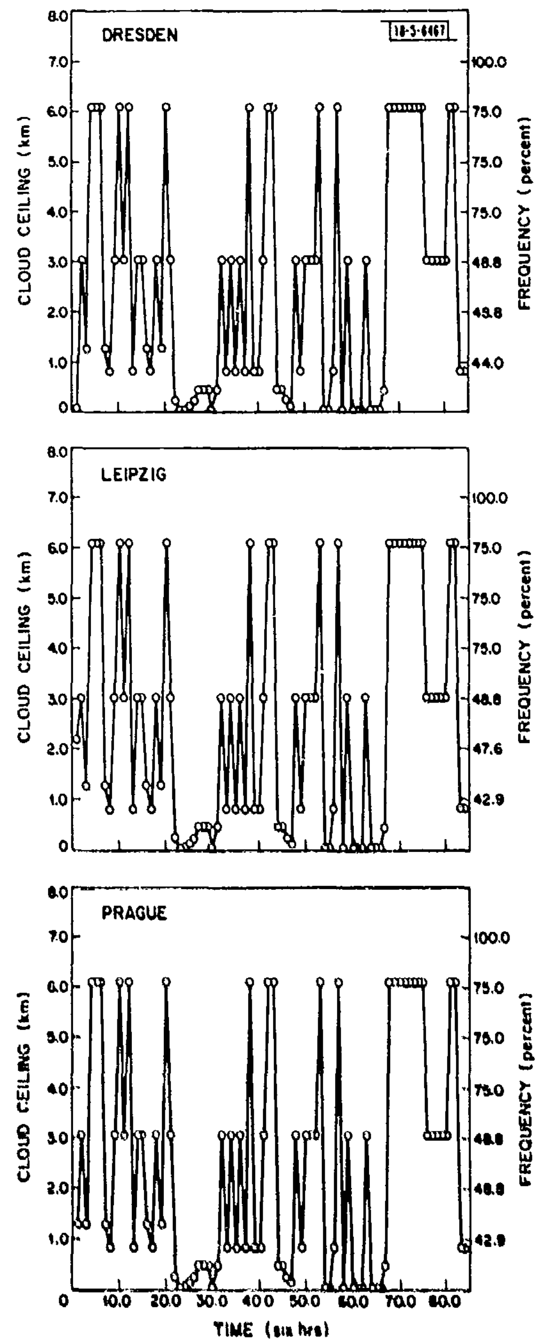

Fig. 10. Short-term variability of cloud ceiling height for three European cities.

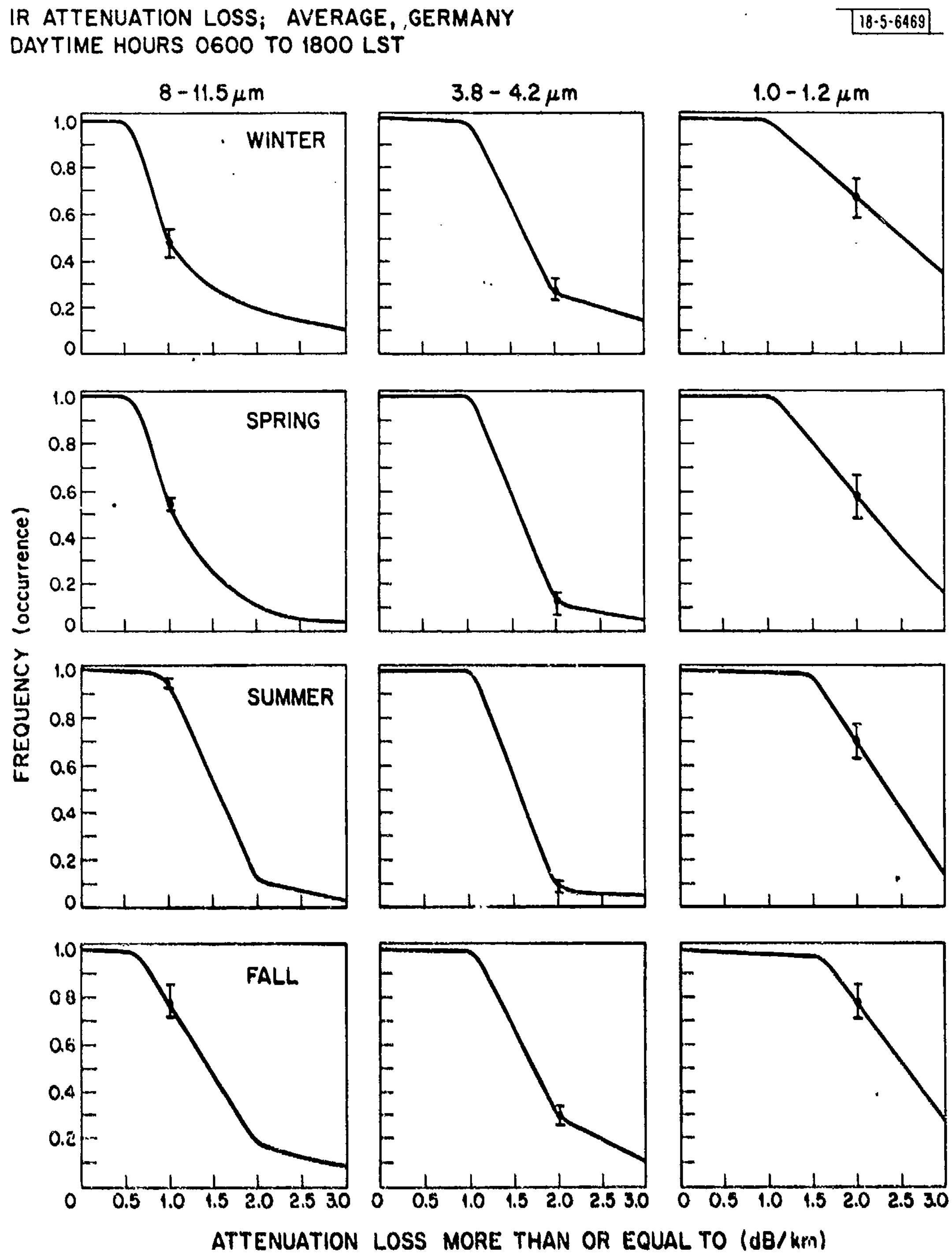

Fig. 11. German average IR attenuation losses for the (1.0-1.2), (3.8-4.2), and (8.0-11.5)μm wavelength bands.

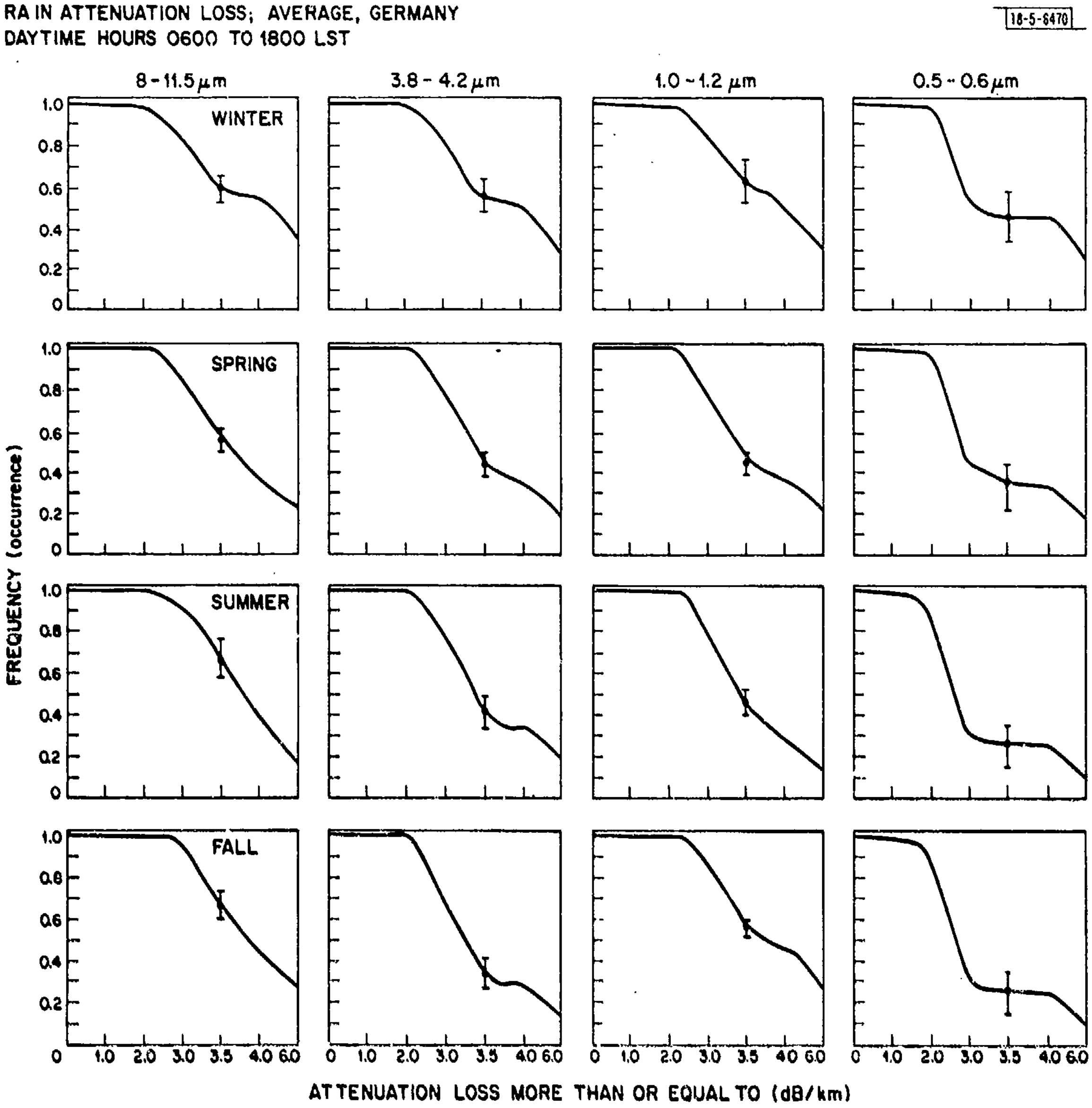

Fig. 12. Average rain attenuation losses in Germany.

18-5-6367

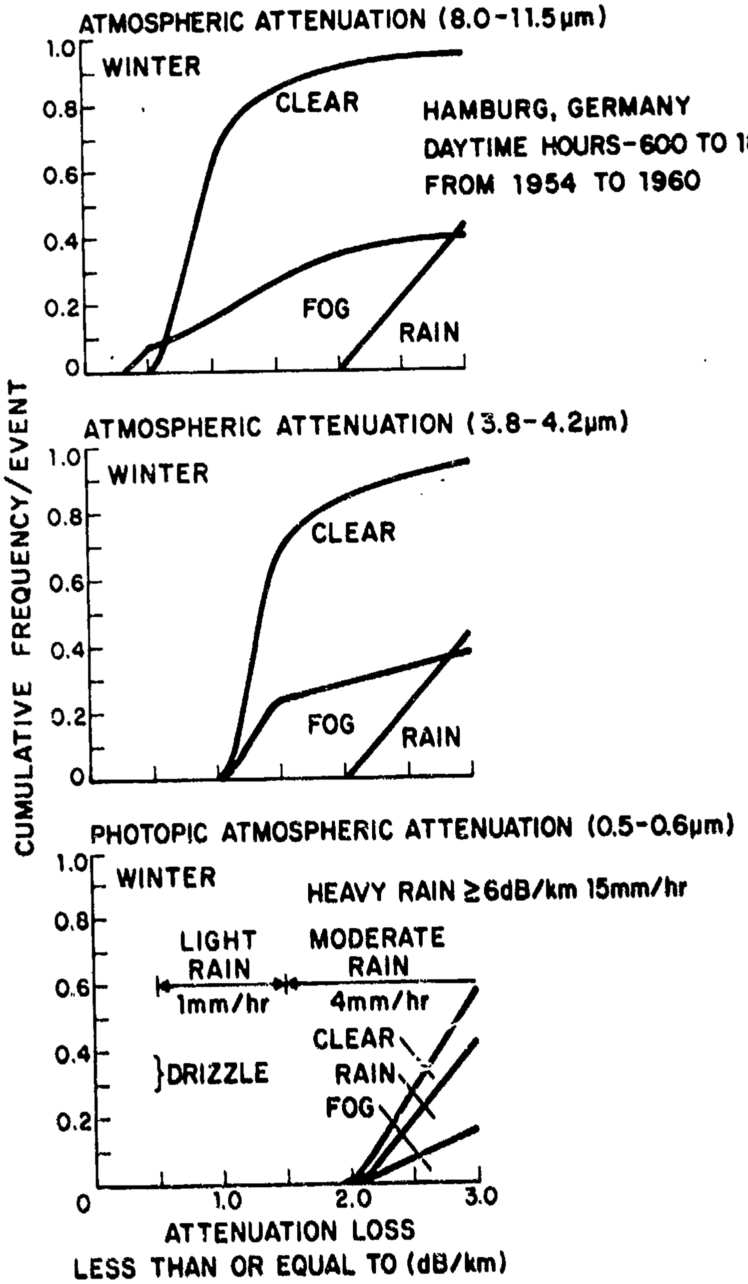

Fig. 13. Comparison of atmospheric attenuation losses for clear weather, fog-haze and rain during winter for Hamburg, Germany.

Meterorological data not available.

Fig. A 1.1 Probability of Synoptic Weather

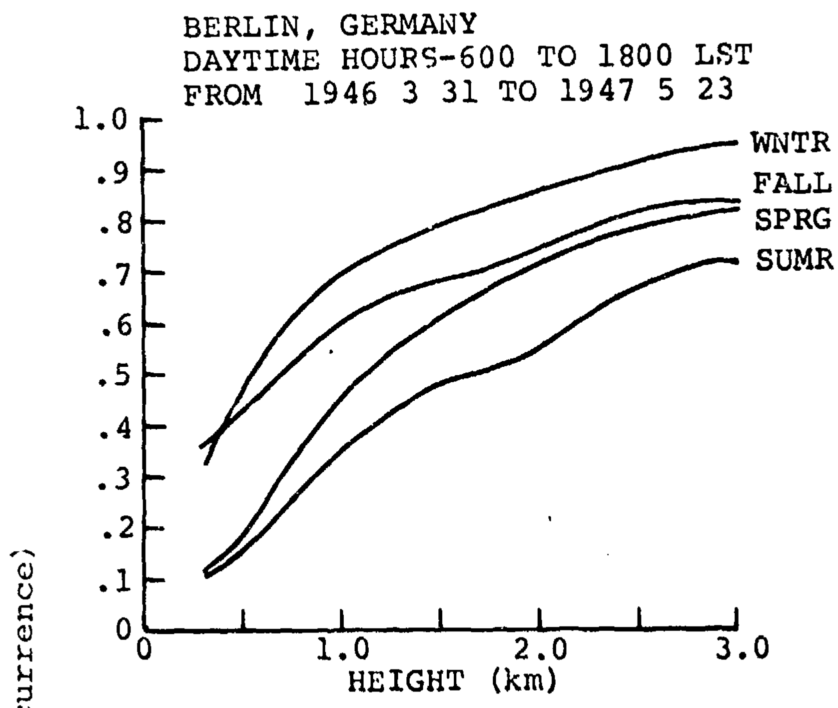

Fig. A 1.2 Probability of Cloud Ceiling Height

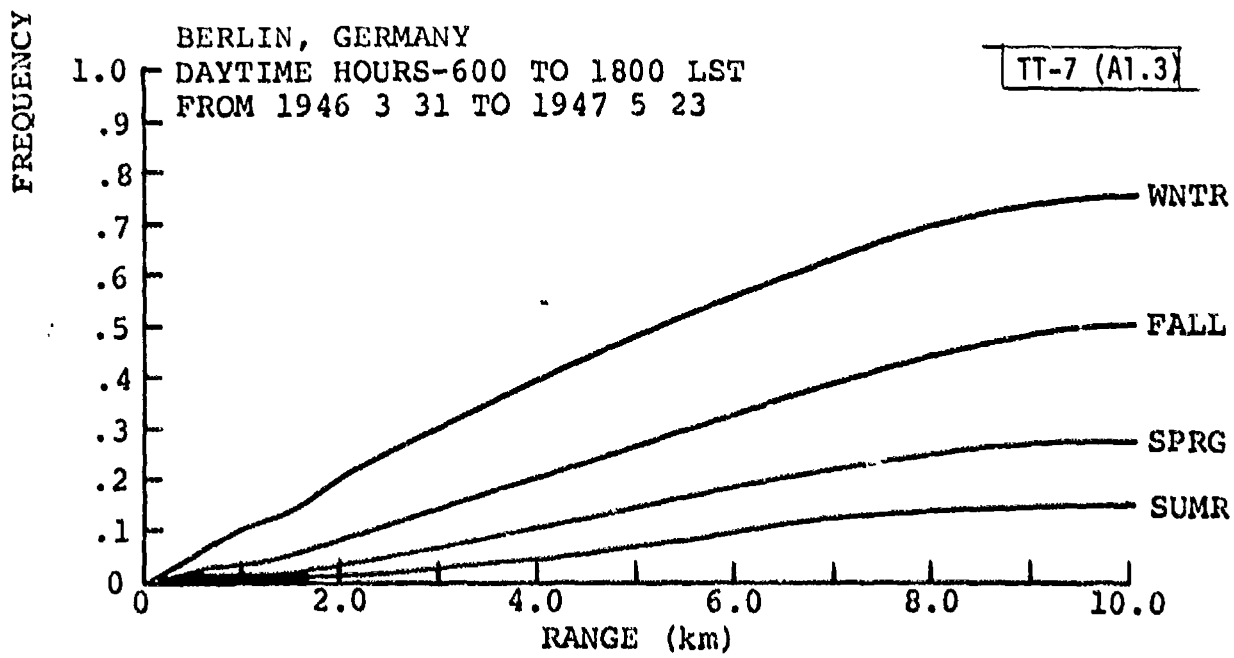

Fig. A 1.3 Probability of Photopic Visibilities

TT-7 (A1.4)

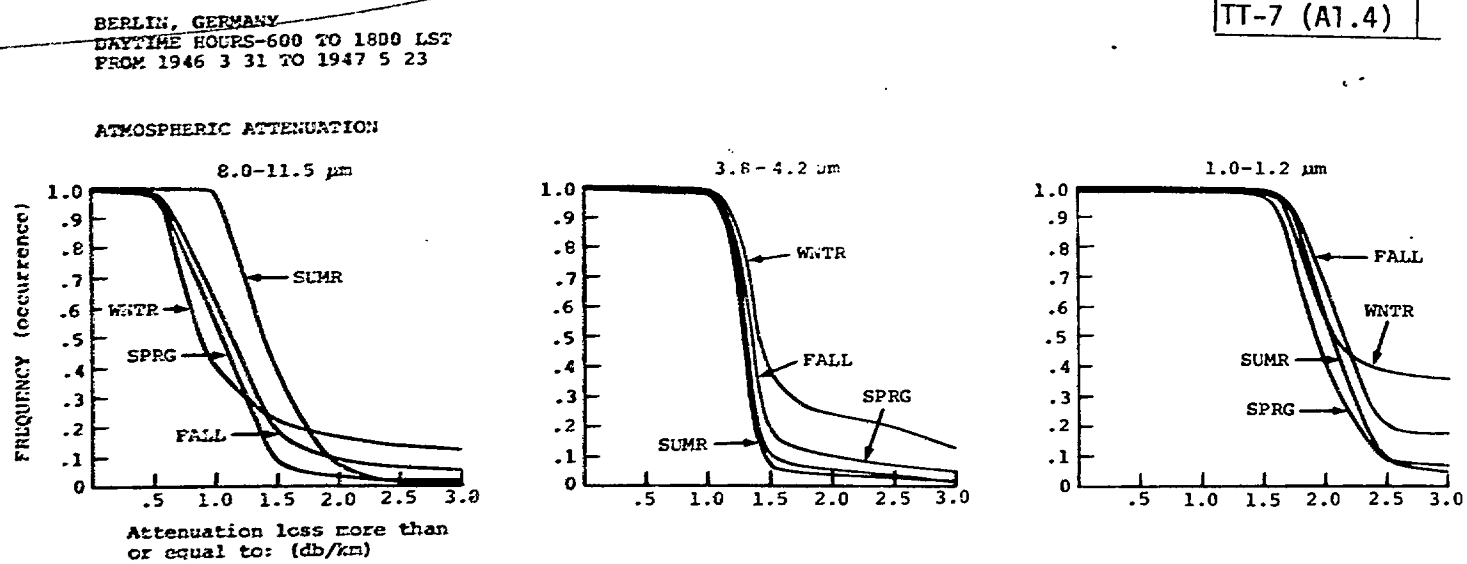

Fig. A 1.4 Probability of Clear Air/Fog-Haze Atmospheric Attenuation for IR Radiation Bands

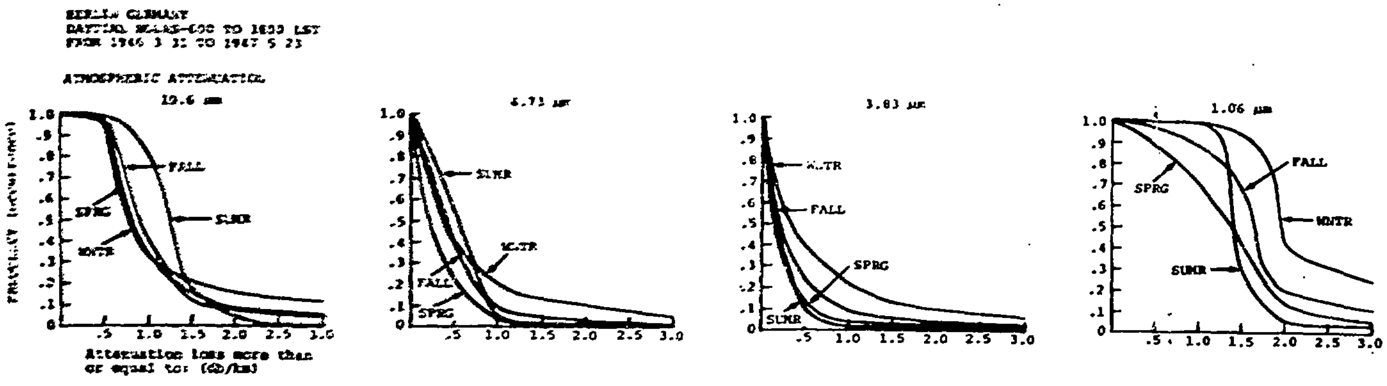

Fig. A 1.5 Probability of Clear Air/Fog-Haze Atmospheric Attenuation for Laser Lines

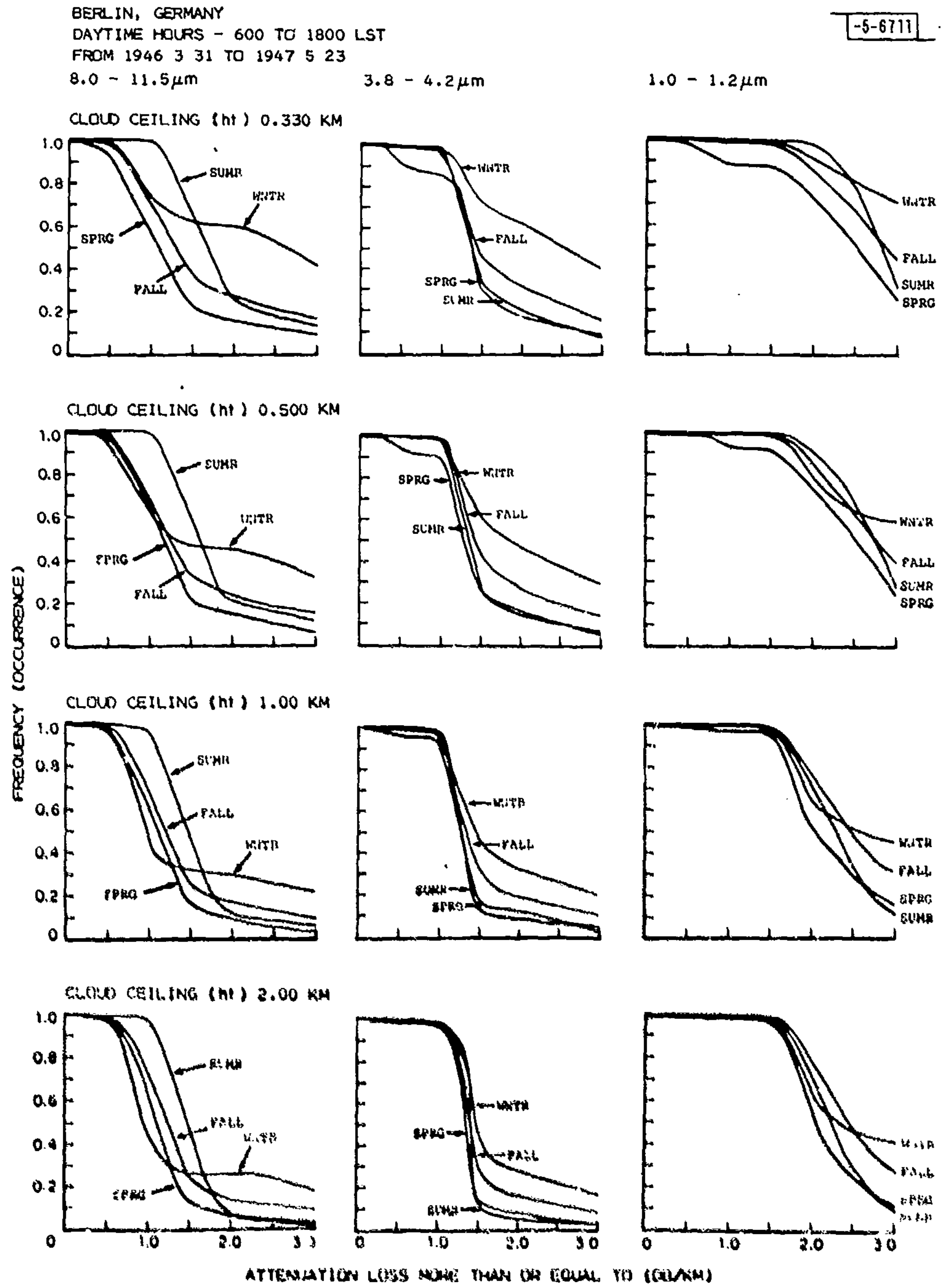

Fig. A 1.6 Joint Probability of Cloud Height and Clear Air/Fog-Haze Attenuation for IR Radiation Bands

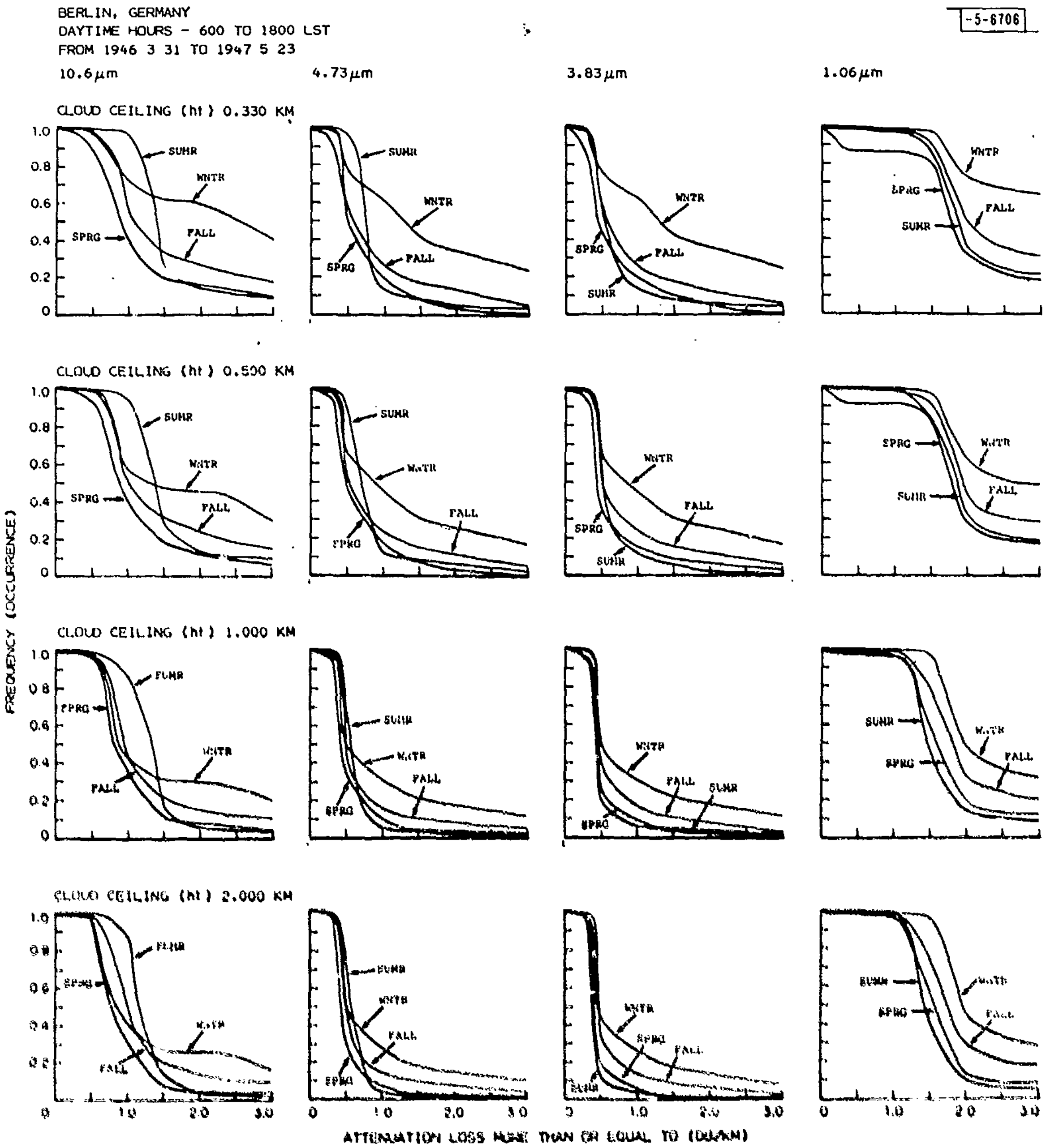

Fig. A 1.7 Joint Probability of Cloud Height and Clear Air/Fog-Haze Attenuation for Laser Lines

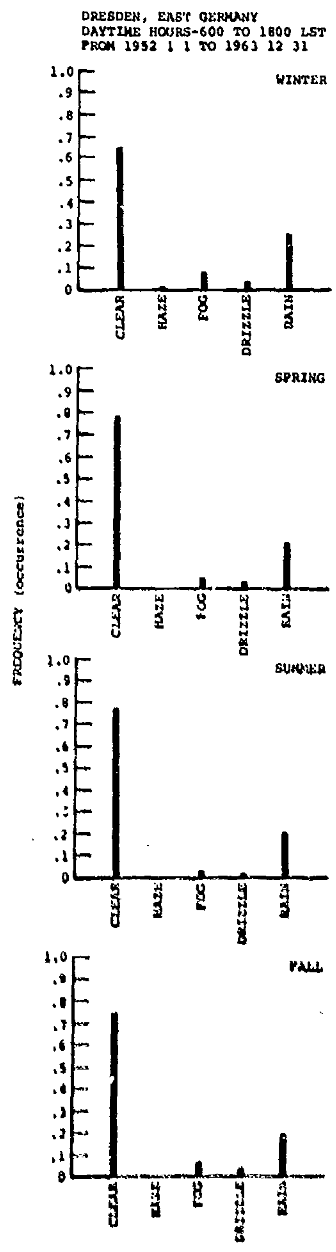

Fig. A 2.1 Probability of Synoptic Weather

Meterorological data not available.

Fig. A 2.2 Probability of Cloud Ceiling Height

TT-7 (A2.3)

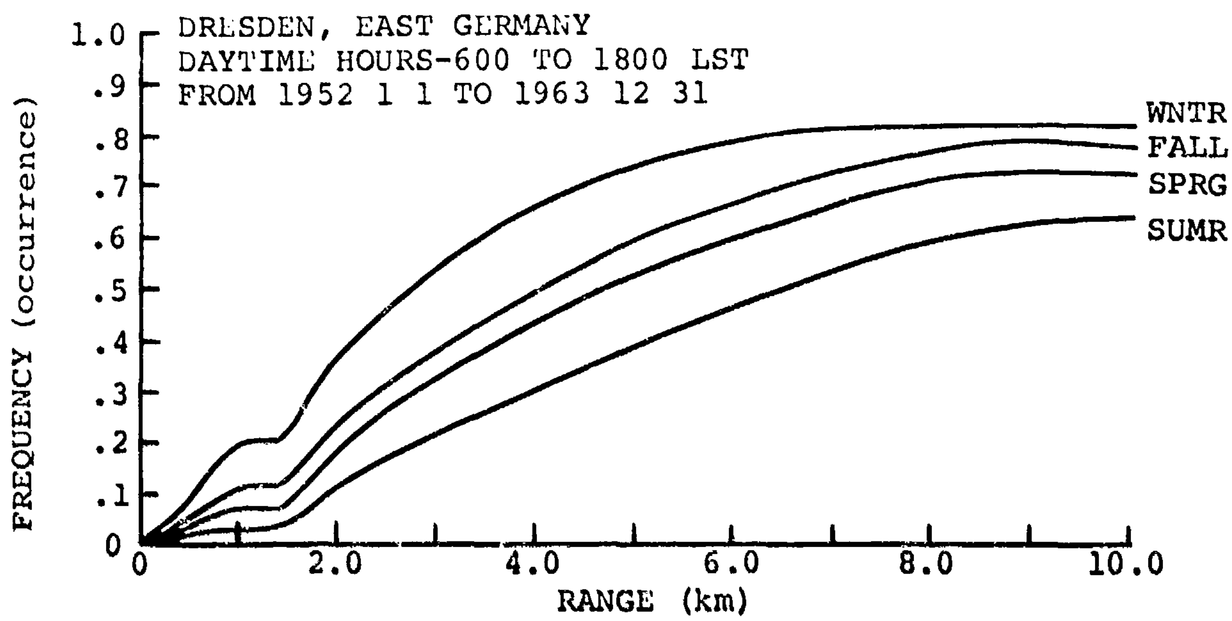

Fig. A 2.3 Probability of Photopic Visibilities

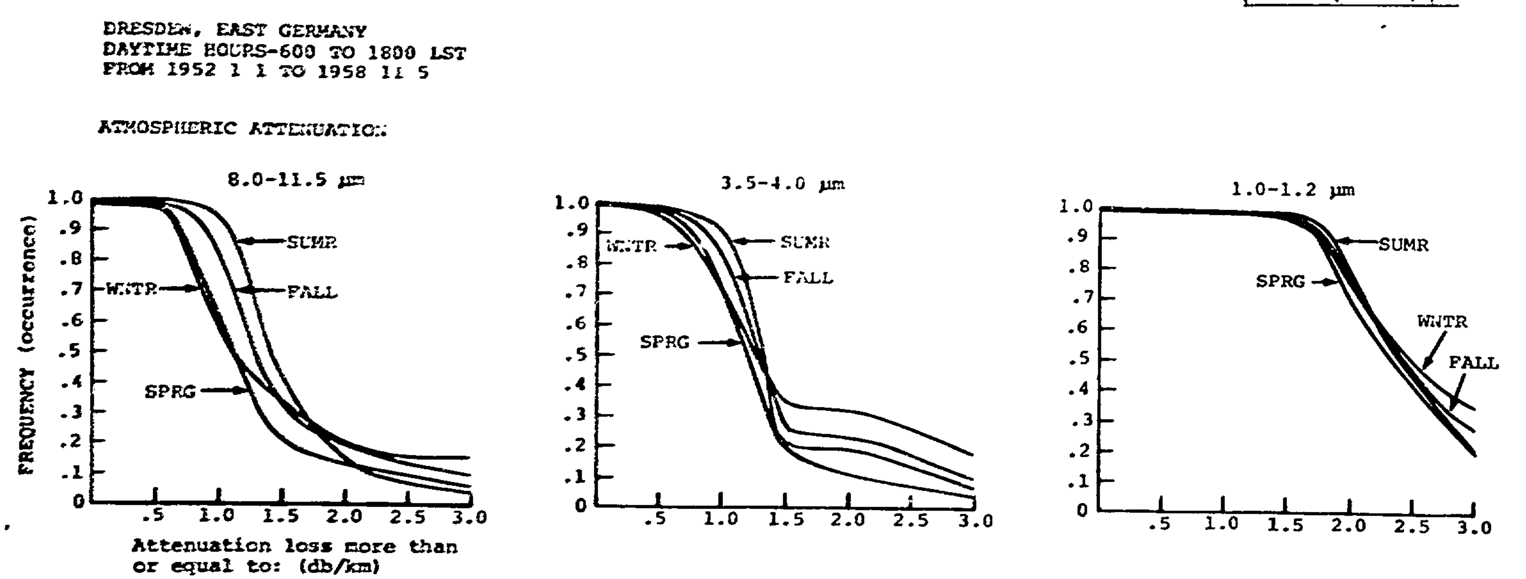

Fig. A 2.4 Probability of Clear Air/Fog-Haze Atmospheric Attenuation for IR Radiation Bands

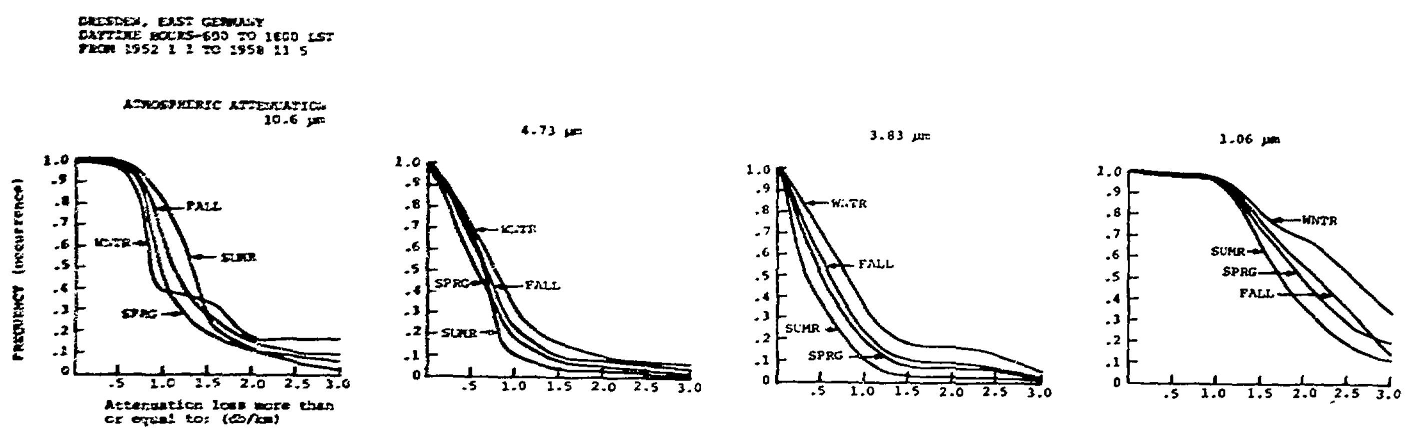

Fig. A 2.5 Probability of Clear Air/Fog-Haze Atmospheric Attenuation for Laser Lines

Joint meterorological data not available.

Fig. A 2.6 Joint Probability of Cloud Height and Clear Air/Fog-Haze Attenuation for IR Radiation Bands

Joint meterorological data not available.

Fig. A 2.7 Joint Probability of Cloud Height and Clear Air/Fog-Haze Attenuation for Laser Lines

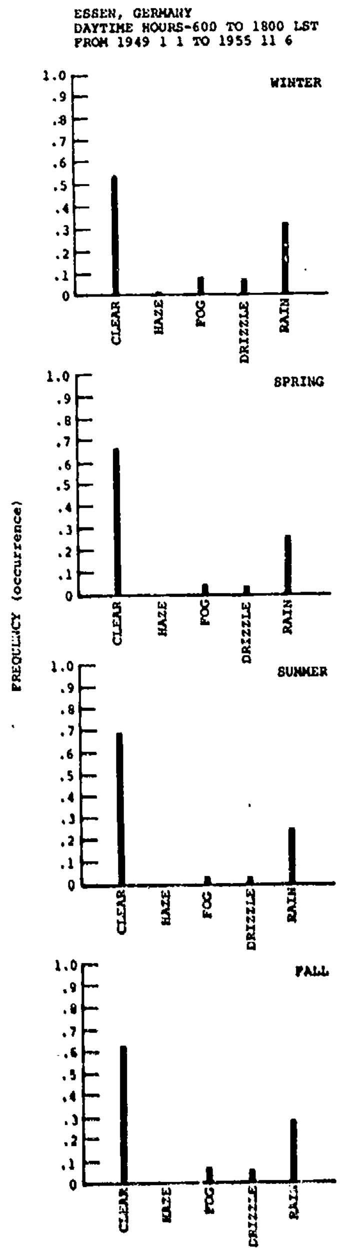

Fig. A 3.1 Probability of Synoptic Weather

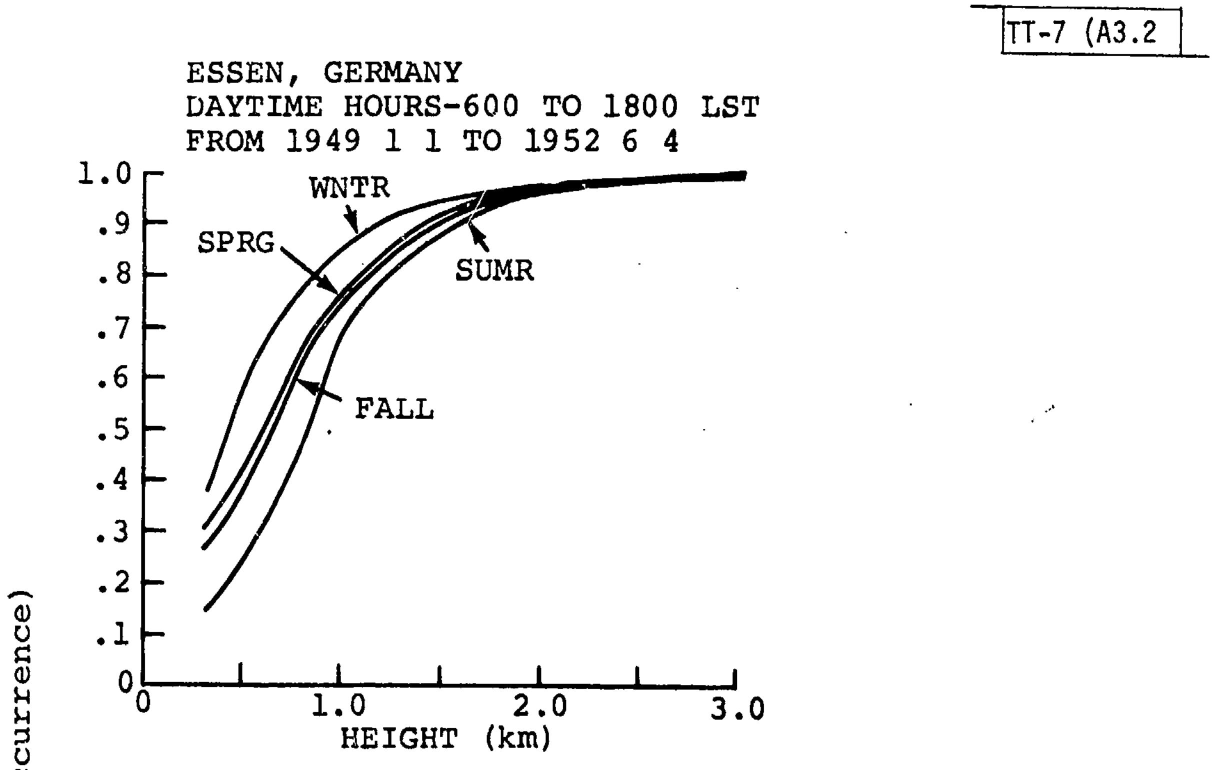

Fig. A 3.2 Probability of Cloud Ceiling Height

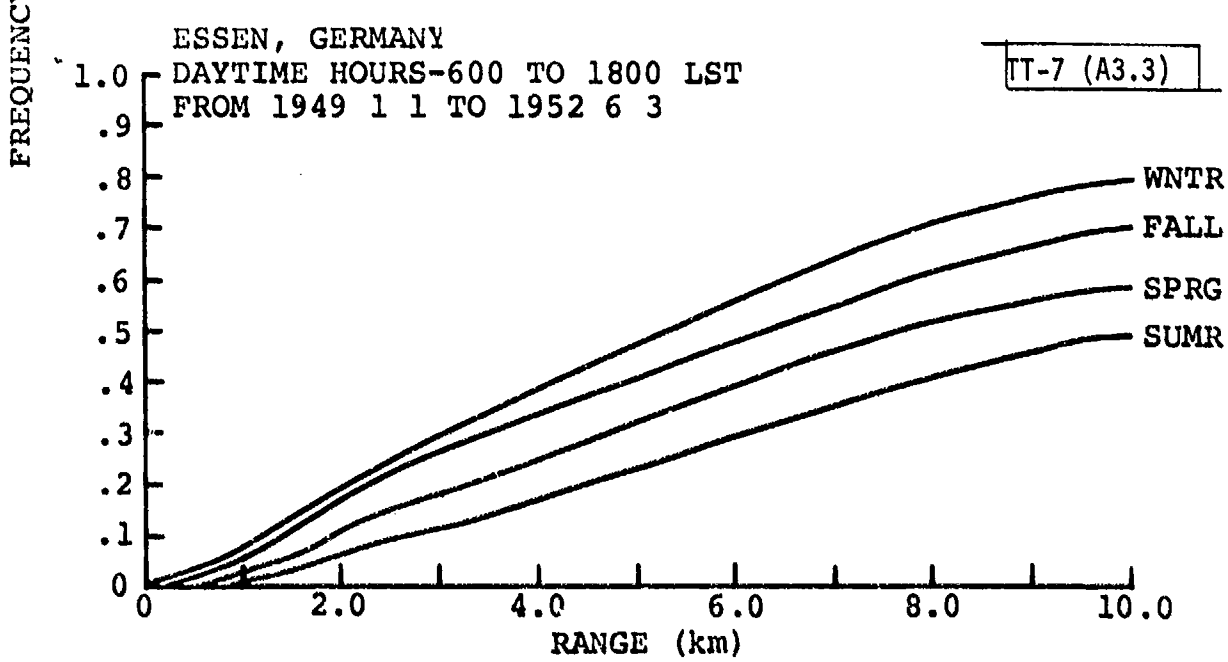

Fig. A 3.3 Probability of Photopic Visibilities

TT-7 (A3.4)

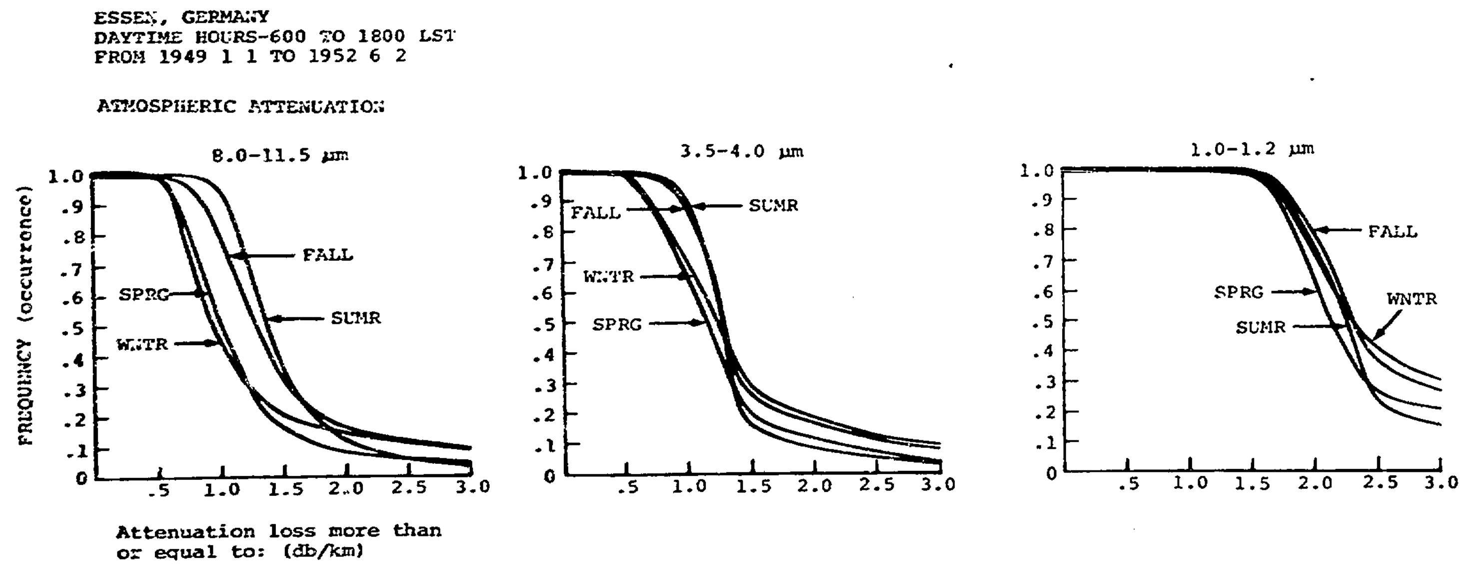

Fig. A 3.4 Probability of Clear Air/Fog-Haze Atmospheric Attenuation for IR Radiation Bands

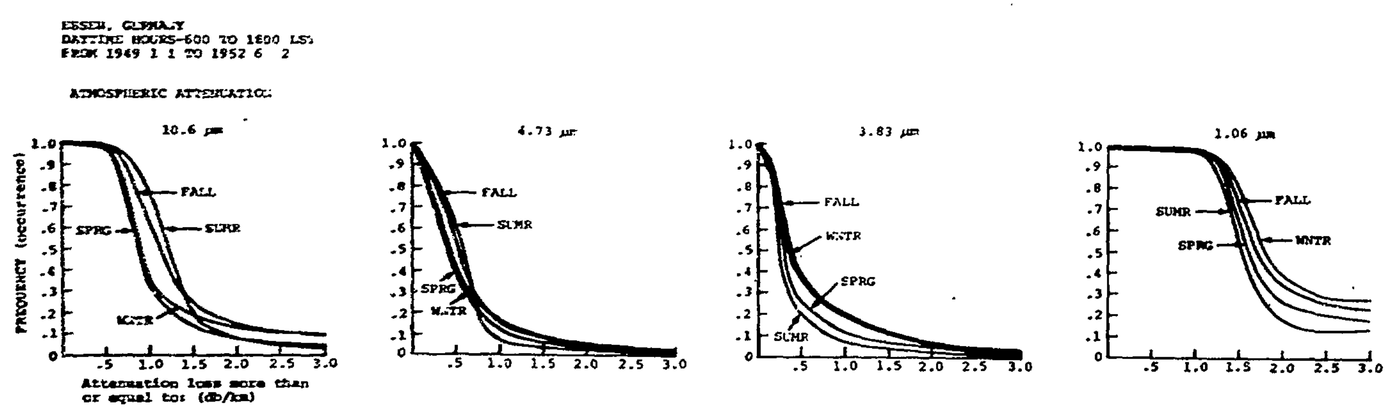

Fig. A 3.5 Probability of Clear Air/Fog-Haze Atmospheric Attenuation for Laser Lines

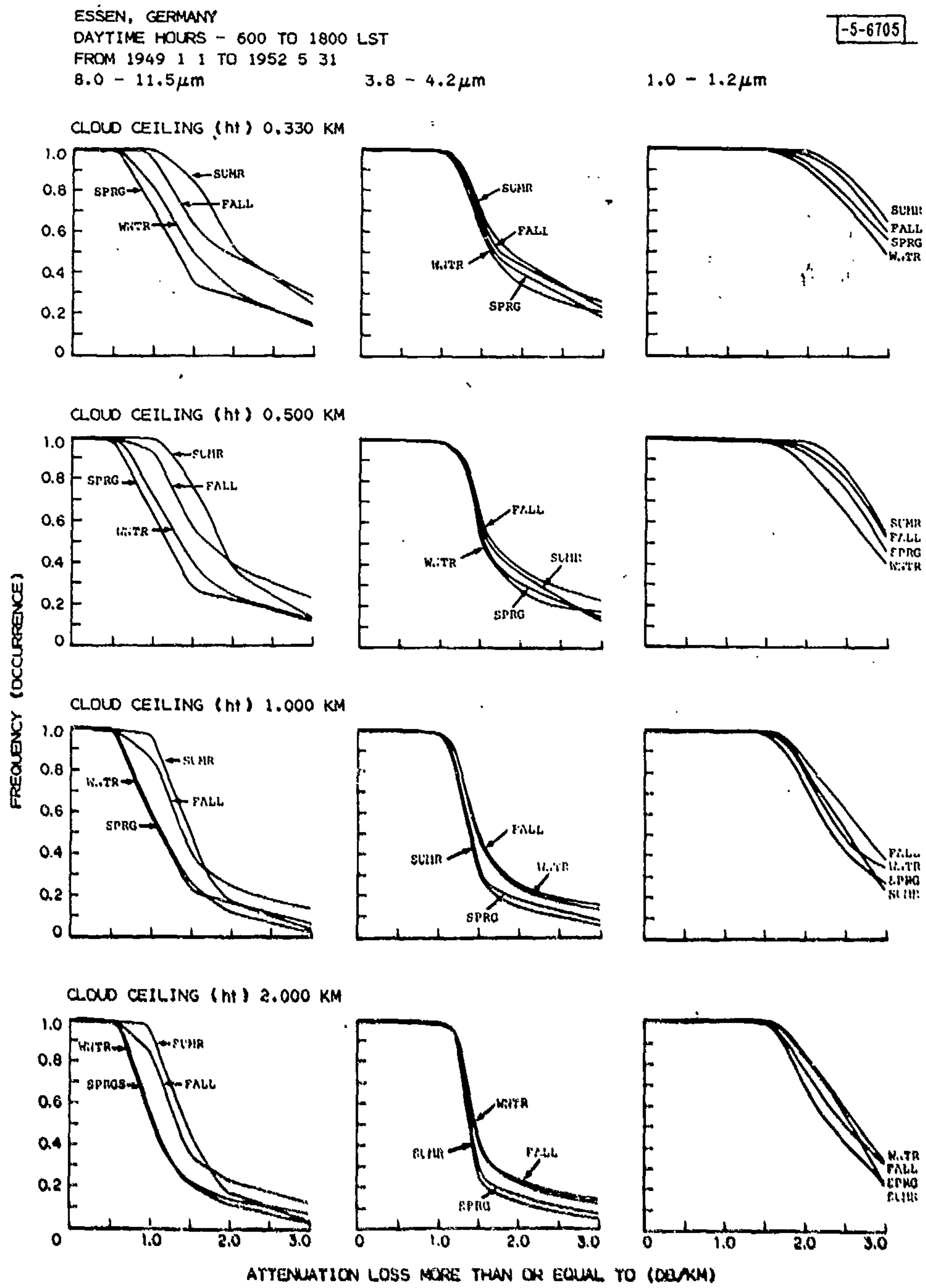

Fig. A 3.6 Joing Probability of Cloud Height and Clear Air/Fog-Haze Attenuation for IR Radiation Bands

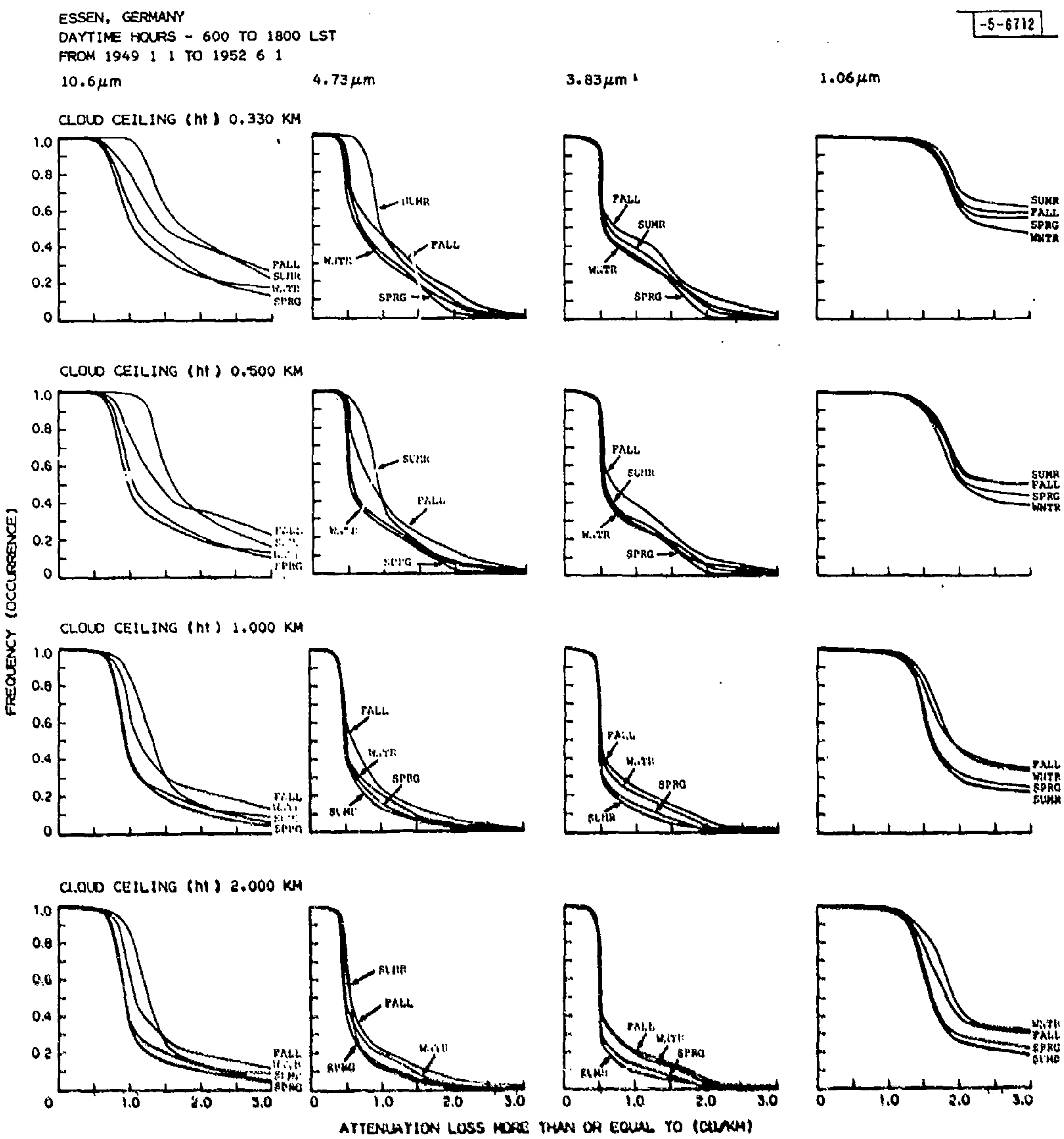

Fig. A 3.7 Joint Probability of Cloud Height and Clear Air/Fog-Haze Attenuation for Laser Lines

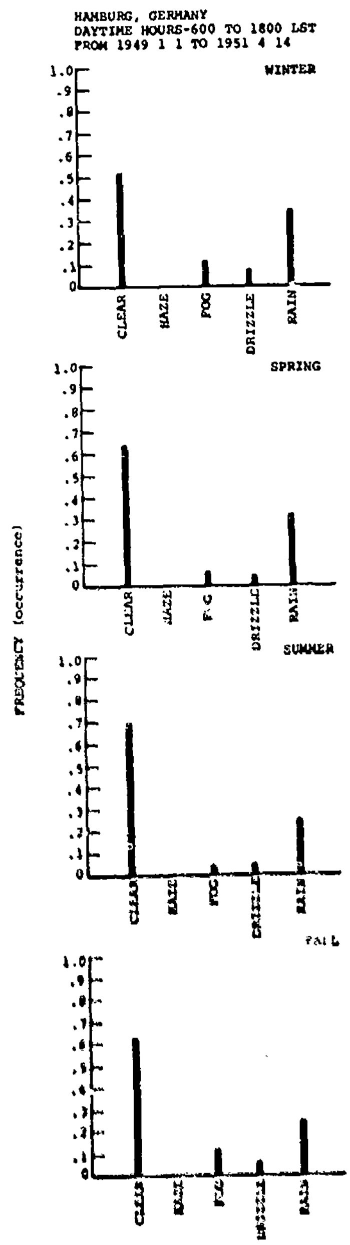

Fig. A 4.1 Probability of Synoptic Weather

TT-7 (A4.2)

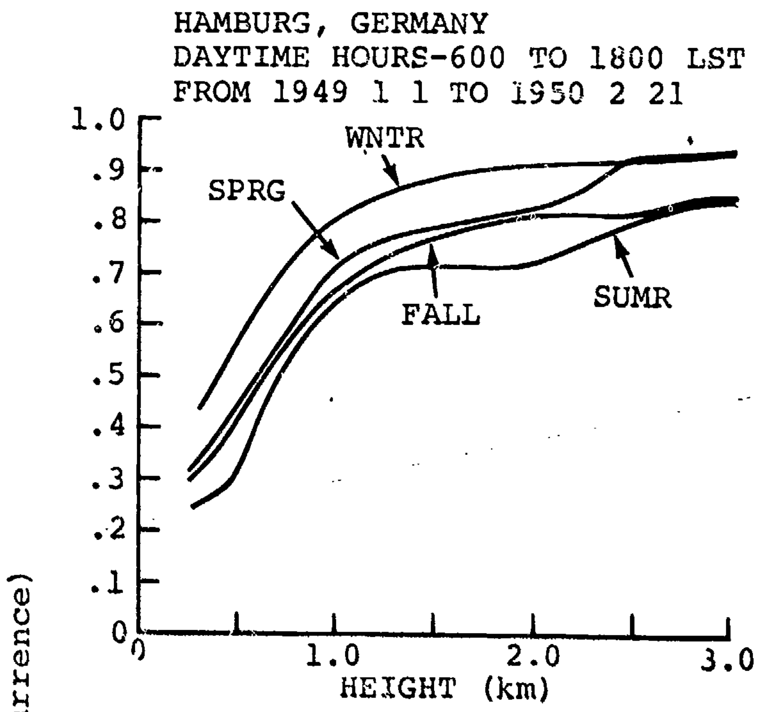

Fig. A 4.2 Probability of Cloud Ceiling Height

TT-7 (A4.3)

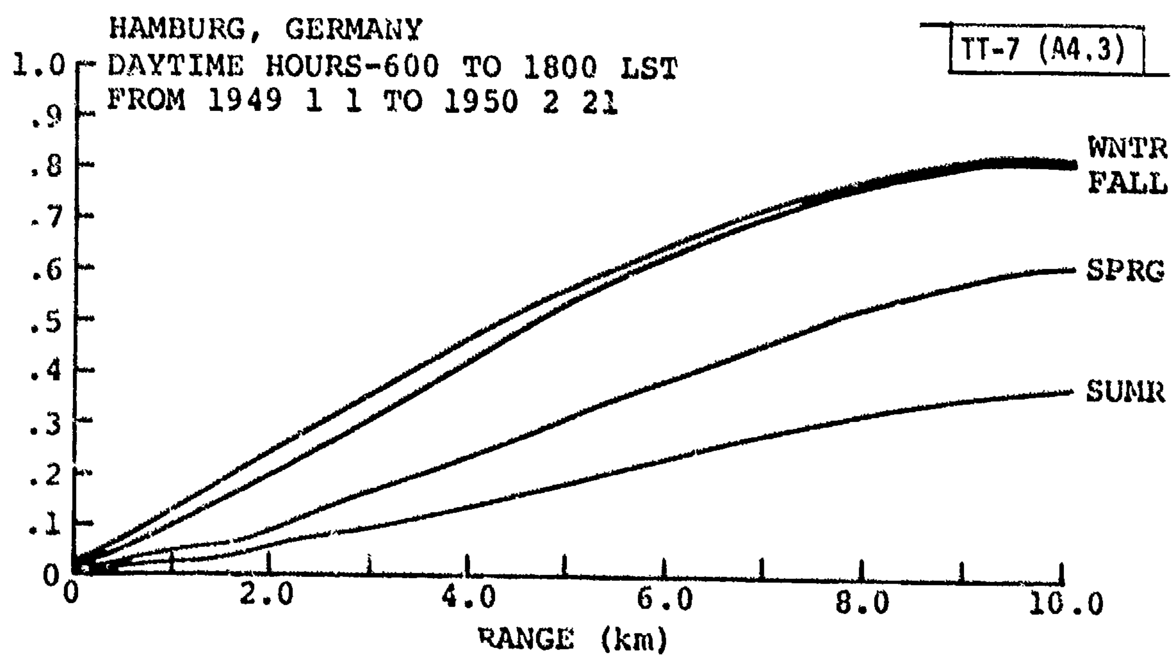

Fig. A 4.3 Probability of Photopic Visibilities

TT-7 (A4.4)

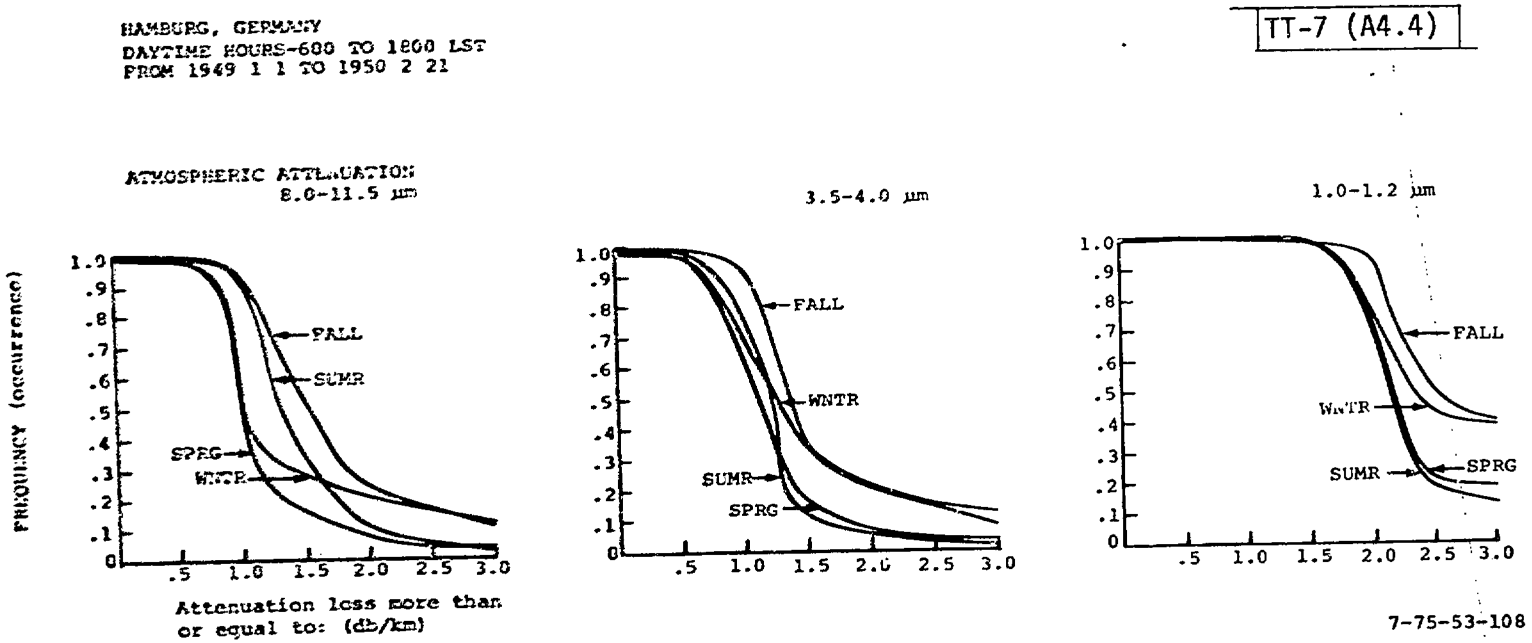

Fig. A 4.4 Probability of Clear Air/Fog-Haze Atmospheric Attenuation for IR Radiation Bands

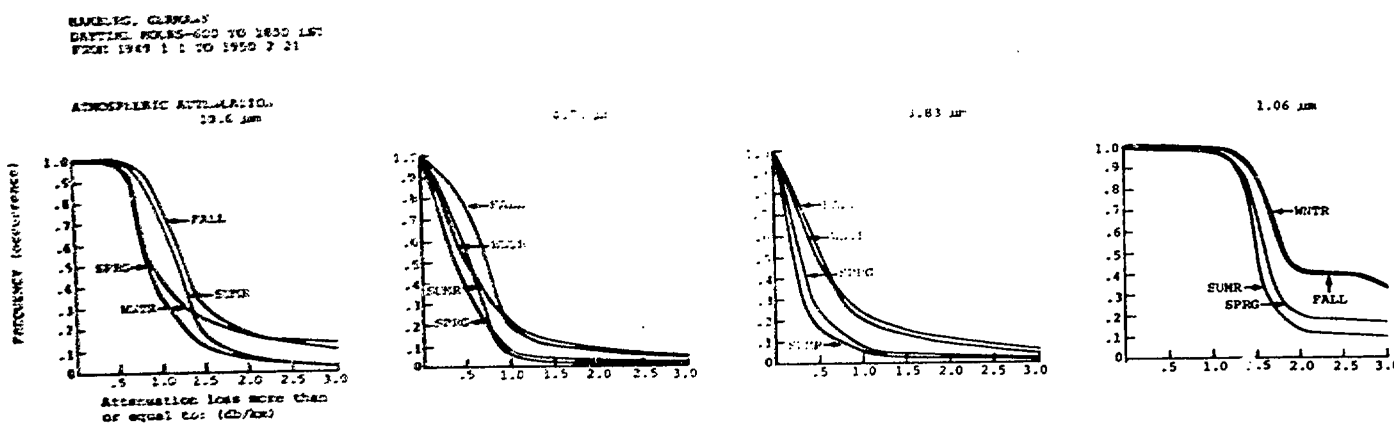

Fig. A 4.5 Probability of Clear Air/Fog-Haze Atmospheric Attenuation for Laser Lines

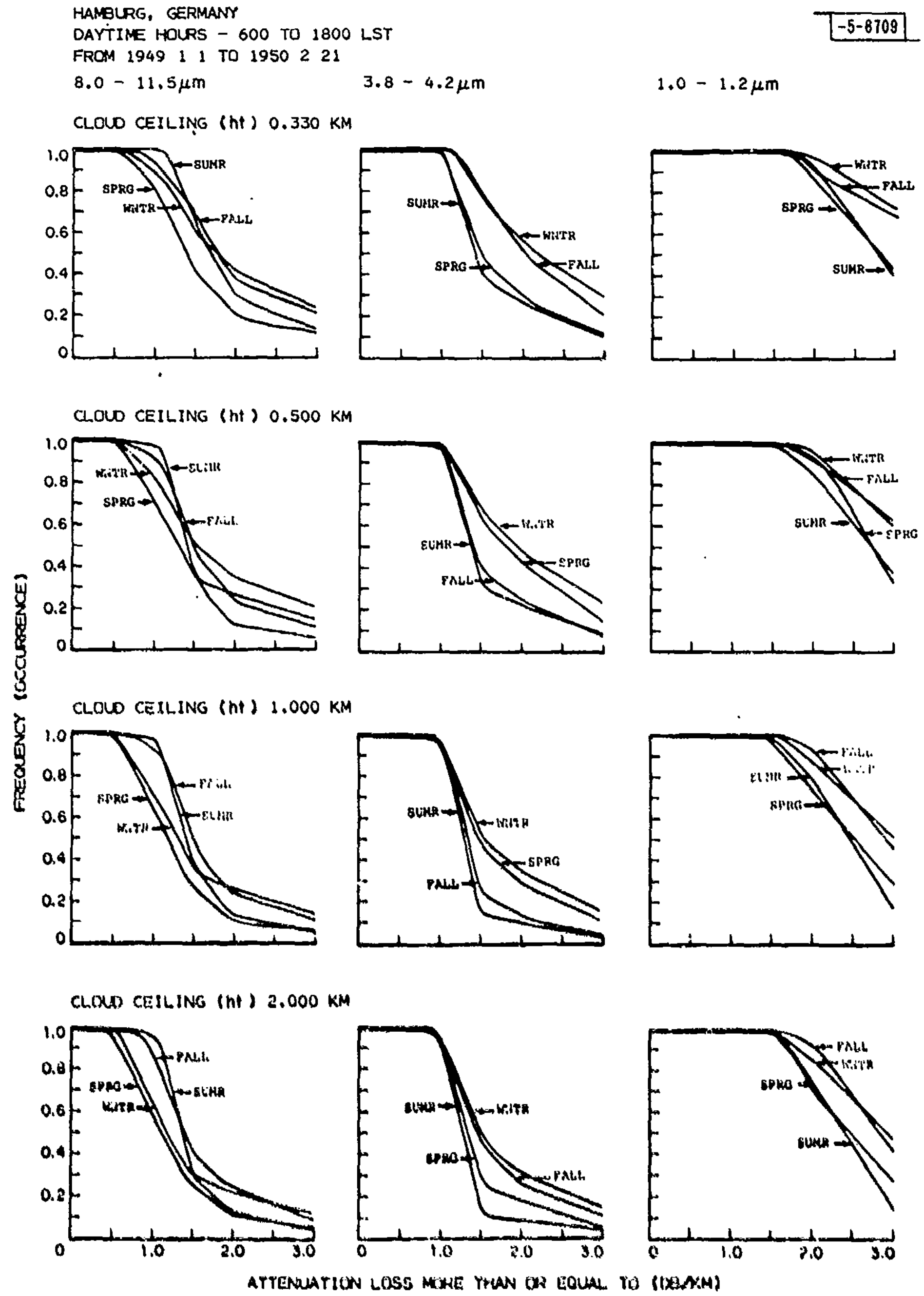

Fig. A 4.6 Joint Probability of Cloud Height and Clear Air/Fog-Haze Attenuation for IR Radiation Bands

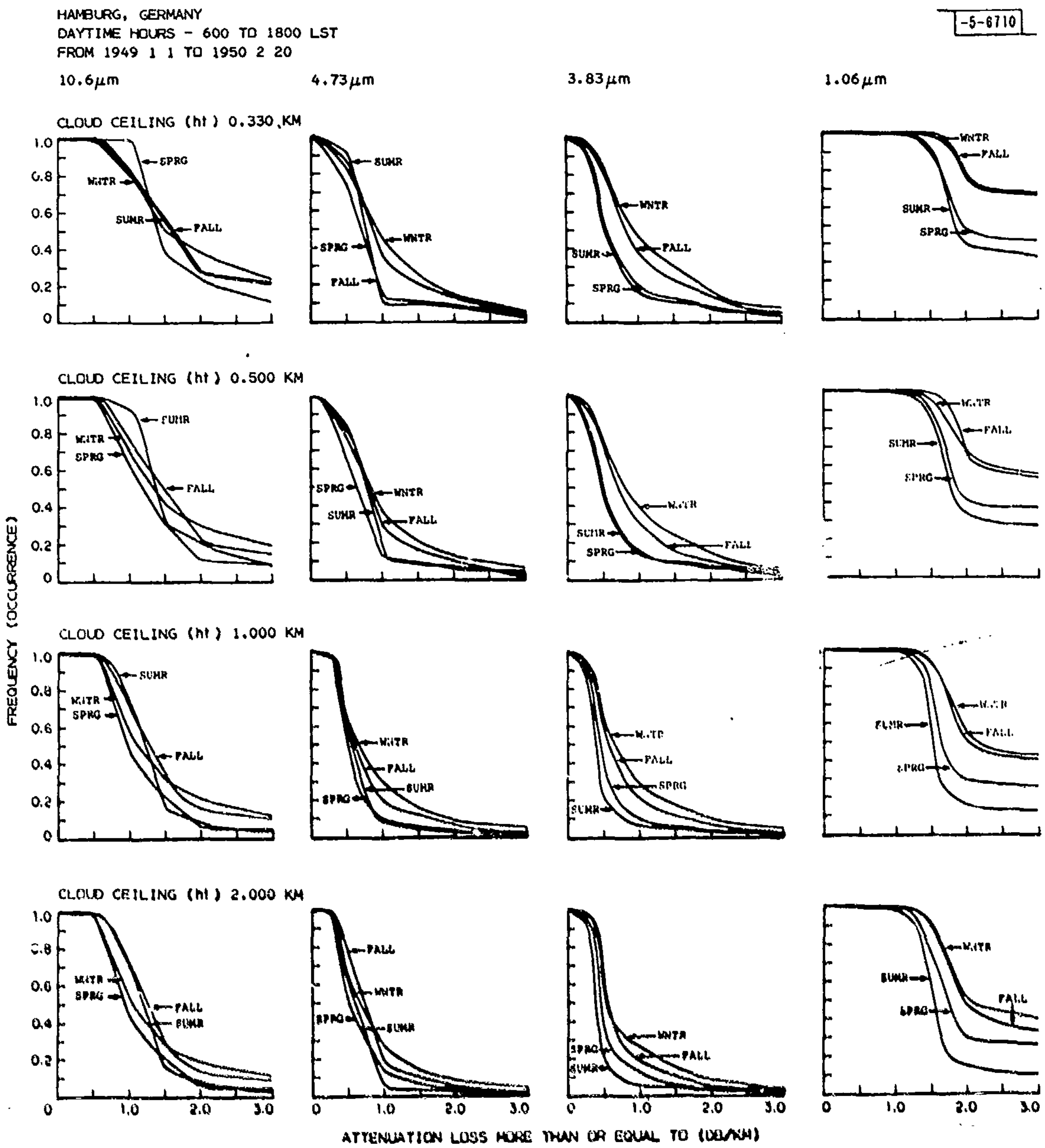

Fig. A 4.7 Joint Probability of Cloud Height and Clear Air/Fog-Haze Attenuation for Laser Lines

TT-7 (A5.1)

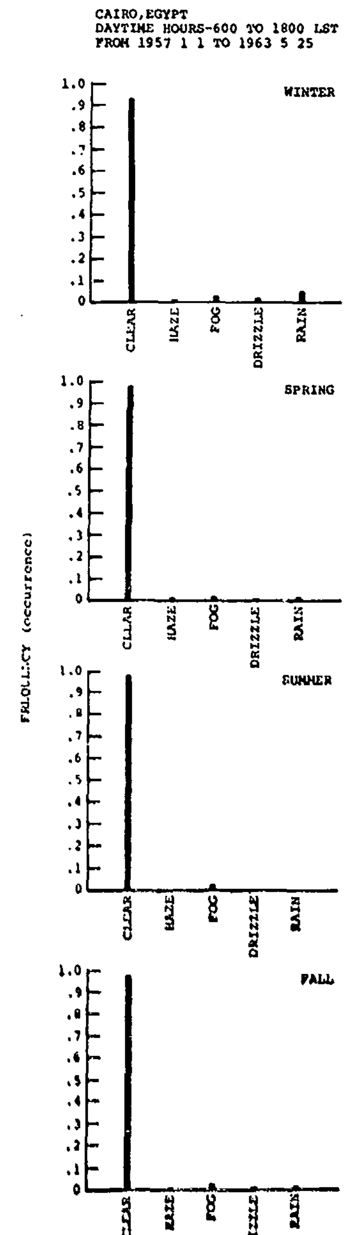

Fig. A 5.1 Probability of Synoptic Weather

TT-7 (A5,2)

CLOUD CEILING HEIGHT GREATER THAN 10KM FOR >.90
FREQUENCY OF OCCURRENCE ALL SEASONS.

Fig. A 5.2 Probability of Cloud Ceiling Height

TT-7 (A5.3)

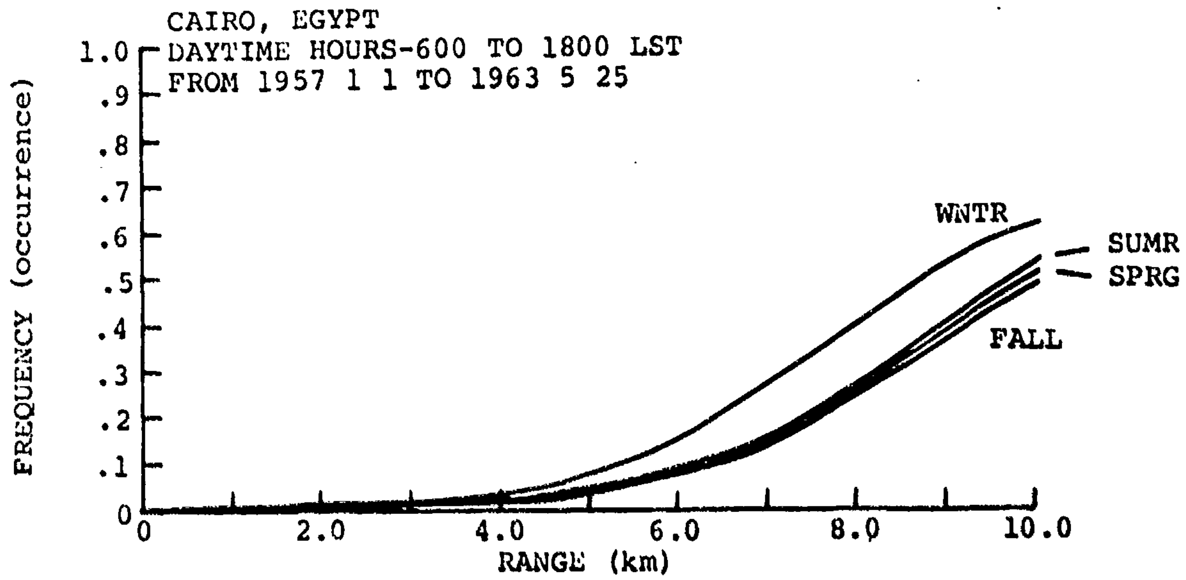

Fig. A 5.3 Probability of Photopic Visibilities

TT-7 (A5.4)

CAIRO EGYPT
DAYTIME HOURS-600 TO 1800 LST
FROM 1957 1 1 TO 1963 5 25

ATMOSPHERIC ATTENUATION

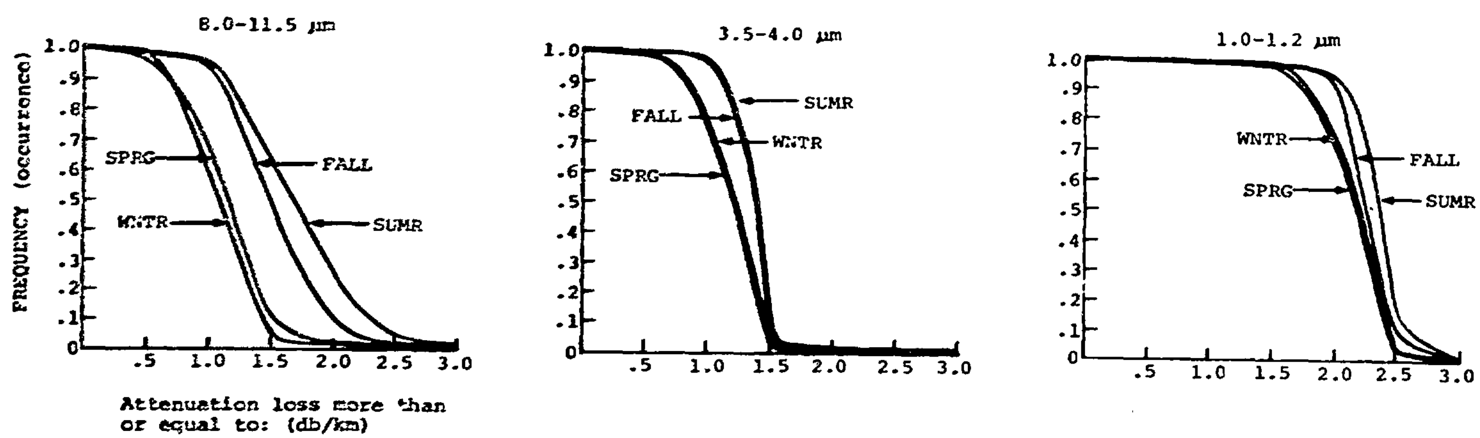

Fig. A 5.4 Probability of Clear Air/Fog-Haze Atmospheric Attenuation for IR Radiation Bands

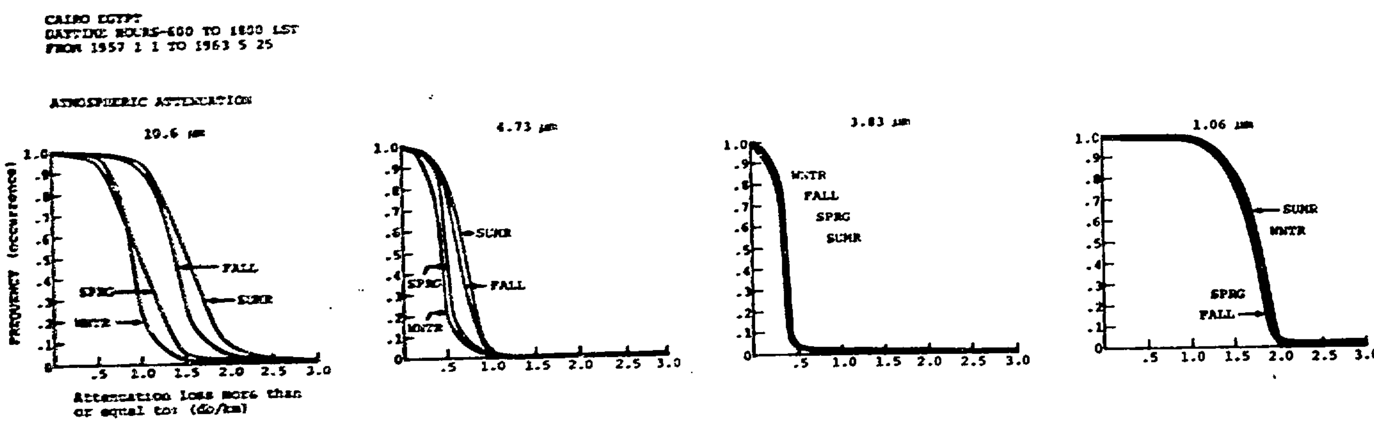

Fig. A 5.5 Probability of Clear Air/Fog-Haze Atmospheric Attenuation for Laser Lines

Joint meterorological data not available.

Fig. A 5.6 Joint Probability of Cloud Height and Clear Air/Fog-Haze Attenuation for IR Radiation Bands

Joint meterorological data not available.

Fig. A 5.7 Joint Probability of Cloud Height and Clear Air/Fog-Haze Attenuation for Laser Lines

TT-7 (A6.1)

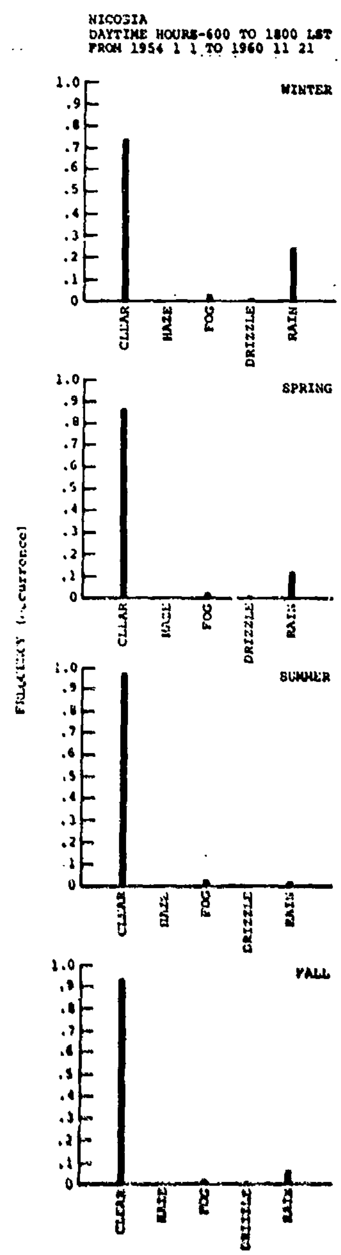

Fig. A 6.1 Probability of Synoptic Weather

TT-7 (A6.2)

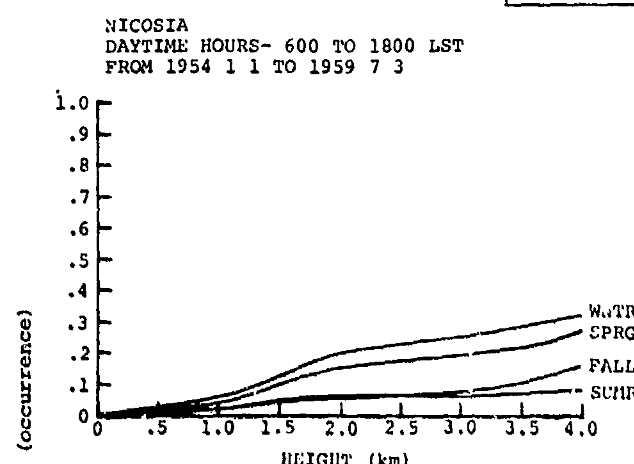

Fig. A 6.2 Probability of Cloud Ceiling Height

TT-7 (A6.3)

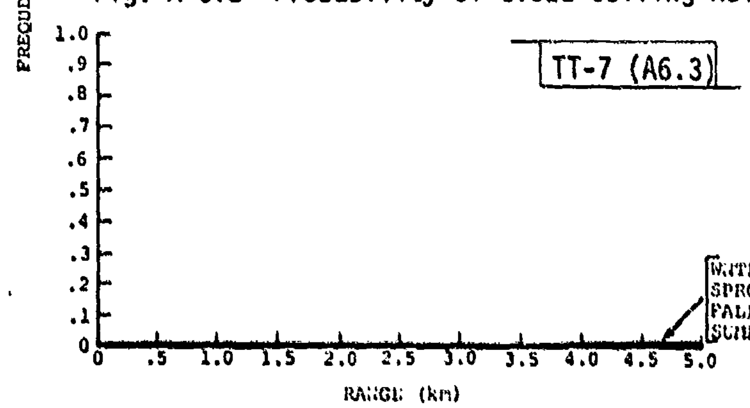

Fig. A 6.3 Probability of Photopic Visibilities

TT-7 (A6,4)

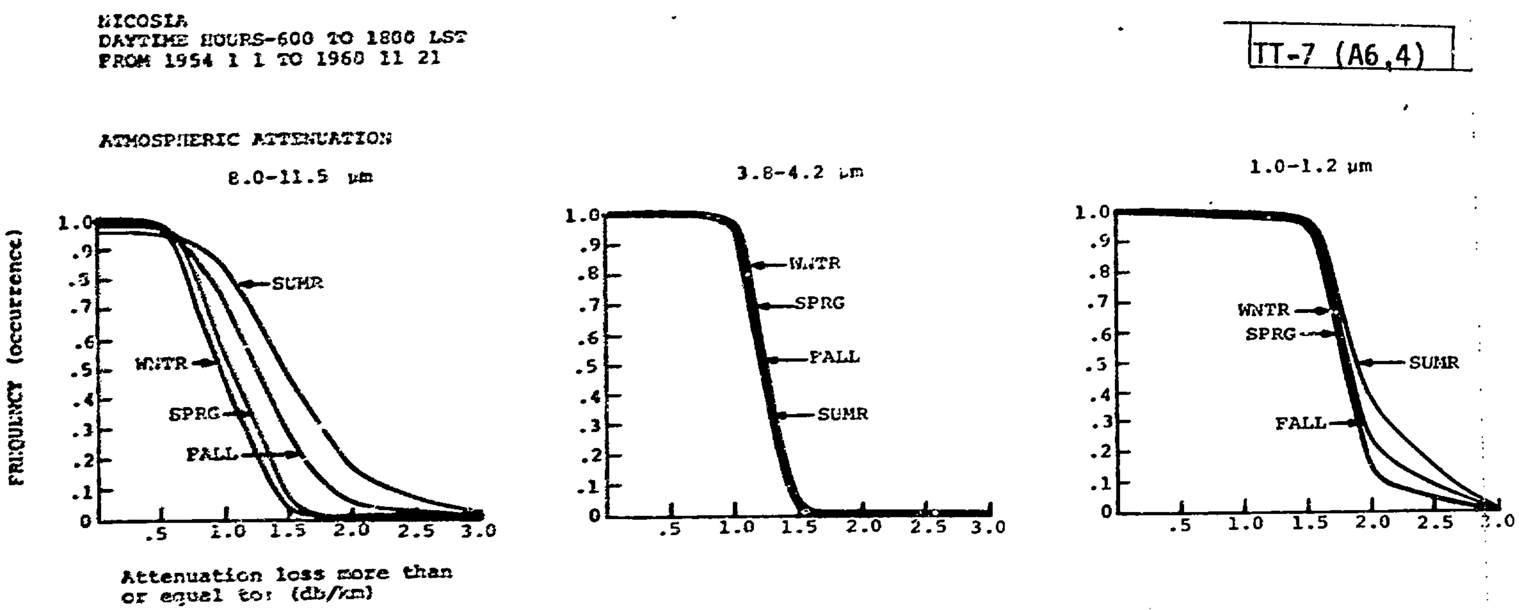

Fig. A 6.4 Probability of Clear Air/Fog-Haze Atmospheric Attenuation for IR Radiation Bands

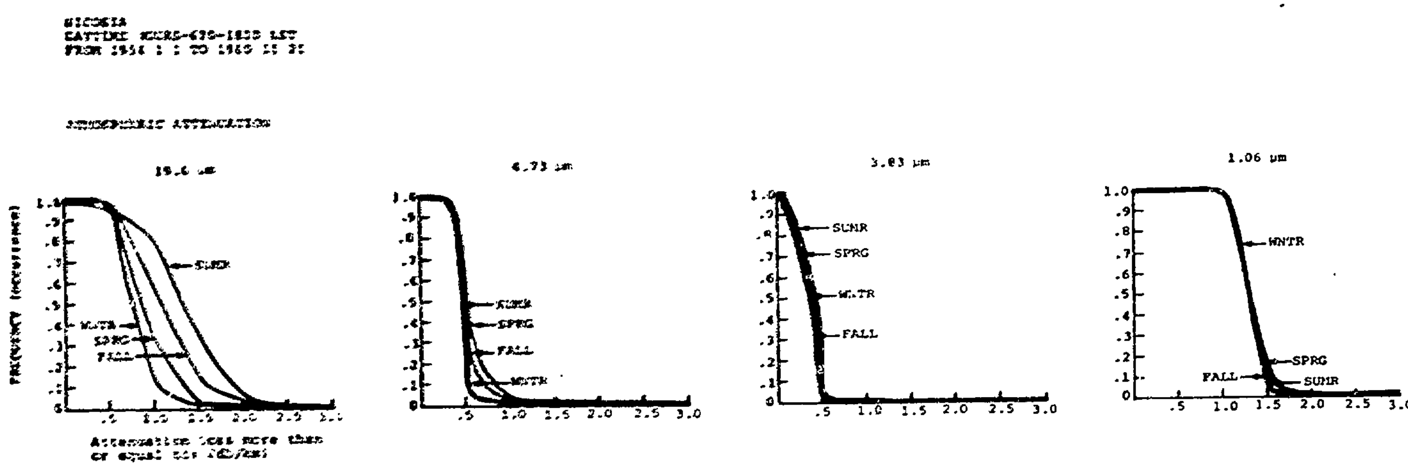

Fig. A 6.5 Probability of Clear Air/Fog-Haze Atmospheric Attenuation for Laser Lines

TT-7 (A6.5)

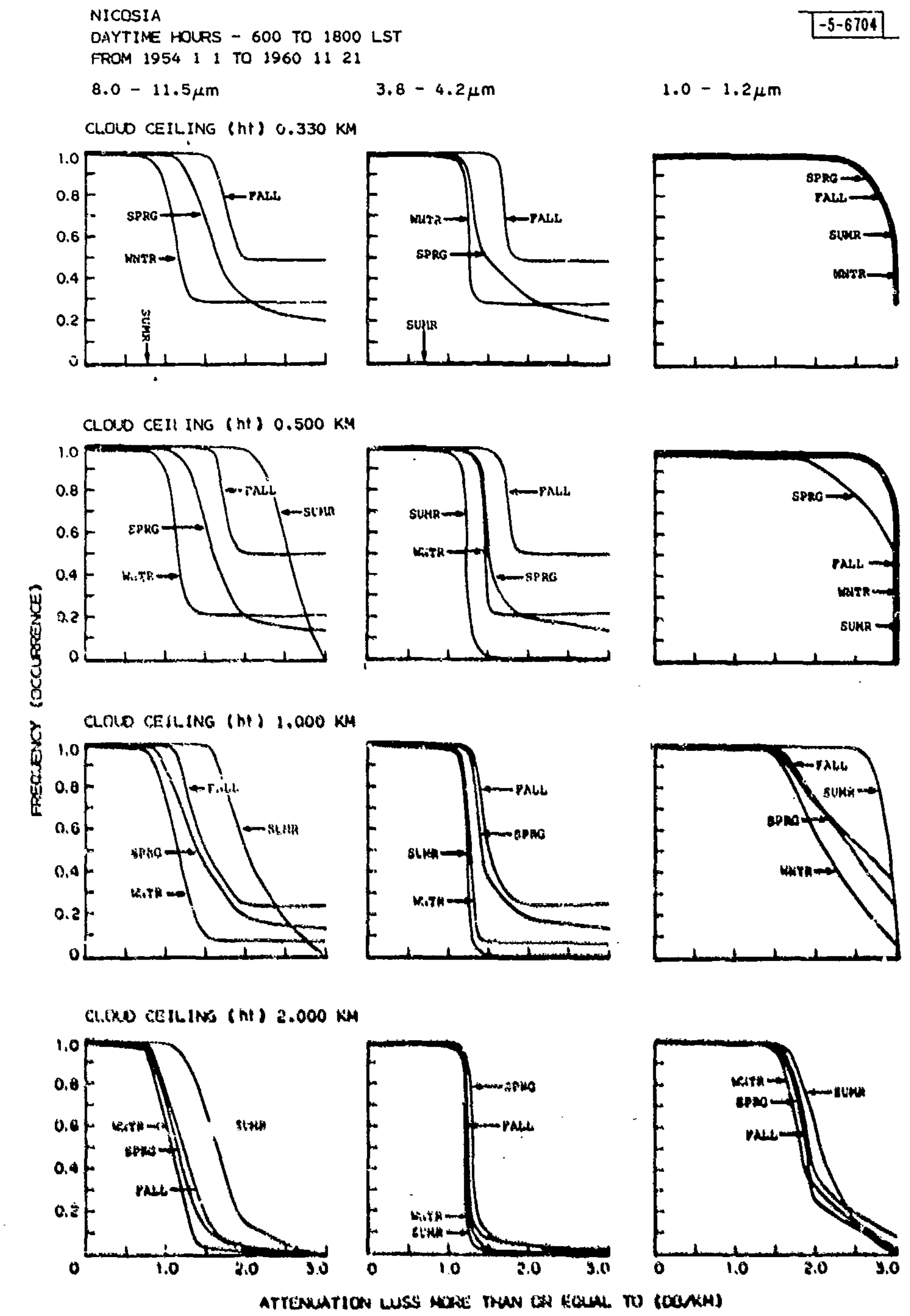

Fig. A 6.6 Joint Probability of Cloud Height and Clear Air/Fog-Haze Attenuation for IR Radiation Bands

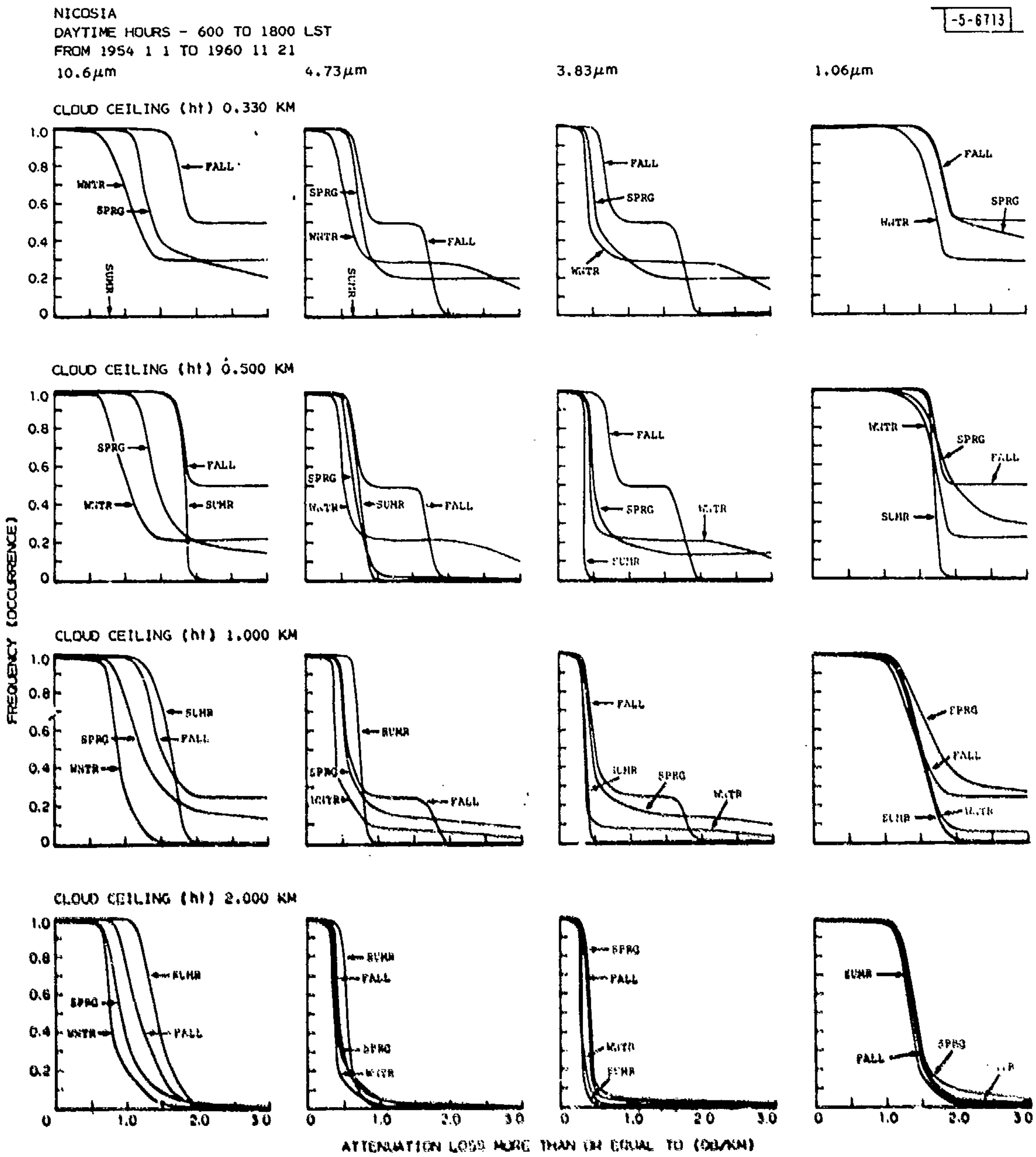

Fig. A 6.7 Joint Probability of Cloud Height and Clear Air/Fog-Haze Attenuation for Laser Lines

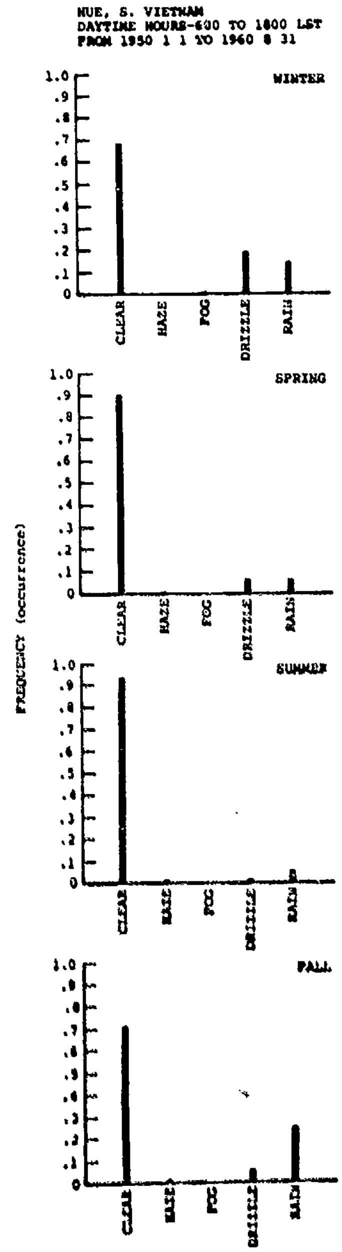

Fig. A 7.1 Probability of Synoptic Weather

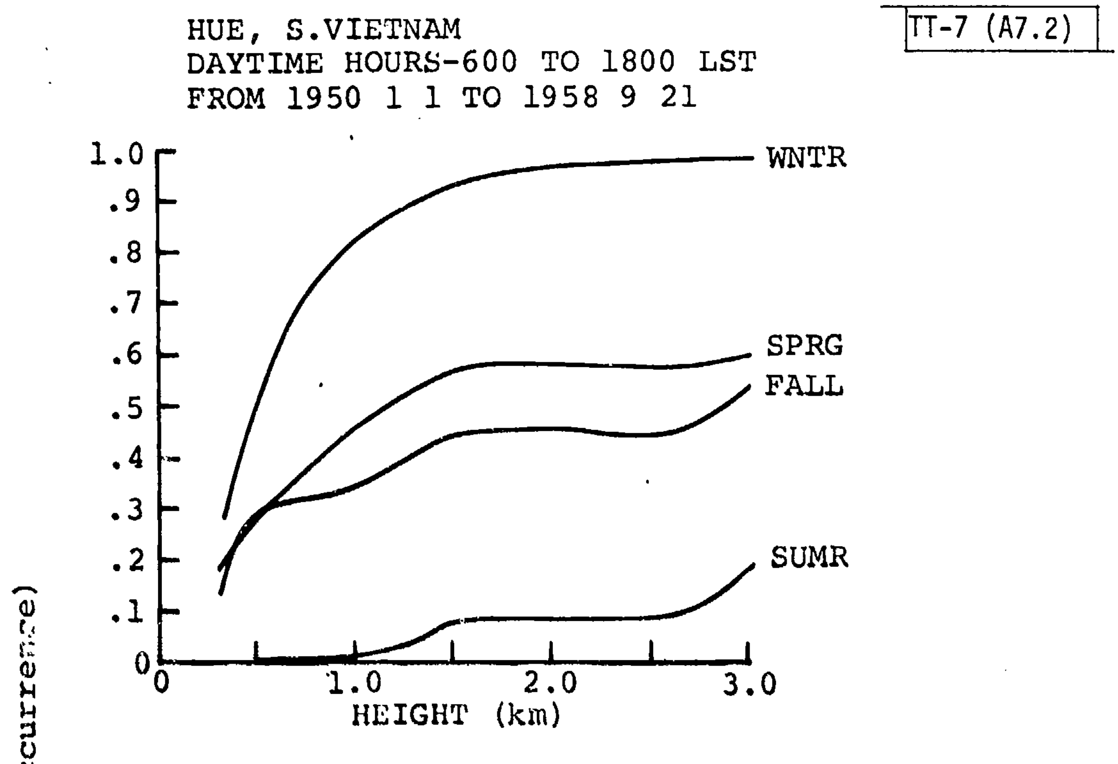

. Fig. A 7.2 Probability of Cloud Ceiling Height

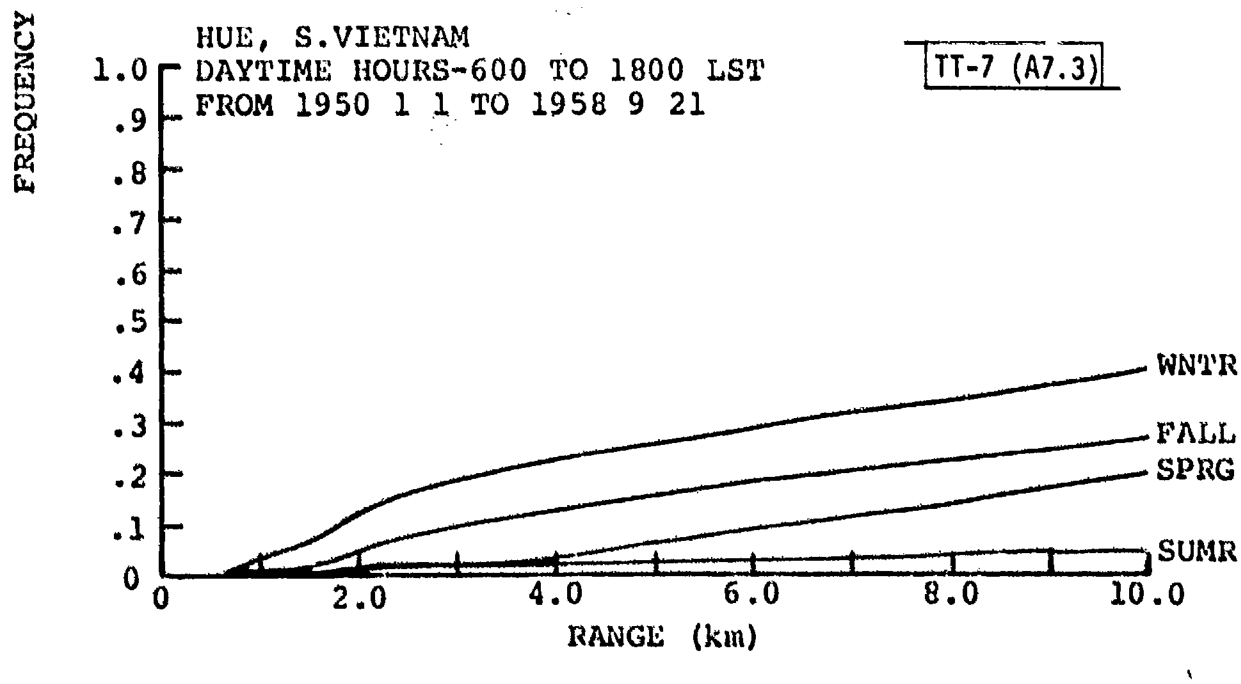

Fig. A 7.3 Probability of Photopic Visibilities

TT-7 (A7.4)

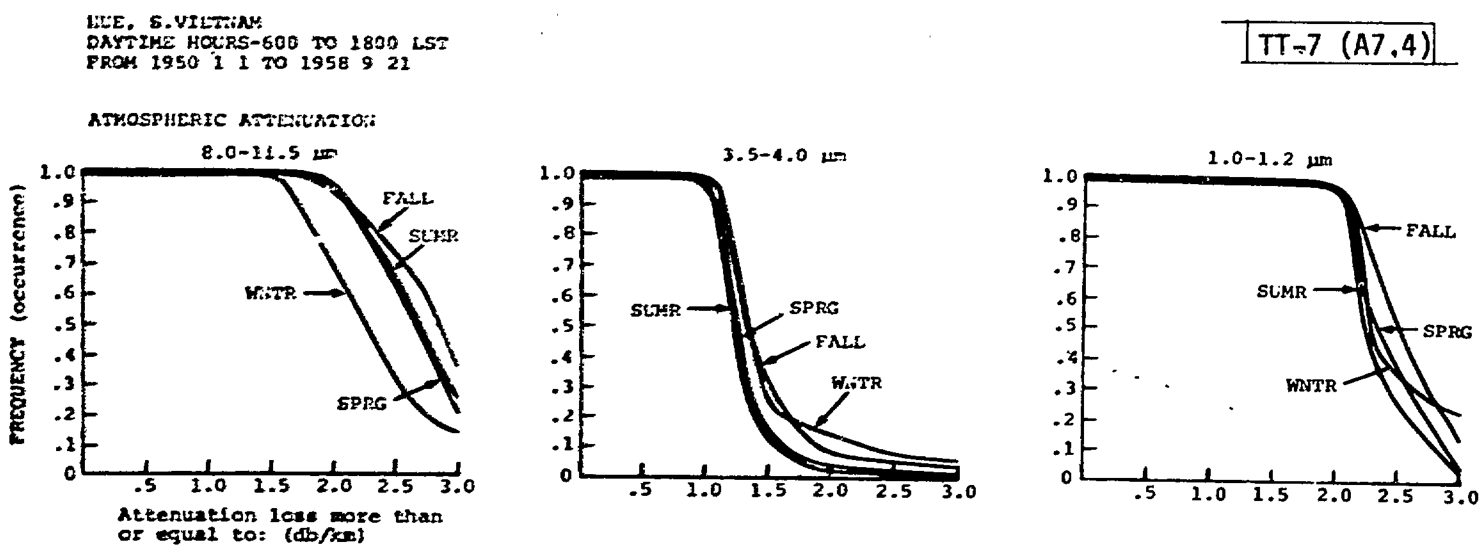

Fig. A 7.4 Probability of Clear Air/Fog-Haze Atmospheric Attenuation for IR Radiation Bands

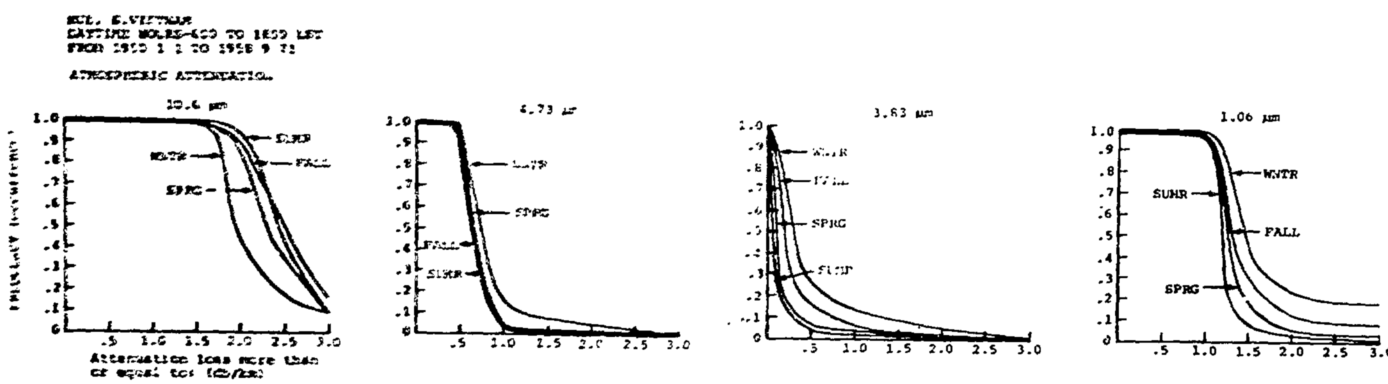

Fig. A 7.5 Probability of Clear Air/Fog-Haze Atmospheric Attenuation for Laser Lines

Joint meterorological data not available.

Fig. A 7.6 Joint Probability of Cloud Height and Clear Air/Fog-Haze Attenuation for IR Radiation Bands

Joint meterorological data not available.

Fig. A 7.7 Joint Probability of Cloud Height and Clear Air/Fog-Haze Attenuation for Laser Lines

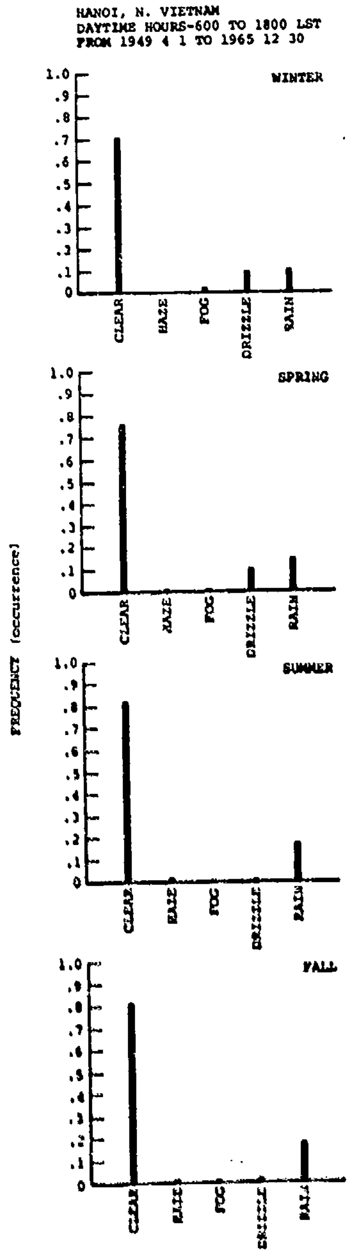

Fig. A 8.1 Probability of Synoptic Weather

Meterorological data not available.

Fig. A 8.2 Probability of Cloud Ceiling Height

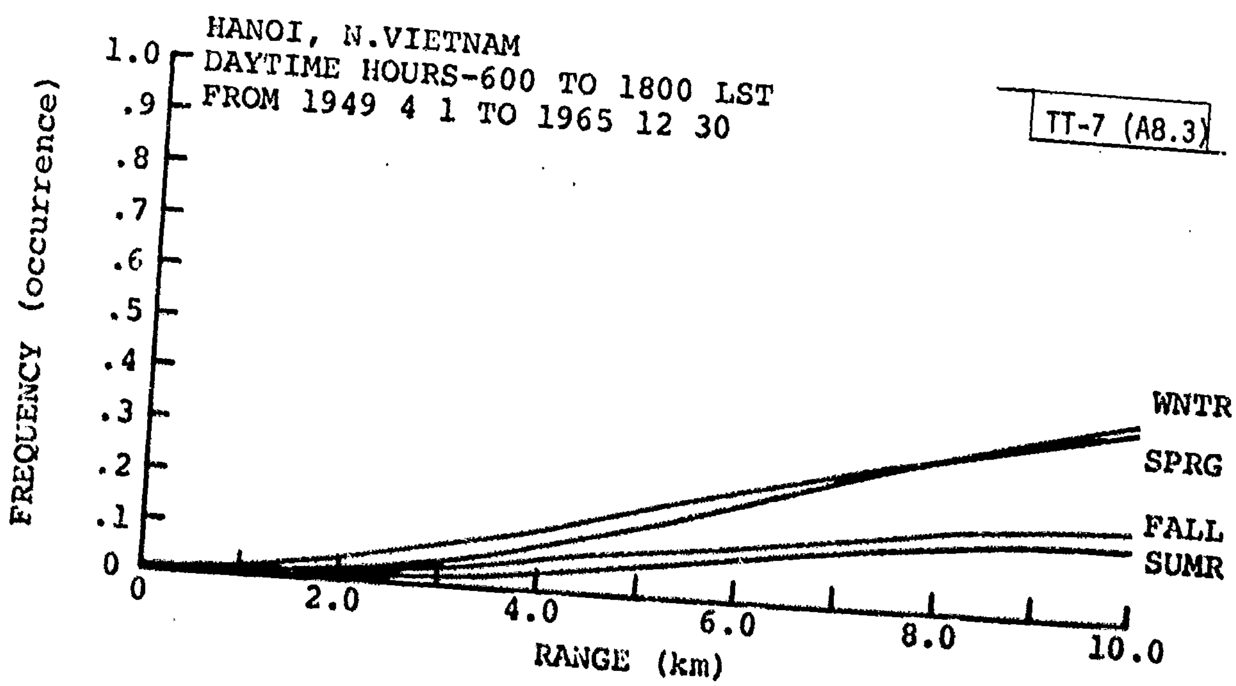

Fig. A 8.3 Probability of Photopic Visibilities

TT-7 (A8.4)

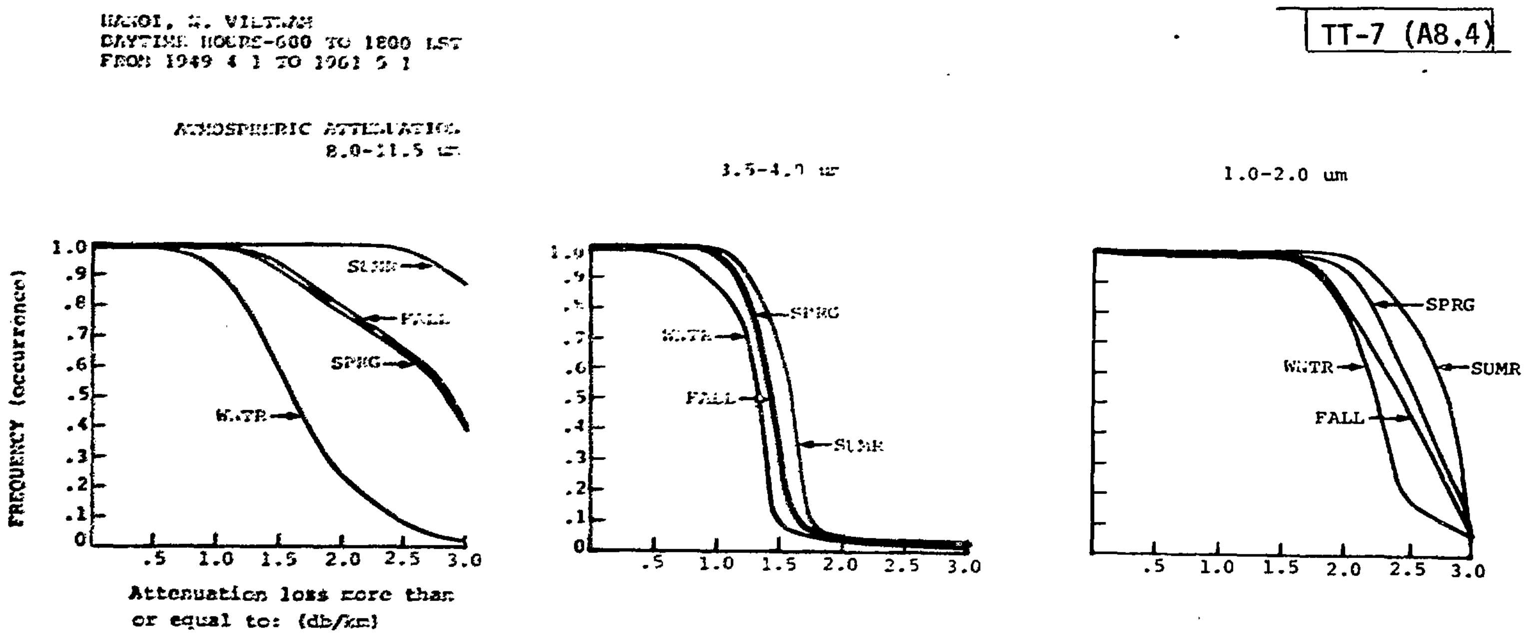

Fig. A 8.4 Probability of Clear Air/Fog-Haze Atmospheric Attenuation for IR Radiation Bands

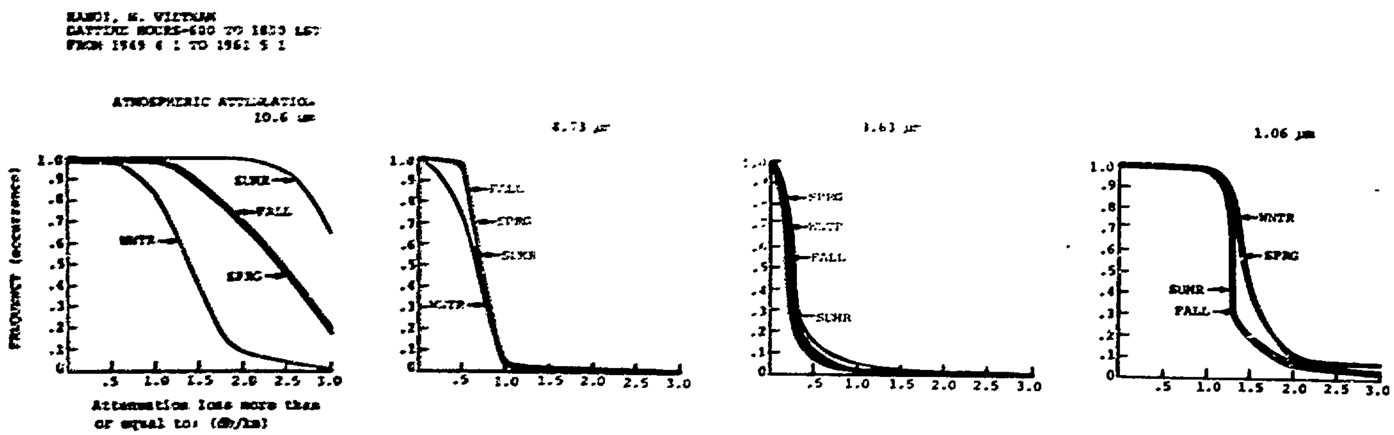

Fig. A 8.5 Probability of Clear Air/Fog-Haze Atmospheric Attenuation for Laser Lines

Joint meterorological data not available.

Fig. A 8.6 Joint Probability of Cloud Height and Clear Air/Fog-Haze Attenuation for IR Radiation Bands

Joint meterorological data not available.

Fig. A 8.7 Joint Probability of Cloud Height and Clear Air/Fog-Haze Attenuation for Laser Lines

Meteorological data not available

Fig. A 9.1 Probability of Synoptic Weather

TT-7 (A9.2)

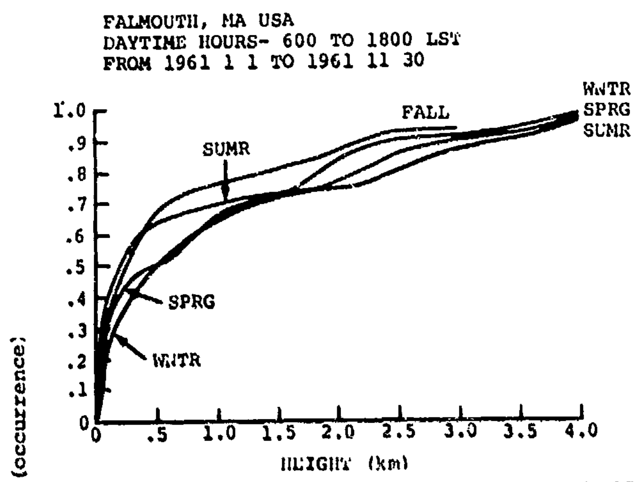

Fig. A 9.2 Probability of Cloud Ceiling Height

TT-7 (A9.3)

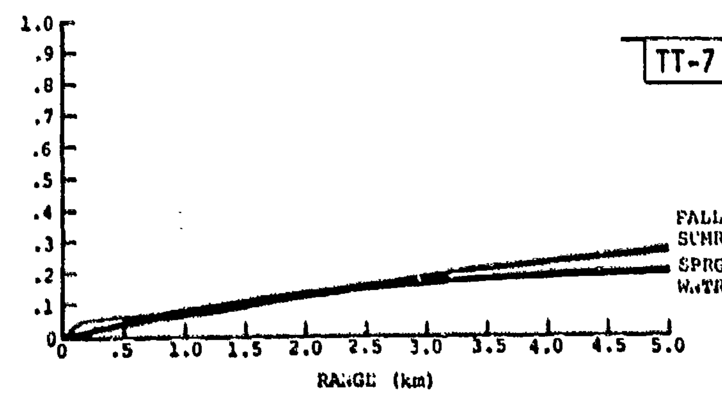

Fig. A 9.3 Probability of Photopic Visibilities

TT-7 (A9.4)

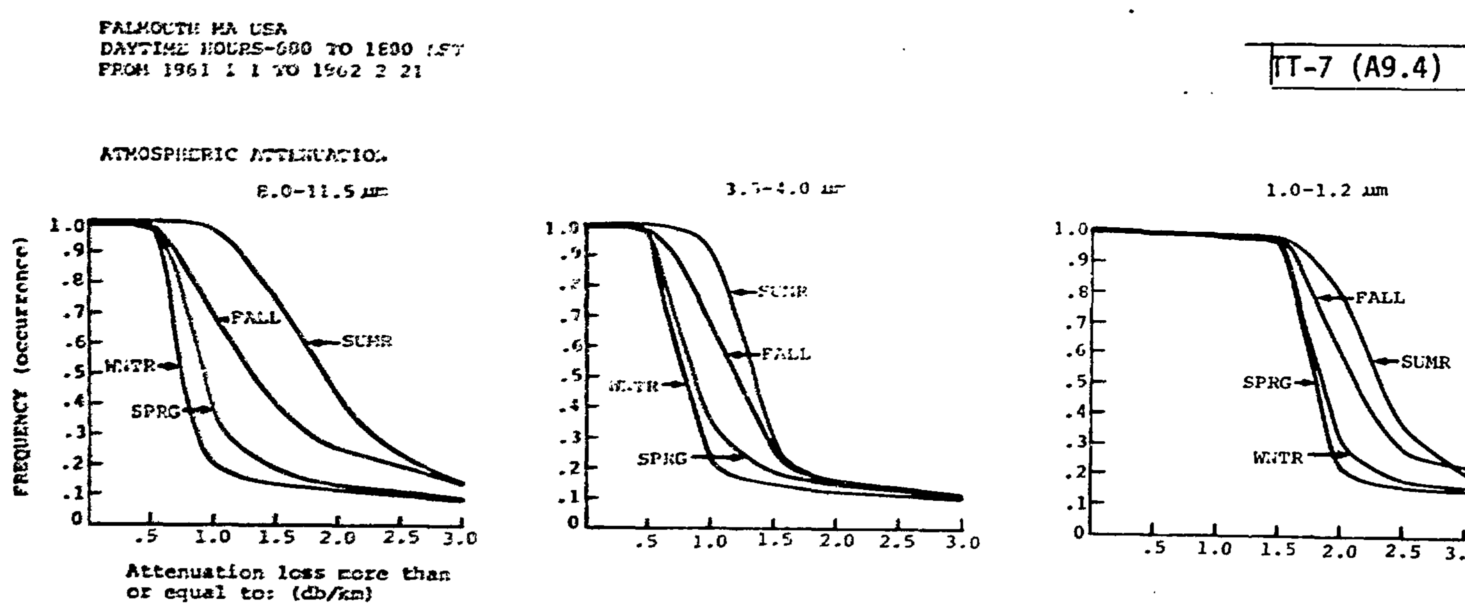

Fig. A 9.4 Probability of Clear Air/Fog-Haze Atmospheric Attenuation for IR Radiation Bands

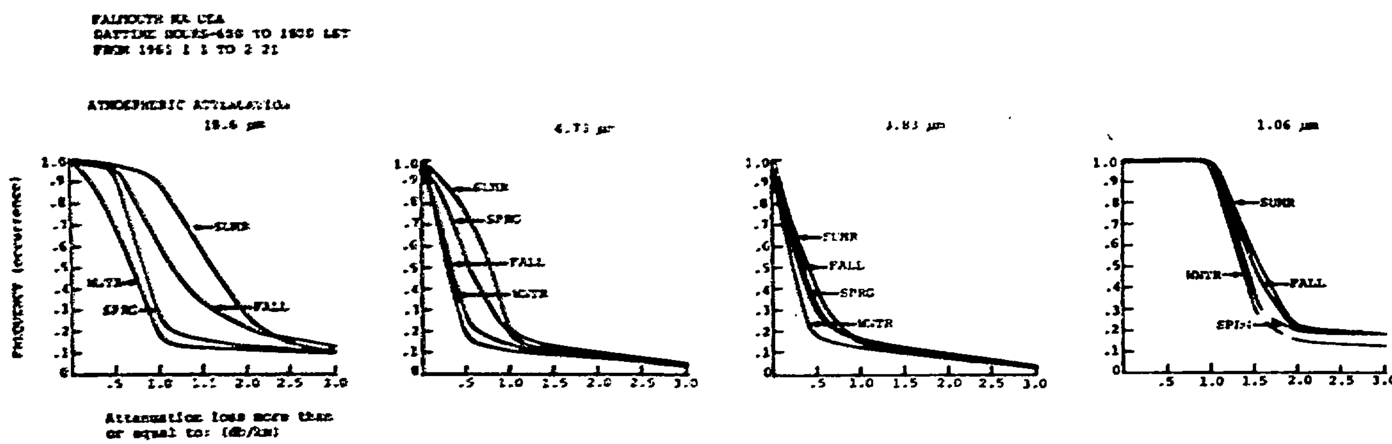

Fig. A 9.5 Probability of Clear Air/Fog-Haze Atmospheric Attenuation for Laser Lines

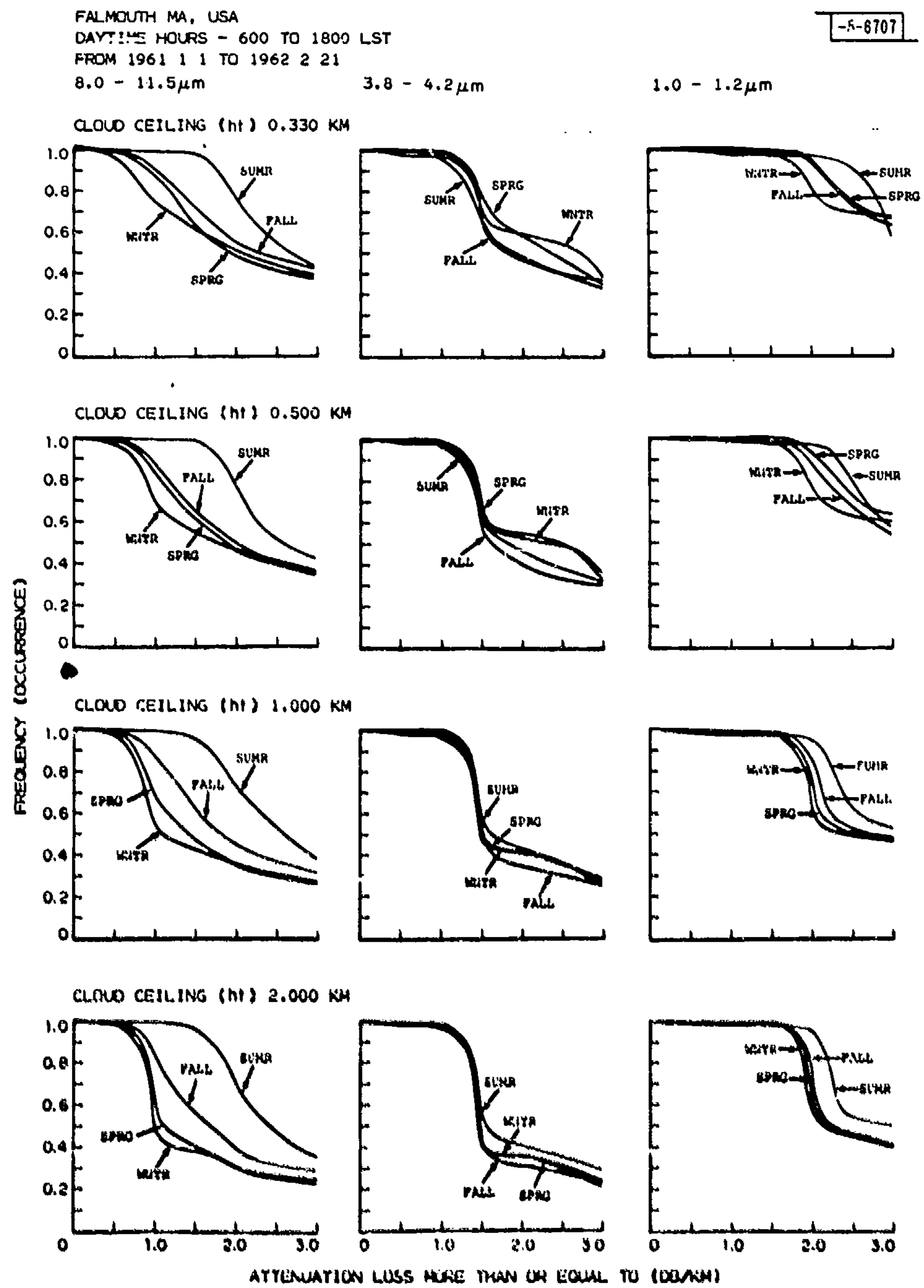

Fig. A 9.6 Joint Probability of Cloud Height and Clear Air/Fog-Haze Attenuation for IR Radiation Bands

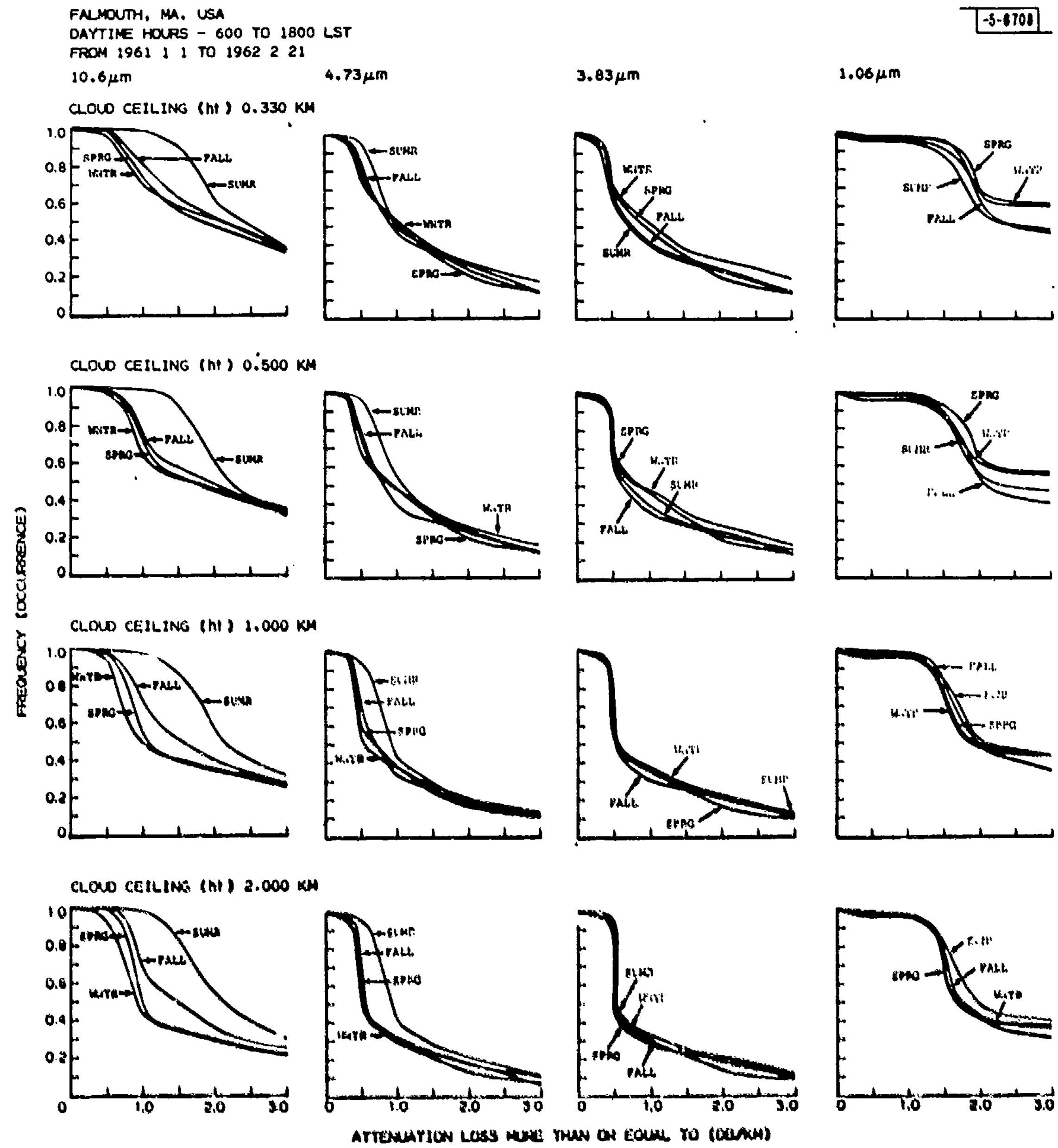

Fig. A 9.7 Joint Probability of Cloud Height and Clear Air/Fog-Haze Attenuation for Laser Lines

UNCLASSIFIED

SECURITY CLASSIFICATION OF THIS PAGE (When Data Entered)

REPORT DOCUMENTATION PAGE

READ INSTRUCTIONS BEFORE COMPLETING FORM

1. REPORT NUMBER: ESD-TR-76-67
2. GOVT ACCESSION NO.
3. RECIPIENT'S CATALOG NUMBER
4. TITLE (and Subtitle): Statistics of Global IR Atmospheric Transmission
5. TYPE OF REPORT & PERIOD COVERED: Project Report
6. PERFORMING ORG. REPORT NUMBER: Project Report TT-7
7. AUTHOR(s): Anthony P. Modica and Herbert Kleiman
8. CONTRACT OR GRANT NUMBER(s): F19628-76-C-0002
9. PERFORMING ORGANIZATION NAME AND ADDRESS: Lincoln Laboratory, M.I.T., P.O. Box 73, Lexington, MA 02173
10. PROGRAM ELEMENT, PROJECT, TASK AREA & WORK UNIT NUMBERS: ARPA Order 2752; Program Element No. 6[illegible]10; Project No. 62702E
11. CONTROLLING OFFICE NAME AND ADDRESS: Defense Advanced Research Projects Agency, 1400 Wilson Boulevard, Arlington, VA 22209
12. REPORT DATE: 3 March 1976
13. NUMBER OF PAGES: 102
14. MONITORING AGENCY NAME & ADDRESS (if different from Controlling Office): Electronic Systems Division, Hanscom AFB, Bedford, MA 01731
15. SECURITY CLASS. (of this report): Unclassified

15a. DECLASSIFICATION DOWNGRADING SCHEDULE

16. DISTRIBUTION STATEMENT (of this Report): Approved for public release; distribution unlimited.
17. DISTRIBUTION STATEMENT (of the abstract entered in Block 20, if different from Report)
18. SUPPLEMENTARY NOTES: None
19. KEY WORDS (Continue on reverse side if necessary and identify by block number)

weather statistics	transmission losses	Project OPAQUE
atmospheric attenuation	LOWTRAN	electro-optical
narrow IR bands	HOWLS Program	systems

20. ABSTRACT (Continue on reverse side if necessary and identify by block number)

RAND weather data tapes have been used to obtain statistics of visibility, relative humidity and cloud ceiling heights for weather stations throughout the Northern Hemisphere to generate global probabilities for atmospheric attenuation in the infrared spectral region. The present analysis predicts seasonal probabilities for horizontal sea level transmission losses for several narrow IR bands (1.0-1.2), (3.8-4.2), (8.0-11.5 μm) and four laser lines (1.06), (3.83), (4.73) and (10.6 μm). The results also include cloud-free line-of-sight probabilities and attenuation losses through rain.

DD FORM 1473, 1 JAN 73 — EDITION OF 1 NOV 65 IS OBSOLETE

UNCLASSIFIED

SECURITY CLASSIFICATION OF THIS PAGE (When Data Entered)